The role of diacylglycerol acyltransferase 1 in hepatic medium-chain fatty acid metabolism

Dissertation

zur

Erlangung des Doktorgrades

(Dr.rer.nat.)

der

Mathematisch-Naturwissenschaftlichen Fakultät

der

Rheinischen Friedrich-Wilhelms-Universität Bonn

vorgelegt von

Klaus Wunderling

aus

Bonn

Bonn, 2019

Angefertigt mit Genehmigung der Mathematisch-Naturwissenschaftlichen Fakultät der
Rheinischen Friedrich-Wilhelms-Universität Bonn

1. Gutachter

Herr Professor Dr. Christoph Thiele

2. Gutachterin

Frau PD Dr. Heike Weighardt

Tag der Promotion: 16.01.2020

Erscheinungsjahr: 2020

Table of Contents

Abbreviations ..... **- 1 -**
Summary ..... **- 3 -**
1. Introduction ..... **- 4 -**
1.1. Medium-chain fatty acids and medium-chain TAG ..... - 5 -
1.2. The function, biosynthesis and catabolism of TAG ..... - 7 -
1.2.1. Function of TAG ..... - 7 -
1.2.2. TAG biosynthesis ..... - 8 -
1.2.3. DGAT enzymes: catalyzing the final step in TAG synthesis ..... - 9 -
1.2.4. TAG mobilization and mitochondrial β-oxidation ..... - 12 -
1.3. Click labeling in lipid research ..... - 14 -
2. Aim of the Thesis ..... **- 19 -**
3. Material ..... **- 20 -**
3.1. Chemicals and reagents ..... - 20 -
3.2. Cell culture media and supplements ..... - 21 -
3.3. Consumables ..... - 21 -
3.4. Small molecule inhibitors ..... - 22 -
3.5. General solutions ..... - 22 -
3.6. Equipment ..... - 23 -
3.7. Computer programs ..... - 24 -
3.8. Alkyne labeled lipids and their nomenclature ..... - 25 -
4. Methods ..... **- 28 -**
4.1. Animal experiments ..... - 28 -
4.1.1. Induction of an *in vivo* LPS-stimulation ..... - 28 -
4.2. Primary hepatocyte cell culture ..... - 29 -
4.2.1. Collagen coating of cell culture plates ..... - 29 -
4.2.2. Liver perfusion and isolation of primary hepatocytes ..... - 29 -
4.3. Metabolic lipid tracing ..... - 31 -
4.3.1. Pulse experiments ..... - 31 -
4.3.2. Pulse-chase experiments ..... - 32 -

4.4. Lipid extraction and click reaction ..... - 33 -
4.4.1. Lipid extraction and click reaction for TLC ..... - 33 -
4.4.2. Lipid extraction and click reaction for MS ..... - 34 -
4.5. Detection methods for alkyne labeled Lipids ..... - 36 -
4.5.1. Detection of clicked alkyne labeled lipids by TLC ..... - 36 -
4.5.2. Multiplexed MS of reporter-labeled alkyne lipids ..... - 37 -
4.6. Live cell oxygen consumption rate (OCR) measurements ..... - 38 -
4.7. Statistical analysis and data evaluation ..... - 40 -
5. Results ..... - 41 -
5.1. Analysis of C11-FA and C19-FA incorporation into TAGs upon DGAT inhibition ..... - 41 -
5.2. Etomoxir and a DGAT1-Inhibitor show similar effects on C11-TAG levels ..... - 44 -
5.3. DGAT1 acts as the main enzyme for MCFA incorporation into TAG ..... - 49 -
5.3.1. Pulse-chase experiments upon DGAT1 inhibition ..... - 49 -
5.3.2. Analysis of the lipid profile in hepatocytes isolated form DGAT1$^{-/-}$ mice upon treatment with DGAT-specific inhibitors and Etomoxir ..... - 55 -
5.4. DGAT inhibition during a short time *in vivo* LPS-stimulation ..... - 68 -
5.5. Comparison of two CPT1 inhibitors: Etomoxir and Teglicar ..... - 73 -
6. Discussion ..... - 79 -
6.1. DGAT1 primarily facilitates murine hepatic MCFA incorporation into TAG ..... - 79 -
6.2. Etomoxir can act as a DGAT inhibitor, predominantly targeting DGAT1 ..... - 82 -
6.3. DGAT inhibition upon an LPS-induced steatotic phenotype ..... - 86 -
6.4. Concluding hypothesis ..... - 87 -
7. Outlook ..... - 89 -
8. References ..... - 90 -
9. Table of figures ..... - 105 -
10. Supplements ..... - 107 -
10.1. Validation of the MCFA-TAG effects with a different set of DGAT inhibitors ..... - 107 -
10.2. Supplementary data for chapter 5.3.1. ..... - 109 -
10.3. Double alkyne-labeled TAG ..... - 110 -
10.4. Internal standard validation ..... - 112 -
10.5. MFQL scripts ..... - 113 -

10.6. Wt vs ΔDGAT1 experiments: total labeled lipids ..... - 120 -

10.7. Supplementary data for chapters 5.3.2 and 5.5 ..... - 121 -

Acknowledgements..... - 125 -

Abbreviations

2-MAG	2-monoacylglycerol
ACAD	acyl-CoA dehydrogenase
ACAT	acyl-CoA:cholesterol acyltransferases
ACN	acetonitrile
ACTH	adrenocorticotropic hormone
ADP	adenosine diphosphate
AGPAT	1-acylglycerol-3-phosphate acyltransferase
AMP	adenosine monophosphate
ATGL	adipose triglyceride lipase
ATP	adenosine triphosphate
BMDMs	bone marrow-derived macrophages
BSA	bovine serum albumin
C10	decanoic acid
C11	C11 alkyne fatty acid
C16	palmitate
C17:2	alkyne palmitate
C18	oleate
C19	alkyne oleate
CACT	carnitine-acylcarnitine translocase
CE	cholesterol ester
Cer	ceramide
CoA	coenzyme A
CPT1/2	carnitine palmitoyltransferase 1/2
DAG	diacylglycerol
DGAT1/2	diacylglycerol acyltransferase 1/2
DHAP	dihydroxyacetone phosphate
DMEM	Dulbecco’s Modified Eagle Medium
ER	endoplasmic reticulum
Eto	Etomoxir
FA	fatty acid
FABPpm	plasma membrane associated fatty acid binding protein
$FADH_2$	flavin adenine dinucleotide
FATP	fatty acid transport proteins
FAO	fatty acid oxidation

FFA	free fatty acid
G3P	glycerol-3-phosphate
GPAT	glycerol-3-phosphate acyltransferase
HESI	high voltage electrospray ionization
HSL	hormone sensitive lipase
LCFA	long chain fatty acid
LCT	long-chain triglyceride
LD	lipid droplet
LPA	lysophosphatidic acid
LPAAT	lysophosphatidic acid acyltransferase
LPC	lysophosphatidylcholine
LPCAT	lysophosphatitylcoline acyltransferase
LPS	lipopolysaccharides
MCDG	medium-chain diglyceride
MCFA	medium chain fatty acid
MCT	medium-chain triglyceride
MFQL	molecular fragment query language
MGAT	monoacylglycerol acyltransferase
MGL	monoacylglycerol lipase
MS	mass spectrometry
NADH	nicotinamide adenine dinucleotide
NAFLD	non-alcoholic fatty liver disease
NFC	normalized fold change
PA	phosphatidic acid
PA	phosphatidic acid
PBS	phosphate buffered saline
PC	phosphatidylcholine
PE	phosphatidylethanolamine
PG	phosphatidylglycerol
PI	phosphatidylinositol
PKA	cyclic AMP dependent protein kinase
PPAR	peroxisome proliferators
SD	standard deviation
TAG	triacylglycerol
TLC	thin layer chromatography
VLDL	very low-density lipoprotein
WT	wildtype

Summary

Fatty acids form a class of important biomolecules, serving as essential elements of lipid molecules. Stored in triacylglycerol (TAG), the main constituent of plant oils and animal fats, they from an inseparable part of the daily human diet. Differing carbon chain length and saturation degrees, lead to a great variety of fatty acids in which long-chain-fatty acids (LCFAs) from the major part. The class of medium-chain fatty acids (MCFAs) are mainly found in a variety of plant oils like palm kernel oil and they possess different biochemical and physiochemical properties then LCFAs. Although the cellular metabolism of MCFAs has been object to research for many decades, it is still insufficiently studied in certain details. This thesis connects to previous work in our laboratory where it was proposed that diacylglycerol acyltransferase 2 (DGAT2) plays predominant role in MCFA-TAG synthesis and that cytosolic MCFA-CoAs for TAG synthesis are provided in a carnitine palmitoyltransferase 1 (CPT1)-dependent manner, as treatment with the CPT1 inhibitor Etomoxir reduced MCFA-TAG levels. This present work puts its emphasis on investigating the hepatic metabolism of DGAT-dependent MCFA incorporation into TAG upon treatment with small molecule inhibitors, targeting either DGAT enzymes or mitochondrial CPT1. Freshly isolated primary hepatocytes from wildtype (WT)- or DGAT1$^{-/-}$-mice were treated with inhibitors and pulsed with alkyne fatty acids, followed by lipid extraction and subsequent analysis of the lipid metabolites via thin layer chromatography or mass spectrometry (MS). Here, a novel MS- based methodology to analyze alkyne labeled lipids which was recently developed in our group, was utilized. As observed with the Etomoxir treatment, it was found that a DGAT1 inhibition in WT hepatocytes resulted as well in a MCFA-TAG reduction. Also, a combination of both inhibitors reduced MCFA-TAG levels even further. A DGAT2-inhibition, however, did not alter MCFA-TAG levels. Further, pulse-chase analysis with unlabeled decanoic acid revealed similar effects upon DGAT1 and Etomoxir treatment. Analysis of the lipid profile in DGAT1$^{-/-}$-mice revealed altered MCFA-TAG levels, independent from inhibitory treatment. Interestingly, in DGAT1$^{-/-}$ hepatocytes, Etomoxir-treatment did lead to a similar change in TAG levels as in the WT control. Additionally, *in vivo* lipopolysaccharide (LPS)-stimulated mice showed overall enhanced lipid levels, but similar responses to the DGAT inhibitor and Etomoxir treatment. Teglicar, another CPT1 inhibitor, did show enhanced TAG synthesis upon treatment. This thesis was concluded by introducing the hypothesis, that hepatic DGAT1 but not DGAT2 is responsible for MCFA incorporation into TAG, which can be compensated partially by DGAT2. It was postulated, that Etomoxir can also act as a potent DGAT inhibitor, predominantly targeting DGAT1, when both DGATs are present. This putative off target effect was not seen with the second CPT1 inhibitor Teglicar.

1. Introduction

One of the most important class of biomolecules are fatty acids (FA). Fatty acids are carboxylic acids with a hydrocarbon chain, usually consisting of an even number of carbon atoms. They are essential elements of many lipid molecules (e.g. phospholipids) and serve as an energy source for catabolic processes, covalent modification of some proteins, as signaling molecules in metabolic processes or as regulators of gene expression.

Fatty acids are classified according to their chain length and their number of double bonds within the acyl chain (saturation). Fatty acids with under 8 carbon atoms are called short-, with 8 to 12 carbon atoms medium-, over 12 carbon atoms as long- and over 22 carbon atoms very long-chain fatty acids. Monounsaturated fatty acids possess one double bond within the acyl chain. Fatty acids which possess more than one double band are called polyunsaturated and fatty acids with no double bonds are classified as saturated. These structural differences cause different biochemical and physical properties of the fatty acids, influencing water solubility, lipophilicity and oxidative capacity. According to their chain length and saturation, fatty acids undergo different metabolic fades in terms of uptake, transport, storage and catabolism.

Long chain fatty acids (LCFA) with 16 or 18 c-atoms, including oleic acid (C18:1) and palmitic acid (C16:0), are the most abundant FAs within animal tissues and most animal diets (Bruss, 2008) and therefore have been well characterized research objects for many decades.

In most plant oils (e.g. rapeseed, sunflower and olive oil) which are used for nutritional purposes throughout the globe and especially in the western world, saturated and unsaturated LCFA, stored as triacylglycerols (TAG), comprise the main fatty acids. With globally increasing prevalence of diet induced obesity and its associated metabolic disorders like non-alcoholic fatty liver disease (NAFLD), type 2 diabetes mellitus and hypertension (Botchlett and Wu, 2018), the interest in research on defining more healthy, alternative nutrients arises.

In the course of this, medium-chain triglycerides (MCT) came into focus. Naturally occurring as a component of coconut- or palm kernel oil and milk (Marten et al., 2006), MCT mainly consist of saturated medium chain fatty acids (MCFAs) (Papamandjaris et al., 1998). Ongoing research on MCFA has revealed several possible positive associations with MCT as a healthy alternative to LCFA-rich TAGs (McCarty and DiNicolantonio, 2016). The cellular metabolism of MCFAs, however, is still insufficiently studied in certain aspects. In this thesis, the murine hepatic metabolism of MCFAs is investigated in more detail, focusing on the DGAT-dependent incorporation of MCFAs into TAGs.

1.1. Medium-chain fatty acids and medium-chain TAG

Medium chain fatty acids are comprised of a fully saturated acyl chain containing 8-12 carbon atoms namely C8:0 (Octanoic acid), C10:0 (Decanoic acid) and C12:0 (Dodecanoic acid) (Papamandjaris et al., 1998). The lack of double bonds and the length of the acyl chain gives MCFA different physiochemical properties than LCFA, leading as well to differences within the metabolism of these two groups of fatty acids and their TAG counterparts. Upon digestion there is already a metabolic discrimination between MCT and long-chain TAG (LCT) within the stomach and gut. The digestion of dietary MCT and LCT starts with the hydrolysis through lingual lipase in the stomach and continues through hydrolysis with pancreatic and gastric lipases within the duodenum. All these enzymes preferably hydrolyze TAG ester bonds at 1 and 3 position, resulting in 2-monoacylglycerol (2-MAG) and two free fatty acids and show a higher activity on MCFA than LCFA (Bach and Babayan, 1982). LCFA, are usually reesterified with 2-MAG to LCT, incorporated into chylomicrons and transported via the lymphatic system, initially bypassing the liver (Bach and Babayan, 1982) (You et al., 2008). In contrast, MCFA can be absorbed directly from the small intestinal cells, where they are afterwards transported to the liver, bound to albumin, via the portal vein for hepatic metabolism (Bach and Babayan, 1982; You et al., 2008), see Figure 1.

In the liver, MCFA can be reesterified to MCT to some extent, when longer fatty acids are present to generate diacylglycerol (DAG) first, which serves, together with the MCFA, as a substrate for DGAT enzymes (Mayorek and Bar-Tana, 1983) The majority of the MCFA, however, undergo rapid catabolism through oxidative pathways including mitochondrial β-oxidation and peroxisomal oxidation (Papamandjaris et al., 1998). In summary, dietary MCTs are hydrolyzed faster than LCTs and the resulting MCFAs are absorbed quickly into the intestinal lumen and transported directly to the liver via the portal vein. In the liver, they undergo mainly catabolic processes and only a small amount is stored in TAG, implicating a shorter half-life in the body and therefore pose a reduced risk of promoting obesity through direct storage in adipocytes (Bach et al., 1996; McCarty and DiNicolantonio, 2016) . Within the last decades, many studies discuss specialized MCFA- and MCT-rich foods as a dietary option for prevention or treatment of certain diseases. Apart from the already mentioned lower incorporation into TAGs, MCTs have been shown to trigger thermogenesis (Hill et al., 1989) and might help to reduce body weight, when used as an alternative oil source, compared to LCT-rich oils (Papamandjaris et al., 1998; Mumme and Stonehouse, 2015). One of the key pathological features in patients suffering from a metabolic syndrome is the increased level of “ectopic fat metabolites” in the affected tissues (McCarty and DiNicolantonio, 2016). These include DAG, which is associated with hepatic insulin resistance via activation of protein kinase Cε (Jornayvaz and Shulman, 2012), and Ceramide, de novo synthetized from palmitate, promoting inflammatory processes (Gao et

al., 2012). On the contrary, MCFAs do not give rise to these metabolites in such extend (Mayorek and Bar-Tana, 1983) and have the potential to partly restore mitochondrial respiration rates under inflammatory conditions (Hecker et al., 2014). Additionally, medium chain diglycerides (MCDGs) have been shown to reduce inflammatory responses *in vitro* (Yu et al., 2017).

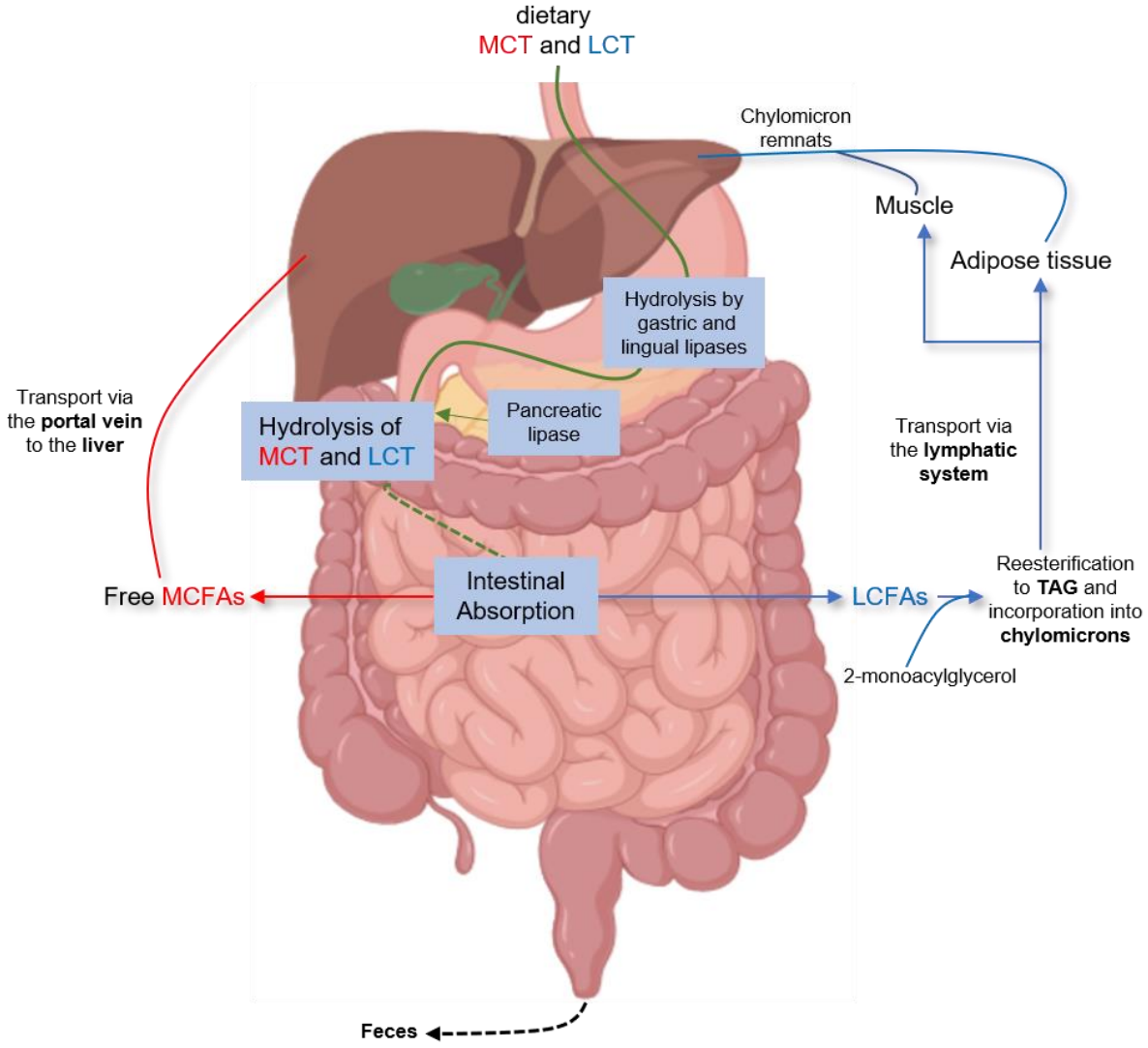

Figure 1: Schematic representation of the digestion and absorption process of dietary MCTs and LCTs. Upon digestion, the hydrolysis of TAG is mediated first by lingual lipases followed by gastric and pancreatic lipases in the small intestine. After hydrolysis to 2-MAG and free fatty acids, the intestinal absorption follows. The main part of MCFAs are directly transported to the liver via the portal vein, bound to albumin. LCFAs are reesterified with 2-MAG to LCT and incorporated into chylomicrons and enter the lymphatic system, where they are transported to adipose tissue or muscle tissue for either storage or oxidation. Remnants of chylomicrons are finally transported to the liver. Scheme of the intestine is adapted from: https://biorender.com/.

Taken together, MCFAs have been identified as promising candiates in alternative diets, beneficial for the treatment of patients suffering from metabolic diseases involving accessive accumulation of fatty acids and their metabolites.

Previous studies in our group described the ability of freshly isolated hepatocytes to incorporate MCFAs into TAGs, in accordance with already published data (Mayorek and Bar-Tana, 1983; Brandes et al., 1985; Klizaite, 2017). It was also shown by our group, that after 8-18 hours, de-differentiating hepatocytes start losing the ability to incorporate C11-FA (alkyne labeled decanoic acid) but nor C19-FA (alkyne labeled oleic acid) into TAG (Klizaite, 2017). Transcriptomic analysis of de-differentiating hepatocytes showed a correlation between the loss of C11-FA incorporation into TAG and DGAT2-expression *in vivo*, but not *in vitro* using cell lysates (Klizaite, 2017). Inspired by these findings, our group hypothesized that hepatic DGAT2 is essential for *in vivo*-C11-FA incorporation into TAG. In the study by Klizaite, it was also shown, that the inhibition of CPT1 through Etomoxir (Turnbull et al., 1984) reduced the C11-FA incorporation intro TAG in hepatocytes. It was hypothesized, that hepatic CPT1 converts mitochondrial MCFA-carnitines to acyl-CoAs, which are shuttled into the cytosol via the carnitine shuttle (Pande, 1975; Klizaite, 2017). The second hypothesis, stating that cytosolic MCFA-CoAs are needed for TAG synthesis by DGAT enzymes in a CPT1-dependent manner was termed “the Etomoxir-effect”.

1.2. The function, biosynthesis and catabolism of TAG

As the work in this thesis focuses mainly on the hepatic incorporation of MCFAs into TAG, the following chapters will give an introduction on the cellular processes involved in TAG synthesis with a special emphasis on the acylation of DAG to TAG via diacylglycerol acyltransferases (DGATs).

1.2.1. Function of TAG

Being the major group of neutral lipids, TAGs form a heterogenous group of molecules, consisting of three fatty acids esterified to a glycerol backbone (Yen et al., 2008). The major function of TAG in living organisms is the storage of fatty acid molecules for energy utilization (Yen et al., 2008). In the adipose tissue TAGs are produced for energy storage (Yen et al., 2008). In the liver, TAGs are produced for the assembly in very low-density lipoprotein (VLDL) particles to enable the transportation of neutral lipids to other tissues (Yen et al., 2015). In the mammary gland, TAGs are synthetized in the form of milk fat globules, enabling fatty acid delivery to mammalian neonates (Yen et al., 2015). In the intestine, the synthesis of TAG is associated with the enterocytic absorption of dietary fats (Bach and Babayan, 1982; Yen et al., 2015).

The synthesis of TAG and their storage in lipid droplets functions also as a protection mechanism of cells against the potential toxic effects of excessive intracellular free fatty acids and their acyl-CoAs (Yen et al., 2008; Aon et al., 2014). TAGs also play an important role in forming the moisture barrier of the skin and serve as an insulator (Coleman and Mashek, 2011).

Unphysiologically high concentrations of TAG in adipose tissue, however, are a key pathological feature of obesity (Yen et al., 2008). In the liver, an excessive TAG accumulation is associated with the pathology of NAFLD and insulin resistance (Ipsen et al., 2018). In the heart, pathological TAG accumulation associates with cardiomyopathy (Unger, 2002).

1.2.2. TAG biosynthesis

Biosynthesis of TAG can be accomplished via two different pathways, namely the glycerol phosphate pathway or the monoacylglycerol pathway (Yen et al., 2008). In the following, both pathways will be described in brief and are schematically summarized in Figure 2.

In both pathways, fatty acids are utilized as acyl-CoAs by the enzymes involved in the respective steps. First, free fatty acids from the blood need to enter the cell. Although passive translocation is possible, this is mainly accomplished by fatty acid transport proteins (FATPs) and the fatty acid translocase, together with the plasma membrane associated fatty acid binding protein (FABPpm) (Doege and Stahl, 2006). In order to maintain high oxidation rates, tissues like the liver, heart and skeletal muscle also have cytoplasmatic fatty acid binding proteins, facilitating faster intracellular fatty acid movement (Houten and Wanders, 2010). Once inside the cell, the fatty acids are quickly activated as acyl-CoAs. Acyl-CoAs are synthetized via a thioesterification from a fatty acid with coenzyme A (CoA) by enzymes called acyl-CoA synthetases. Currently 26 genes were identified in the human genome encoding for this enzyme class (Watkins et al., 2007). Acyl-CoA synthetase are categorized in short-chain (ACSS), medium-chain (ACSM) and long chain (ACSL) CoA-synthetases according to the chain length of their preferred fatty acid substrate (Grevengoed et al., 2014).

Glycerol-3-phosphate (G3P) is the initial acceptor substrate for the TAG synthesis via the glycerol phosphate pathway. In the liver it can be synthetized either from the glycolysis intermediate dihydroxyacetone phosphate (DHAP), from free plasma glycerol via glycerol kinase and from pyruvate originating from gluconeogenesis (Kalhan et al., 2001).

The rate limiting step in TAG synthesis via the glycerol phosphate pathway is the *sn1*-acylation of G3P with acyl-CoA, catalyzed by the glycerol-3-phosphate acyltransferase (GPAT) enzymes (Yamashita et al., 2014). This enzyme class has four known isoforms, with GPAT1 and 2 residing on mitochondria and GPAT3 and 4 locating to the ER, whereas GPAT4 has also been found on lipid droplets (Takeuchi and Reue, 2009; Wilfling et al., 2013). The resulting 1-acyl-*sn*-glycerol-3-phosphate (lysophosphatidic acid (LPA)) is further acylated with another acyl-CoA at the *sn2* position of the glycerol backbone by enzymes of the 1-acylglycerol-3-phosphate acyltransferase (AGPAT) family, also named lysophosphatidic acid acyltransferases (LPAATs) (Takeuchi and Reue, 2009). This family consists of at least 10 described isoforms, having different enzymatic activities like GPAT- or lysophosphatidylcholine acyltransferase (LPCAT) activity (Yamashita et al., 2014). AGPAT1

and 2 are best characterized, both showing LPAAT activity for a broad spectrum acyl-CoAs in terms of chain length and saturation (Yamashita et al., 2014). Although both AGPAT1 and 2 have a broad tissue distribution, AGPAT1 is mainly expressed in the testis, spleen and gut, whereas AGPAT2 is mainly expressed in the adipose tissue, liver, pancreas and heart (Yamashita et al., 2014). Both AGPAT1 and 2 are localized at the endoplasmic reticulum (ER) (Eberhardt et al., 1999). This reaction marks an important branching point in TAG synthesis, as the resulting phosphatidic acid (PA) is not only a precursor for diacylglycerol (DAG) but also for Cytidine-diphosphate diacylglycerol (CDP-DAG), which itself is further metabolized to phosphatidylglycerol (PG) and phosphatidylinositol (PI) (Yamashita et al., 2014).

PA is dephosphorylated by a subfamily of enzymes from the phosphatidic acid phosphatase (PAP) family, also known as lipins. This gene family encodes for three members (Reue, 2009). All three lipins show a unique tissue expression pattern, which suggests different physiological roles (Reue, 2009). PAPs in general have been shown to be localized in the cytosol and being translocated to the ER upon activation (Takeuchi and Reue, 2009); (Gomez-Muñoz et al., 1992). It has been shown that lipin1 is phosphorylated and translocated in an insulin-dependent manner (Harris et al., 2007).

DAG is also synthetized via the monoacylglycerol (MAG) pathway, and both pathways converge at the final step of TAG synthesis, acylating DAG to TAG (Yen et al., 2015).

The MAG pathway occurs predominantly in the intestinal enterocytes, where MAG, as a product of dietary TAG hydrolysis, is acylated with acyl-CoA to DAG via monoacylglycerol acyltransferase (MGAT) activity (Shi and Cheng, 2009; Yen et al., 2015). So far, three isoforms of MGATs have been identified, all showing strong MGAT activity and are localized to the ER (Yen et al., 2002; Cheng et al., 2003; Cao et al., 2003). MGAT3 is only found in higher mammals and possesses a stronger sequence homology to DGAT2 than the other MGATs and is also shown to have DGAT activity (Cao et al., 2007). DAG itself is not only the immediate precursor for TAG but also for the two phospholipids phosphatidylcholine (PC) and phosphatidylethanolamine (PE). Eventually, the last step of TAG synthesis is carried out by DGAT enzymes.

1.2.3. DGAT enzymes: catalyzing the final step in TAG synthesis

There are two enzymes known to catalyze the final step in TAG synthesis, namely DGAT1 and DGAT2. These enzymes do not share a sequence homology and thus are associated with different gene families (Yen et al., 2008). The DGAT1 gene sequence is associated with the gene family of acyl-CoA:cholesterol acyltransferases (ACAT) (Cases et al., 1998), whereas the DGAT2 gene sequence is associated with a family which also includes MGATs and wax synthases (Yen et al., 2005a). Both enzymes exist in a variety of eukaryotes (Yen et al., 2008). DGAT1 and 2, have been proven experimentally to catalyze TAG synthesis from a

variety of FA-CoAs and DAG substrates, when overexpressed in either plant, insect or mammalian cells (Cases et al., 1998; Cases et al., 2001; Yen et al., 2008). DGAT1 has been shown to exhibit additional acyltransferase activity, catalyzing the synthesis of diglycerides, waxes and retinol esters (Yen et al., 2005b). The expression pattern of DGAT enzymes in humans is mostly similar to those in mice (Cases et al., 1998; Cases et al., 2001). Both enzymes are ubiquitously expressed but show distinct cellular and tissue specific expression patterns (Cases et al., 1998; Cases et al., 2001; Buhman et al., 2002). DGAT1 has its highest expression in the small intestine, adipose tissue and the mammary gland, but is also expressed in the liver (Li et al., 2015; Yen et al., 2015). DGAT2 has its highest expression level in the liver, the adipose tissue and as well in the mammary gland and the intestine (Yen et al., 2015; McLaren et al., 2018). Both DGATs are located at the ER and DGAT2 is also shown to localize on lipid droplets (LDs) (Stone et al., 2006; Kuerschner et al., 2008; Stone et al., 2009; Wurie et al., 2011). The metabolic importance of both DGATs is underlined through the phenotypes resulting from a global knockout of the enzymes in mouse models. A loss of DGAT2 is not compatible with life, as the newborn mice die shortly after birth, with severely reduced TAG levels and an impaired barrier function of the skin (Stone et al., 2004). A suppression of DGAT2 with antisense oligonucleotides has been shown to reverse a diet induced NAFLD phenotype in rats (Choi et al., 2007). DGAT1 knockout mice are viable, show a delayed intestinal fat absorption, have a higher energy expenditure and show a resistance towards high-fat diet induced obesity, insulin resistance and hepatic steatosis (Smith et al., 2000; Chen et al., 2002; Buhman et al., 2002). Additionally, a pharmacological inhibition of DGAT1 in Leptin deficient db/db mice also leads to reduced body weight, reduced hyperlipidemia and reduced hepatic steatosis in these animals (Zhang et al., 2010). Intestine specific overexpression of DGAT1 in a DGAT1$^{-/-}$-background reverses the effects of a global DGAT1 knockout. Despite of lacking DGAT1 in the liver and adipose tissue, the animals show no resistance towards HF diet-induced hepatic steatosis or obesity any more (Lee et al., 2010). In mice, DGAT1 deficiency is also associated with a congenital diarrheal disorder (Haas et al., 2012). Interestingly, this phenotype has also been shown for humans suffering from loss-of-function mutations of DGAT1 in the intestine (van Rijn et al., 2018). A intestine specific overexpression of DGAT2 leads to increased TAG secretion from the enterocytes and an increased response of hepatic TAG storage resulting in an exacerbated steatotic phenotype (Uchida et al., 2013).

There are several publications, dealing with distinct preferences of acyl-CoAs in terms of chain length and saturation for both DGAT enzymes, as well as and the roles of both enzymes in cellular energy metabolism. In a study, using specific small molecules inhibitors against either DGAT enzymes in murine hepatocytes, it has been shown that DGAT1 and 2 can compensate for each other in TAG synthesis, but that triacylglycerol synthesized by

DGAT1 is preferentially used for β-oxidation, whereas TAG synthetized by DGAT2 is destined for very low–density lipoprotein assembly (Li et al., 2015). It has been reported, that DGAT2 may act upstream of DGAT1 in utilizing nascent diglycerides with *de-novo* synthesized fatty acids (Wurie et al., 2012) and that DGAT1 catalyzes the synthesis of TAGs via utilization of exogenously supplied fatty acids (Qi et al., 2012).

In an *in vitro* competition assay, mammalian DGAT1 which was expressed in insect cells favored monounsaturated oleoyl-CoA (C18:1) over saturated palmitoyl-CoA (C16:0), whereas another study concluded otherwise (Cases et al., 2001; Hiramine and Tanabe, 2011). DGAT2 purified from the fungus *Mortierella Ramanniana* showed an enhanced activity towards the medium-chain acyl-CoA dodecanoic acid-CoA (C12:0-CoA) in comparison to oleoyl-CoA (C18:1) as well as higher activities with medium chain DAGs as acceptor substrates (Lardizabal et al., 2001). However, a seed specific DGAT1 isoform from the plant *Cuphea avigera var pulcherrima* has been identified, showing an enhanced activity towards the medium-chain acyl-CoA decanoic acid-CoA (C10:0-CoA) (Iskandarov et al., 2017). This enhanced activity of DGAT1 towards medium-chain fatty acid acyl-CoAs has also been shown in seed oil production from other plant species (Aymé et al., 2015; Rigouin et al., 2018). A study, dealing with the genetic diversity of DGAT1 transcripts in lactating river buffalos, revealed a variety of polymorphisms of the DGAT1 enzyme with association towards extreme phenotypes in milk fat content (Gu et al., 2017).

Taken together, even though both DGAT enzymes have been subject to intensive research for decades, there are still many open questions regarding the distinct metabolic properties of both enzymes in cellular-, tissue and species-specific function on TAG synthesis.

As the inhibition of both DGAT enzymes have been of interest as targets for the treatment of metabolic diseases like hepatic steatosis, obesity and diabetes, a variety of well characterized small molecule inhibitors, selectively targeting either DGAT1 or DGAT2, were developed and have also been utilized in this present work (Yen et al., 2008; King et al., 2010; Qi et al., 2010; Qi et al., 2012; Li et al., 2015).

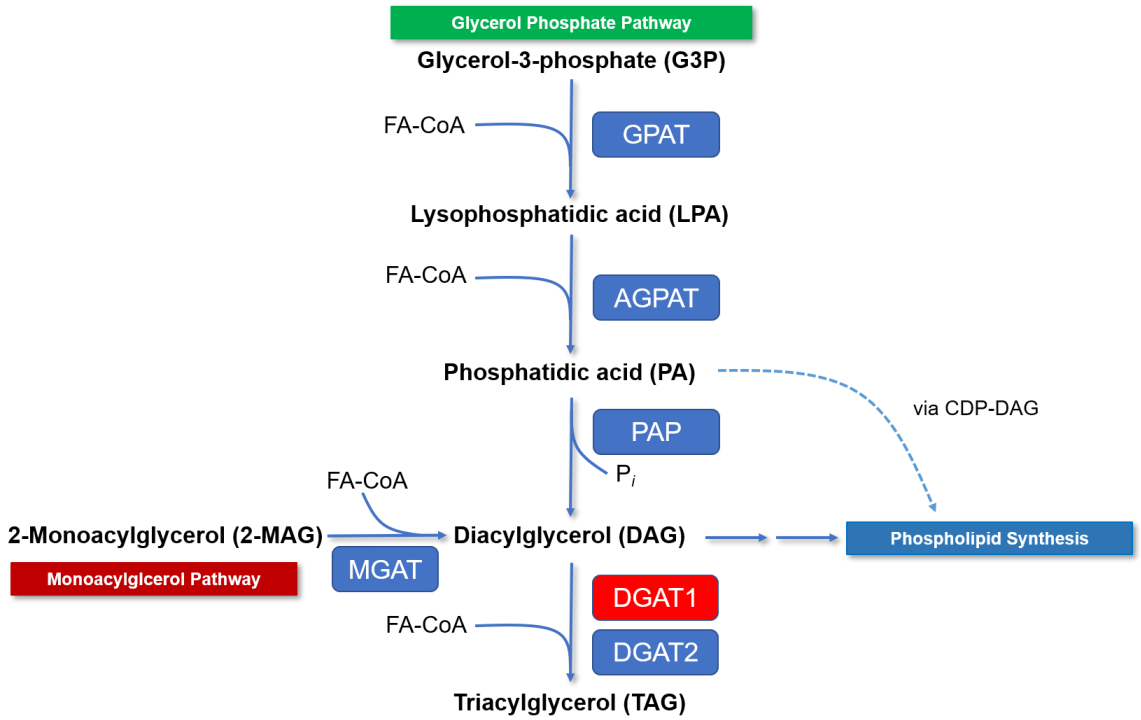

Figure 2: Schematic overview on the pathways involved in TAG synthesis as described in chapters 1.2.2 and 1.2.3. Abbreviations: FA-CoA: fatty acid-coenzyme A, GPAT: glycerol-phosphate acyltransferase, AGPAT: acylglycerol-phosphate acyltransferase, CDP-DAG: Cytidine-diphosphate diacylglycerol, PAP: phosphatidic acid phosphohydrolase, MGAT: acyl CoA: monoacylglycerol acyltransferase and DGAT1/2: diacylglycerol acyltransferases 1/2. Scheme is adapted from: (Yen et al., 2008).

1.2.4. TAG mobilization and mitochondrial β-oxidation

Upon cellular energy demand of the organism, the TAG depot, stored in the adipose tissue, is broken down and the generated free fatty acids (FFA) are transported to other tissues via the bloodstream bound to albumin for mitochondrial β-oxidation and ATP production (Lass et al., 2011). The process of cellular TAG storage and subsequent mobilization upon energy demand is not restricted to adipocytes (Lass et al., 2011). However, non-adipose cells do not secrete FFA, derived from intracellular TAG depots, but rather use them in an autonomous intracellular manner for β-oxidation or lipid synthesis (Lass et al., 2011). The lipolysis of TAG is achieved by three lipases, the adipose triglyceride lipase (ATGL), the hormone sensitive lipase (HSL) and the monoacylglycerol lipase (MGL), which sequentially hydrolyze TAG, forming FFAs and glycerol. ATGL is the key enzyme which catalyzes the initial, rate limiting step in TAG hydrolysis in both adipose and non-adipose tissues (Zimmermann et al., 2004; Watt and Steinberg, 2008). In this first step, ATGL predominantly generates *sn*-1,3 and *sn*-2,3 DAG (Eichmann et al., 2012). In the hepatic metabolism, resulting FFAs are either used for oxidation or for re-esterification at the ER, where newly synthetized TAGs are incorporated into apolipoprotein-B-containing VLDL for secretion and transportation to other tissues (Yao et al., 2013; Grasselli et al., 2015). DAG can be further hydrolyzed by HSL,

resulting in monoacylglycerol and a free fatty acid. HSL is mainly expressed in adipose tissue, and is stimulated by hormones like catecholamines, ACTH and glucagon, which is facilitated via phosphorylation through cyclic AMP dependent protein kinase (PKA) (Yeaman, 1990; Kraemer and Shen, 2002). The resulting MAG is finally hydrolyzed by MGL, forming a last FFA and glycerol. MGL is a serine hydrolase, both found in the brain and peripheral tissues such as adipose tissue and heart (Karlsson et al., 1997). The free fatty acids from the subsequent hydrolysis steps are activated by thioesterification with CoA (see: Chapter 1.2.2). On demand, they will be used for lipid synthesis or for mitochondrial or peroxisomal β-oxidation. Mitochondrial β-oxidation covers the major part of oxidation of short-, medium-, and long-chain fatty acids. LCFAs, originating from dietary fats represent the predominant source for energy production via oxidative phosphorylation generating ATP (Reddy and Hashimoto, 2001). The translocation of acyl-CoAs trough the mitochondrial membrane is facilitated by the carnitine shuttle system, although it has been proposed that the translocation of MCFA-CoAs can also be facilitated without the carnitine shuttle system (Bremer, 1983; Odle et al., 1991; Violante et al., 2013). The first enzyme involved is the carnitine palmitoyl transferase 1 (CPT1), catalyzing the conversion of acyl-CoAs to acyl-carnitines (McGarry and Brown, 1997; Houten and Wanders, 2010). There exist at least two known isoforms of CPT1, namely the liver isoform (CPT1A), which has its highest expression in the liver, and the skeletal muscle isoform (CPT1B) which is highly expressed in the heart and skeletal muscle (Houten and Wanders, 2010). CPT1 is evidently induced by peroxisome proliferators (PPAR) and by fatty acids/ acyl-CoAs and can be inhibited by malonyl-CoA (Reddy and Hashimoto, 2001; Houten and Wanders, 2010). The acyl-carnitines present are translocated through the inner mitochondrial membrane via the carnitine-acylcarnitine translocase (CACT), exchanging carnitines from the mitochondrial matrix with acyl-carnitines form the intermembrane space. The acyl-carnitines are converted back into acyl-CoAs by the carnitine palmitoyltransferase 2 (CPT2), located at the inner mitochondrial membrane (Houten and Wanders, 2010). The acyl-CoAs are then able to enter the mitochondrial β-oxidation cycle.

The peroxisomal β-oxidation has been shown to additionally be present in all cells in which also mitochondrial β-oxidation is facilitated (Reddy and Hashimoto, 2001). Here, the process is catalyzed by different enzymes and plays a functionally complementary but different role (Reddy and Hashimoto, 2001). It has been shown that very long chain fatty acids (VLCFAs) with over 20 carbon atoms are almost exclusively β-oxidized in peroxisomes because mitochondria do not possess a very-long-chain acyl-CoA synthetase (Reddy and Hashimoto, 2001). There is also experimental evidence, showing a compensation in acylcarnitine levels through peroxisomal metabolism, when mitochondrial β-oxidation is deficient or overloaded (Violante et al., 2013).

1.3. Click labeling in lipid research

In order to follow the metabolism or cellular localization of any lipid of interest, preferably the molecule needs to have a label, which can be used for the detection method of choice. In contrast to proteins, lipids cannot be modified with genetically encoded reporters, for instance by attaching a traceable tag to the protein of interest through a molecular cloning approach. Lipids need to be modified chemically and the tags need to be as small as possible, that their structure does not interfere with the biochemical properties of the lipid in the cellular environment. For decades, isotopes such as carbon (^{14}C) or deuterium (D) have been used for this purpose (Rittenberg, D., and R. Schoenheimer, 1937). Isotope labeling does not interfere with the biochemical properties of the lipid and it allows its detection by several methods including chromatography or MS. Drawbacks of this technology however are the high expense of isotope labeled lipids and the need for specialized laboratories and regulations, when working with radioactivity. Also, radioactive isotopes, relevant for fatty acid tracing (^{14}C and ^{3}H), have moderate to low specific activities and therefore this detection method is limited in sensitivity or requires long exposure times to generate meaningful results (Thiele et al., 2012). Another approach to generate a labeled molecule which is traceable in living systems, is the use of biorthogonal chemical reactions and labels (Sletten and Bertozzi, 2009). One of these reactions is the 1,3-dipolar [3+2] cycloaddition of terminal alkynes with an azide under high temperatures or pressures, originally described by Huisgen in 1963 (Huisgen, 1963). In 2002, two independent groups (Tornøe et al., 2002; Rostovtsev et al., 2002) described that the addition of Cu(I) as a catalyst could enable the reaction under mild conditions at room temperature (Figure 3), thus making it more suitable for the use in biological systems.

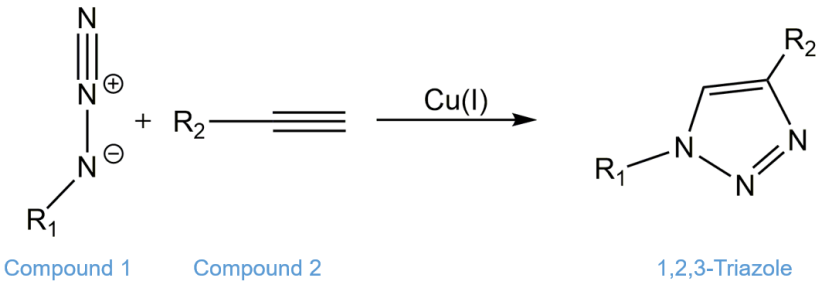

Figure 3: Schematic visualization of the Cu(I) catalyzed click reaction.

Since then, the use of an alkyne group as a small biorthogonal label, found its way into biological applications.

Our group has established several methods in which lipids, labeled with terminal alkynes, are used to trace lipid metabolism (Thiele et al., 2012; Gaebler et al., 2013; Gaebler et al., 2016).

When fed to cells, the fatty acids are incorporated into cellular lipids in a similar manner as their native counterparts (Thiele et al., 2012).

After lipid extraction, the alkyne labeled lipid can be reacted with any suitable azido-labeled reporter group for further detection. In this work, two different detection methods, developed in our group, were used. One is the reaction of the alkyne labeled lipids to azido-coumarin, followed by lipid separation through thin layer chromatography (TLC) and the visualization by fluorescent imaging (Figure 4):

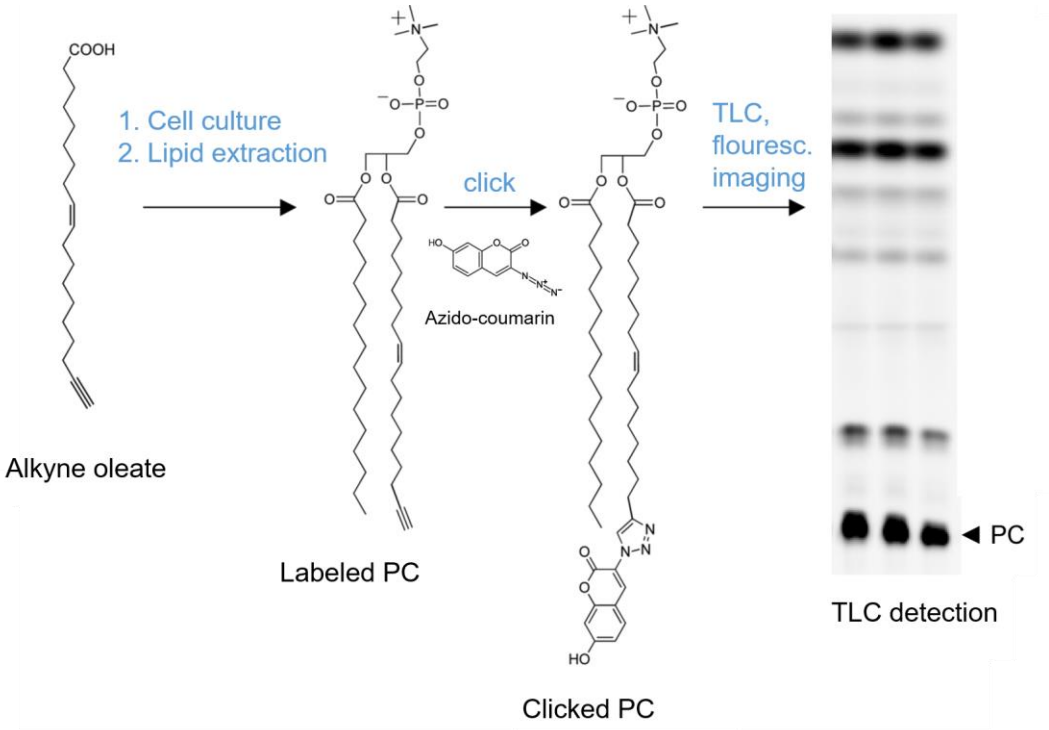

Figure 4: Schematic visualization of the workflow used to trace lipid metabolism with alkyne labeled fatty acids with the use of azido-coumarin as a fluorescent dye. Alkyne labeled oleate is fed to cells and once metabolized, it results in a variety of alkyne labeled lipid species. The lipids are then extracted and clicked to azido-coumarin. The clicked lipids are separated on a TLC and the fluorescent coumarin signal is captured. Figure is adapted from: (Thiele et al., 2012).

Although this method is a fast and versatile tool, enabling a broad range coverage of metabolic pathways in lipid biochemistry, it has limitations in terms of lipid species resolution. Here the sum of all species within a lipid class is represented in one band on the TLC plate. In order to analyze species within the lipid class, a detection method with a higher resolution is required.

The study of the lipidome by MS finds its biggest challenge in the complexity of lipid extracts from biological sources with hundreds of lipid classes subdivided in thousands of lipid species (Brügger, 2014). Brügger and colleagues were the first to approach the quantitative analysis of membrane lipids from unprocessed lipid extracts via tandem MS (Brügger et al., 1997). This approach was further refined by Ejsing and colleagues, who established a global analysis of the yeast lipidome by quantitative shotgun MS, as an efficient resource for eukaryotic lipidome analysis (Ejsing et al., 2009).

Characterization of lipids in MS predominantly uses heated electrospray ionization (heated ESI) as a soft ionization technique with minimal in-source fragmentation, generating positive or negative lipid ions (Fenn et al., 1989). For modern lipidomics, mass spectrometers with high mass resolution and high accuracy such as hybrid orbitrap tandem mass spectrometers are used. In tandem MS (MS/MS), ions are first separated by their mass-to-charge ratio (*m/z*). So called precursor ions with a distinct (*m/z*)-ratio are then selected and collided with an inert gas (e.g. nitrogen) in a collision cell. The process which follows is called collisionally activated dissociation (CAD). Precursor ions are fragmented into product ions and corresponding neutral fragments, which are termed neutral loss (NL). By applying high resolution tandem mass spectrometers with precursor ion and neutral loss scanning to the shotgun-lipidomics approach (Han and Gross, 2005), it became possible to distinguish between most isobaric lipid species from different lipid classes within total cellular lipid extracts (Schwudke et al., 2011).

The use of stable heavy isotopes is an established method for tracing and, to some extent, also applicable for MS. However, identification and quantification of metabolites originated from isotope labeled compounds in cellular extracts comprises an even bigger challenge, especially tracing fatty acid metabolism with hundreds of possible metabolic products (Parks and Hellerstein, 2006).

Our group has recently developed several azido-labeled reporter compounds which can be detected by tandem MS, transferring the advantages of alkyne-labeled lipid tracing to this technology and enabling lipid species resolution with high sensitivity (Thiele et al., 2019)

One of these reporter groups is the compound C171 (Figure 5). It consists of a quaternary ammonium group, a C4 linker and an azido group for click reacting it to terminal alkynes.

This structure offers three features for mass spectrometric detection. First, the permanent positive charge of the quaternary ammonium group enhances the ionization of the labeled lipid. This effectively enhances the transmission into the mass spectrometer, especially for neutral lipid species such as TAG. Second, when reacted, C171 gives all labeled lipids a nominal mass shift of +171 Da, allowing direct detection in the mass spectrometer. Third, upon collision in MS/MS analysis, the reacted C171 shows a characteristic fragmentation pattern with a characteristic neutral loss (NL) of 73.09 Da,

corresponding to the dimethlyethlyamine group eliminated at low collision energies in the orbitrap (Figure 5).

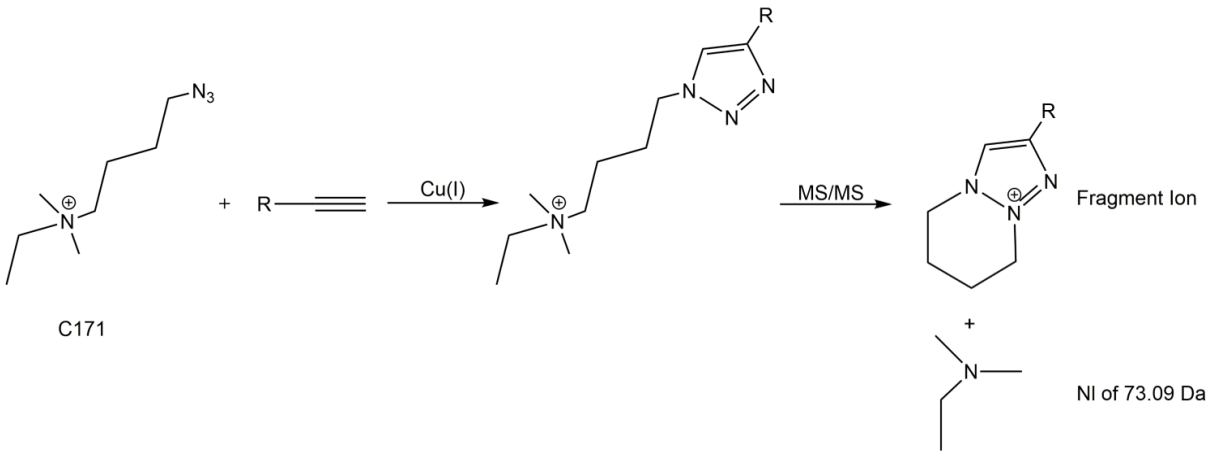

Figure 5: Structure, click reaction and fragmentation pattern of the compound C171. The azido labeled compound is first reacted with an alkyne labeled lipid (R) via the Cu(I) catalyzed click reaction, giving it a mass shift of 171 Da. Upon collision during a tandem MS analysis (MS/MS), reacted C171 shows a fragmentation pattern with a stereotypic neutral loss (NL) of 73.09 Da and the corresponding fragment ion.

This NL can be used as a diagnostic reaction applicable for a variety of lipid species (Thiele et al., 2019). Both, the mass shift of 171 Da and the neutral loss of 73.09 Da in MS/MS analysis, can be used for automated computational identification of the labeled lipids by the LipidXplorer program (Herzog et al., 2011).

Furthermore, our group transferred the methodology of using isobaric labeling for MS/MS-based multiplex analysis on the C171 reporter compound.

In Proteomics, the use of isobaric labeling is a well-established methodology, namely TMT (Tandem Mass Tags (Thompson et al., 2003)) and iTRAQ (isobaric Tags for Relative and Absolute Quantification (Ross et al., 2004)), for analyzing several biological samples at once. This increases sample throughput and reduces inaccuracies such as technical background noise.

Our approach on lipid analysis benefits strongly form multiplexing due to many technical difficulties in sample processing, such as handling small volumes of organic solvents in the extraction process or spray- and fragmentation- variations in the mass spectrometer.

For combining the benefits of multiplex analysis with the properties of the C171 reporter compound for MS, different combinations of deuterium- and ^{13}C-atoms were used to generate four isobarically labeled C171 compounds (Figure 6, A) (Thiele et al., 2019).

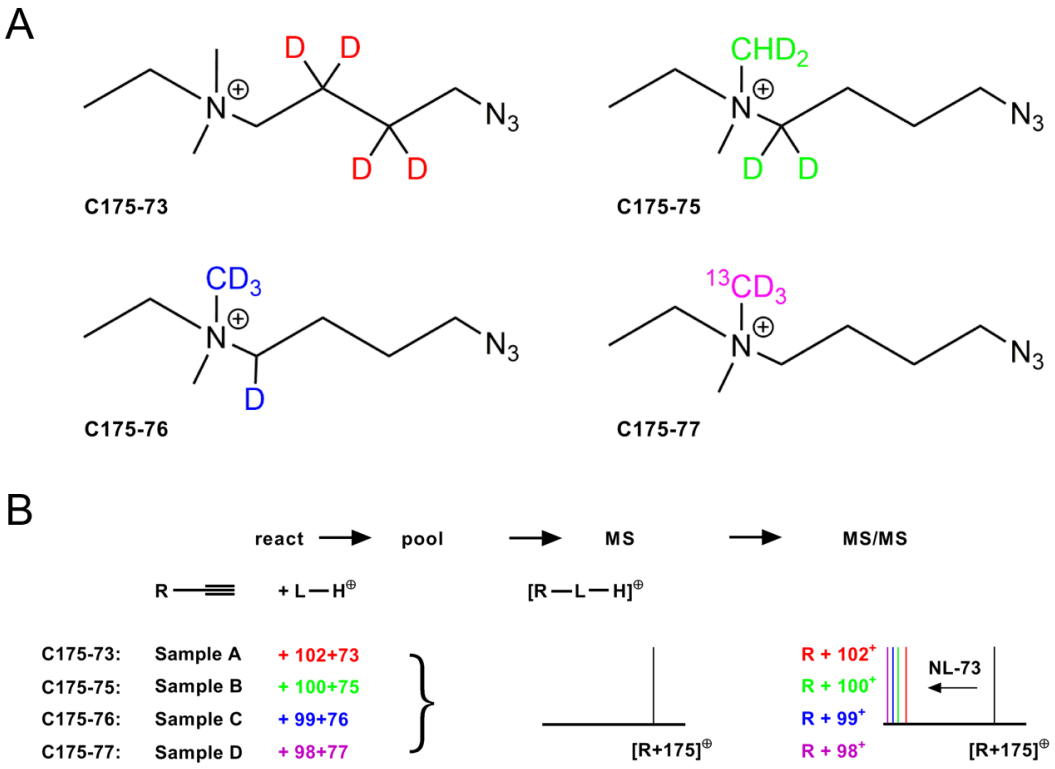

Figure 6: Structures (A) and biological application (B) of the isobarically labeled C171 compounds for multiplex analysis. A: The compound C171 has been modified with specific combinations of deuterium- and ^{13}C-atoms, in order to establish four different compounds bearing nearly identical masses of 175,18 Da. In MS2 fragmentation however, all four compounds generate different neutral losses of either 73 Da (C175-73, A), 75 Da (C175-75, B), 76 Da (C175-76, C) and 77 Da (C175-77, D). B: Lipid extractions from four different biological samples with alkyne labeled lipids are individually reacted with one C175-XX compound each, pooled and analyzed by MS. In MS all labeled lipids from each sample are detected with the same monoisotopic mass. Fragmentation during MS/MS leads to four different neutral losses and their corresponding fragment ion, each representing its original sample. R=lipid residue, L=label, H=Headgroup, MS=Mass spectrometry, MS/MS=tandem mass spectrometry.

All resulting molecules bear nearly identical masses of 175,18 Da in MS1 analysis, but have different neutral losses of 73 Da, 75 Da, 76 Da and 77 Da in their MS/MS fragmentation pattern. In the following work they are referred to as C175-XX. These properties allow the analysis of four biological samples at once using MS/MS (Figure 6, B). Normalization to the internal alkyne labeled standards used in this work, namely TAG, DAG, PC, PA, CE, Cer and a double labeled TAG, allows the absolute quantification of these lipid classes under experimental conditions.

In this work the click labeling method for either TLC or MS application was used to investigate the hepatic metabolism of DGAT-dependent MCFA incorporation into TAG under the influence of small molecule inhibitors, targeting either DGAT enzymes or mitochondrial CPT1.

All MS-based experiments presented in this work were accomplished with the use of the C175-XX compounds.

2. Aim of the Thesis

The work in this thesis continues the previous study from our group by K. Klizaite (Klizaite, 2017). There, it was hypothesized that in hepatocytes DGAT2 might play a predominant role over DGAT1 in MCFA-TAG synthesis and that MCFA-CoAs for DGAT-dependent TAG synthesis are provided in a CPT1-dependent manner.

This thesis aims to deepen the understanding of the MCFA metabolism in primary murine hepatocytes, following the two hypotheses by focusing on these key questions:

- Does one of the DGAT enzymes play a predominant role in hepatic MCFA incorporation into TAG?
- Is the effect of diminished MCFA incorporation into TAG caused by Etomoxir due to its CPT1-specific inhibition, or generated by a possible off-target effect of the inhibitor?
- Does a loss of DGAT1 in hepatocytes affect the MCFA incorporation into TAG, and is this comparable to the effects of a DGAT1-specific inhibition?
- How does the inhibition of DGAT enzymes affect the hepatic lipid metabolism during an LPS-induced short term inflammatory response?
- Are the effects caused by Etomoxir reproducible, using another CPT1 inhibitor?

3. Material

3.1. Chemicals and reagents

Name	Source
3-azido-7-hydroxycoumarin	C. Thiele (Thiele et al., 2012)
Acetic acid (AcA)	VWR International GmbH
Acetonitrile (ACN)	VWR International GmbH
$CaCl_2 \cdot 2H_2O$	AppliChem GmbH
Chloroform ($CHCl_3$), stabilized with 0.9 % EtOH	VWR International GmbH
Collagen (type I) from rat tail	Sigma Aldrich/ Merck KgaA
Collagenase NB G4 from *Clostridium histolyticum*	Nordmark Arzneimittel GmbH
Dimethyl-Sulfoxide (DMSO)	Sigma Aldrich/ Merck KgaA
EGTA	Carl Roth GmbH
Ethanol (EtOH)	VWR International GmbH
Ethyl acetate	VWR International GmbH
HBSS (Hanks' Balanced Salt Solution)	Sigma Aldrich/ Merck KgaA
Heparin-Natrium-25000-ratiopharm®	Ratiopharm GmbH
Hexane (mixture of isomers)	VWR International GmbH
Hünig's base (N,N-diisopropylethylamine)	Sigma Aldrich/ Merck KgaA
isotonic 0.9 % NaCl solution	B. Braun Melsungen AG
KCl	Sigma Aldrich/ Merck KgaA
KH_2PO_4	Sigma Aldrich/ Merck KgaA
LC-MS grade acetic acid (LiChropur®)	Sigma Aldrich/ Merck KgaA
LC-MS grade isopropanol (LiChrosolv®)	VWR International GmbH
LC-MS grade methanol (LiChrosolv®)	VWR International GmbH
LC-MS grade water (Chromanorm®)	VWR International GmbH
LPS O111:B4 from *E. coli*	Sigma Aldrich/ Merck KgaA
Methanol (MeOH)	VWR International GmbH

Na_2HPO_4	Sigma Aldrich/ Merck KgaA
NaCl	AppliChem GmbH
NaOH (sodium hydroxide pellets)	Honeywell
Narketan 100 mg/ml (Ketaminhydrochloride)	Vetoquinol GmbH
Rompun 2% (Xylazinhydrochloride)	Bayer AG
Tetrakis(acetonitrile)copper(I) Tetrafluoroborate	TCI Deutschland GmbH
Trypan blue solution	Sigma Aldrich/ Merck KgaA

3.2. Cell culture media and supplements

Product	Source
Fetal Calf Serum	Thermo Fisher Scientific Inc.
L-glutamine Solution 200 mM (100x)	Thermo Fisher Scientific Inc.
Penicillin-Streptomycin Solution (100x)	Thermo Fisher Scientific Inc.
Seahorse XF RPMI Medium	Agilent Technologies
William's medium E	PAN Biotech GmbH

3.3. Consumables

Product	Source
1.5 ml reaction tubes	Sarstedt AG & Co
1.5 ml reaction tubes "Eppis", for MS applications	Eppendorf AG
Biosphere® filter Tip 10 µl, 200 µl, 1000 µl, for cell culture applications	Sarstedt AG & Co
Cannula BD Neoflon™ 26 G 0.6 x 19 mm, 13 ml/min	BD Biosciences
Capillaries, sodalime-glass, cut ends 100 mm length, 0.1 mm outer diameter	Hilgenberg GmbH
Cell strainer, 100 µm	Sarstedt AG & Co
Falcon™ tubes 25 ml, 50 ml	Corning Inc.
Fast-Read 102® cell counting chambers	VWR International GmbH
Pasteur pipets, glass, long tip	VWR International GmbH

Pipet tips 10 µl, 200 µl, 1000 µl	Sarstedt AG & Co
Pipet tips 10 µl, 200 µl, 1000 µl, for MS applications	Eppendorf AG
Seahorse XF Calibrant solution	Agilent Technologies
Seahorse XF96 cell culture microplates	Agilent Technologies
Seahorse XF96 sensor cartridge	Agilent Technologies
Serological pipets 5ml, 10ml, 25 ml	Sarstedt AG & Co
Syringe 1ml Sub-Q, 26 G, 0.45 mm x 12,7 mm	BD Biosciences
TC 24 well plate, Standard	Sarstedt AG & Co
TLC plates (glass), TLC silica gel 60	Merck KgaA

3.4. Small molecule inhibitors

Name	Producer, CAS or Catalogue Number
Etomoxir (Eto)	Cayman Chemical, CAS № 828934-41-4
A922500 (D1)	Sigma-Aldrich, Cat. No. A1737
JNJ-DGAT2A (D2)	Tocris, Cat. No. 5853
PF-04620110 (PFD1)	Pfizer/Sigma-Aldrich, Cat. No. PZ0207
PF-06424439 (PFD2)	Pfizer/Sigma-Aldrich, Cat. No. PZ0233
ST1326/Teglicar (Tegli)	Avanti Polar Lipids, Cat. No. 870853

3.5. General solutions

Name	Contents
10x Phosphate Buffered Saline (PBS) for 1000 ml	80 g NaCl 2.0 g KCl 14.4 g Na_2HPO_4 2.4 g KH_2PO_4 in ddH_2O adjust to pH 7.4
1x PBS	Diluted from 10x PBS
Ammonium acetate solution (100 mM)	7.708 g ammonium acetate in 1000 ml ddH_2O
EGTA solution (100 mM)	9,509 g in 250 ml ddH_2O, adjust to pH 8.01, sterile filtered

$CaCl_2$ solution (2,5 M)	18.376 g in 50 ml ddH_2O, sterile filtered
HBSS (Hanks' Balanced Salt Solution) with $NaHCO_3^-$	1 Package (HBSS, 9.5 g), 0.35 g $NaHCO_3^-$ in 1 l ddH_2O
Ketamin/Xylazin solution	1:1 in 10 parts isotonic 0.9 % NaCl solution
LPS for injection	1 mg/ml in sterile ddH_2O
Collagen solution	0.33 mg/ml rat tail collagen in sterile 0.2% acetic acid

3.6. Equipment

Name	Company
Accu-Jet® pro, pipette controller	Brand GmbH & Co KG
ATC2000 (Animal Temperature Controller)	World Precision Instruments
Centrifuge 5424	Eppendorf GmbH
Centrifuge Allegra® X-15R	Beckman Coulter GmbH
CO_2 Incubator Midi 40	Thermo Fisher Scientific Inc.
Concentrator Plus Vacuum concentrator	Eppendorf GmbH
Eppendorf Research® plus pipettes: 2,5 µl, 10 µl, 20 µl, 100 µl, 200 µl, 1000 µl	Eppendorf GmbH
Fusion 101, dual channel syringe pump	Chemyx Inc.
Gastight Syringes (500 µl (1700 series), 1000 µl (1000 series) Borosilicate glass, PTFE	Hamilton Company
Heatlamp (150 W)	Local Zoo Shop
Peristaltic Pump Drive PD 5001	Heidolph Instruments GmbH
Q Exactive™ Plus Hybrid Quadrupole-Orbitrap™ mass spectrometer	Thermo Fisher Scientific Inc.
Rolera MGI plus EMCCD camera	Decon science Tec GmbH
ThermoStat Plus, Thermoblock system	Eppendorf GmbH
TLC developing chamber for a 20 x 20 cm plate	VWR International GmbH
Vacuum pump, Vacusafe comfort	INTEGRA Biosciences AG
Vortex Genie 2	Scientific Industries Inc.
Water bath	Memmert GmbH
Seahorse XF 96 Analyzer	Agilent Technologies

3.7. Computer programs

Name	Usage	Company/Developer
ImageJ	Image processing	Wayne Rasband (NIH)
Microsoft Office 2019	Word processing, Spreadsheed calculations, Image processing	Microsoft Corporation
Adobe Illustrator CS5	Image processing	Adobe Systems Inc.
GelPro Analyzer 6.0	Analysis of TLC plates	Media Cybernetics
GraphPad Prism 6, 7	Statistics, Data processing	GraphPad Software Inc.
Seahorse Wave Controller 2.4	Seahorse XF Analyzer: instrument control and data acquisition/ processing	Agilent Technologies

3.8. Alkyne labeled lipids and their nomenclature

All experiments presented in this work used alkyne labeled fatty acids.

Three alkyne fatty acids, termed C11, C17:2 and C19, were chosen to trace MCFA-, saturated LCFA- and monounsaturated LCFA-metabolism, respectively (see: Figure 7).

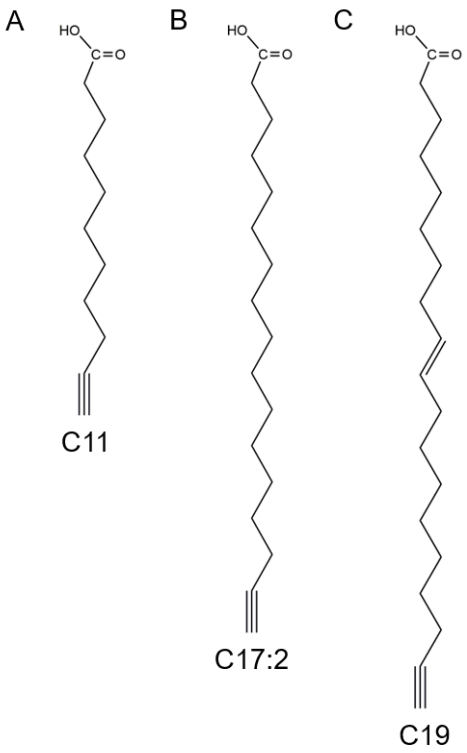

Figure 7: Structure of alkyne labeled lipids used for metabolic tracing. The underlined simplified names are used throughout the text. A (C11): 10-Undecynoic acid (alkyne-decanoic acid, C11:2). B (C17:2): 16-Heptadecynoic acid (alkyne-palmitate). C: (C19): Nonadec-9-cis-en-18-ynoic acid (alkyne-oleate, C19:3).

In experiments, where the alkyne metabolites are detected through TLC, the resulting lipid classes are designated with the addition of the respective alkyne-FA name. For example, TAGs that have one C11-FA incorporated are named C11-TAGs, representing the group of MCFA-TAGs (or MCTs). The same naming scheme is used for C17:2- and C19-FAs, both resembling groups of LCFA-TAGs (or LCTs).

Alkyne-palmitate (C17:2) was used in all experiments in which the labeled lipids were analyzed through MS. Since MS enables lipid species resolution (chapter 1.3), a broad variety of alkyne labeled lipid species within all analyzed lipid classes can be detected and analyzed.

Yet, in comparison to their natural counterparts, all alkyne labeled fatty acids used here contain one more c-atom and two additional double bonds due to the alkyne group. This results in odd numbered and seemingly double unsaturated lipid species, when an alkyne fatty acid was metabolically incorporated. As an example, Figure 8 shows a TAG-molecule where alkyne-palmitate was introduced.

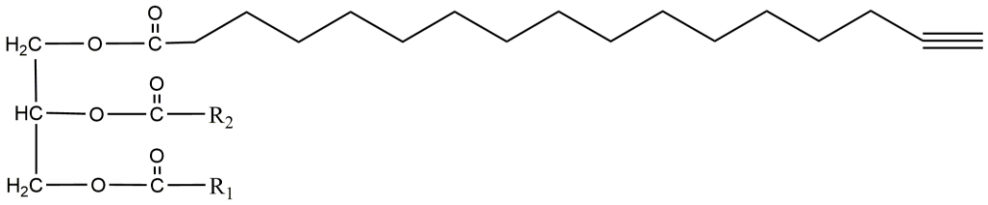

Figure 8: Structure of triacylglycerol labeled with alkyne palmitate (C17:2). R_1 and R_2 stand for any other fatty acid, incorporated into the molecule.

Assuming, that R_1 is decanoic acid (C10:0) and R_2 is oleic acid (C18:1), this TAG molecule would be named as TAG [45:3], for C17:2 + C18:1 + C10:0. In contrary, when natural palmitate (C16:0) would have been introduced the resulting TAG molecule would be stated as TAG [44:1], for C16:0 + C18:1 + C10:0. This applies to all lipid species. In this thesis, a TAG molecule, consisting of alkyne-palmitate (C17:2), one molecule of decanoic acid (C10:0) and one more additional fatty acid, resulting in a total number of carbon atoms of 47 or below is defined as an MCFA-TAG. All analyses of the lipid species TAG, DAG, PC and PA which are presented in this work, were applied on single alkyne labeled lipids. These lipid molecules are a single alkyne labeled FA and are named aTAG, aDAG, aPC and aPA. For information regarding double alkyne-labeled lipid species, see: Supplementary chapter 10.3. Absolute quantification of the lipid classes aTAG, aDAG, aPC, aPA, aCeramide (aCer), aCholesterol ester (aCE) and dlTAG were accomplished using internal standards (see: Table 2). As absolute amounts of alkyne labeled Cer and CE species were very low (always under 10 pmol total), these species were only included in calculations for relative amounts (mol per mille) and not included in any figures. On the validation of the accuracy of the internal standardization, see: Supplementary chapter 10.4.

All alkyne labeled lipids, including all internal standards used for MS analysis, were synthesized by Prof. Dr. C. Thiele (see: Table 1 and 2) except the commercially available C11 FA. Detailed information on the synthesis protocol for alkyne-palmitate and alkyne-oleate is published in: (Thiele et al., 2012). The synthesis protocol for the alkyne labeled lipid

species used as internal standards for MS analysis is published in: (Thiele et al., 2019). As a native MCFA, decanoic acid (C10) was used (see: Table 1).

Table 1: Name and composition of the stock solution from the alkyne labeled fatty acids/ native decanoic acid used for metabolic tracing.

Alkyne/native lipid (Name used in thesis), stock solution compostition	Producer/Source
C11 (alkyne-decanoic acid), 14.7 mM in 80% EtOH	TCI Deutschland GmbH
C17:2 (alkyne-palmitate), 20 mM in 80% EtOH	Synthesis by Prof. Dr. C. Thiele
C19 (alkyne-oleate), 100 mM in 80 % EtOH	Synthesis by Prof. Dr. C. Thiele
C10 (Decanoic acid, C10:0), 20 mM in 80% EtOH	Sigma Aldrich/ Merck KgaA

Table 2: Name, synthesis procedure and masses of alkyne labeled lipids used as internal standards for MS analysis.

Standard name	Synthesis procedure	Calculated and measured masses (m/z)
aPC (16:0/a18:3)	Acylation of LPC (16:0) using EDC/DMAP	$[M+H]^+$ measured: 756.551 calculated: 756.554
aPA (a17:2/17:1)	Acylation of sn-glycerol-3 diethylphosphate and subsequent deprotection with bromotrimethylsilane (Gaebler et al., 2013)	$[M-H]^-$ measured: 669.451 calculated: 669.450
aCer (d18:1/a18:3)	Acylation of sphingosine with a18:3-NHS	$[M+H]^+$ measured: 560.502 calculated: 560.504
aTAG (14:0/17:1/a17:2)	Acylation of DAG (14:0/17:1) using EDC/DMAP	$[M+NH^4]^+$ measured: 818.721 calculated: 818.723
aCE (a18:3)	Acylation of cholesterol using EDC/DMAP	$[M+NH^4]^+$ measured: 664.602 calculated: 664.603
aDAG (a17:2/15:0)	Acylation of MA G (a17:2) using EDC/DMAP	$[M+NH^4]^+$ measured: 582.508 calculated: 582.509
dlTAG (a17:2/15:0/a19:3)	Acylation of DAG (a17:2/15:0) using EDC/DMAP	$[M+NH^4]^+$ measured: 856.735 calculated: 856.739

4. Methods

4.1. Animal experiments

As a mouse strain, the C57Bl/6NCrl strain from Jackson Laboratories was used.

Mice were kept on a regular light-dark cycle (12/12 h) in a specific, pathogen free environment, using ventilation cages at 21± 2ºC room temperature and 55±5 % humidity. The animals were kept *ad libitum* on a regular chow diet (LASQCdiet® **Rod16** (main caloric intake: fat 4.3%, protein 16.9%)) from LASvendi, in Soest, Germany.

For all experiments, male mice aged for 8 weeks were used.

All animal experiments were performed according to the European Directive 2010/63/EU in compliance with national laws (deutsches Tierschutzgesetz vom 01.01.2019, Tierschutz-Versuchstierordnung vom 13.08.2013).

For the experiments done in collaboration with Christina Leopold (PhD) within the group of Prof. Dr. Dagmar Kratky at the Medical University of Graz, Austria, DGAT1$^{-/-}$ mice (Smith et al., 2000) and respective WT control animals were used. These animals were aged for 10-12 weeks, and as well kept at a regular light-dark cycle (12 h/12 h) in a clean and temperature-controlled environment and fed a regular chow diet (11.9% caloric intake from fat; Altromin Spezialfutter GmbH, Lage, Germany). All animal experiments were performed according to the European Directive 2010/63/EU in compliance with national laws and approved by the Austrian Federal Ministry of Education, Science and Research, Division of Genetic Engineering and Animal Experiments, Vienna, Austria

4.1.1. Induction of an *in vivo* LPS-stimulation

For an *in vivo* LPS-stimulation, 8 weeks old, WT C57Bl6/NCrl males were weighted and i.p. injected with 15 mg/kg LPS according to their respective weight. During the incubation time of 1.5 hours, the animals were kept *ad libitum* with water and food. After incubation, the mice were proceeded for liver perfusion, followed by isolation of primary hepatocytes (see: Chapter: 4.2.2.).

4.2. Primary hepatocyte cell culture

All experiments in this work were performed on murine primary hepatocytes, which were freshly isolated on the day of the experiment, using the procedure as described below.

4.2.1. Collagen coating of cell culture plates

The cell culture plates used for cultivation of primary hepatocytes were coated with rat tail collagen, in order to generate an environment which mimics some properties of the liver extracellular matrix, to ensure a good adhesion of the cells. For collagenization, 200 µl sterile collagen-solution (see: Materials 3.5.) was added per well of a 24 well plate and allowed to incubate for 30 minutes at room temperature. This procedure was done under sterile conditions in a cell culture hood. After the incubation, the solution was removed and stored for further usage (up to five times) at 4 ºC. The plates were dried under UV-light radiation in the cell culture hood and stored at room temperature for up to 2 weeks.

4.2.2. Liver perfusion and isolation of primary hepatocytes

Primary hepatocytes were isolated by collagenase perfusion of the liver by an adapted protocol as previously described (Berry, 1969; Kaytor et al., 1997; Stoeckman and Towle, 2002).

All buffers and solutions (see: Table 3) used for the procedure were prewarmed in a water at 37ºC. A mouse was first injected i.p. with 200 µl heparin solution. After 10 minutes the animal was given an intraperitoneal injection of a Ketamin/Xylazin mixture. Anesthetic depth of the animal was monitored by pinching the feet, using surgical forceps. When the mouse was in deep anesthesia, it was fixed at a surgical desk. The abdomen was cut open and the intestine moved to the right side in order to expose the portal vein. Once exposed, the portal vein was picked using a butterfly canula with the catheter attached to a “third hand” in order to keep the catheter in place. Then the catheter was connected to the tube from the peristaltic pump, and the liver was perfused with pre-perfusion buffer (see: Table 3) for 2 min at a flow rate of 4 ml/min corresponding to 52 rpm. During this time a rectal temperature probe was attached on top of the liver and a thermal heat lamp was used so keep the liver at 37ºC. After these procedures the tubing was changed to the perfusion buffer (see: Table 3) containing the collagenase. The liver was perfused with 20 ml of the buffer for about seven minutes. Afterwards the liver was carefully dissected by cutting into the diaphragm and attaching blood vessels. A beaker glass was filled with 40 ml of prewarmed adhesion medium (see: Table 3) in which the liver was shaken and rubbed against the glass in order to dissolve the liver. The achieved liver cell suspension was transferred into a falcon tube and centrifuged at 20 g for 2 minutes.

The supernatant was removed, and the pellet containing the hepatocytes was resuspended again in 40 ml prewarmed adhesion medium. The suspension was passed through a 100 µm

cell strainer into a fresh falcon tube. The living cell number was assessed in a cell counting chamber using trypan blue staining. Once counted, 7.5 x 10^4 cells were plated in every well of a 24-well plate. All plates were pre coated with collagen (see: Chapter: 4.2.1.). The plated hepatocytes were allowed to adhere for two hours. The cells were kept at 37ºC and 5% CO_2 in a humidified incubator. Prior the experiment the medium was removed, and the cells were washed once with prewarmed adhesion medium.

Table 3: Buffers and media used for hepatocyte isolation.

Name	Composition
Pre-perfusion Buffer	50 µl Heparin (25000 i.E/ 5ml) 250 µl EGTA (100 mM EGTA, pH 7.4 in ddH_2O, sterile filtered) in 50 ml HBSS (Hanks' Balanced Salt solution + 0.35 g/l $NaHCO_3$)
Perfusion Buffer	36 µl 2.5 M $CaCl_2$ 250 µl Collagenase (0.35 U/ml) in dd in ddH_2O in 25 ml Williams Medium E (w/o any supplements)
Adhesion Medium	Williams Medium E, supplemented with: 10 % (v/v) fetal calf serum 1 % (v/v) penicillin/streptomycin solution 1 % (v/v) 200 mM L-glutamine solution

4.3. Metabolic lipid tracing

In order to analyze the hepatic lipid metabolism upon different experimental conditions, alkyne labeled lipids were used (see: Chapter 3.8.) in either pulse or pulse-chase experiments. All experimental conditions were carried out as technical triplicate determinations. After the respective labeling experiment, the lipids were extracted and processed for either TLC or quantitative lipidomic MS (see: Chapters 4.4.1 and 4.4.2 for extraction and click reaction and Chapters 4.5.1 and 4.5.2 for detection). In the following these experimental procedures are described.

4.3.1. Pulse experiments

These experiments were carried out in 24-well plates with 7.5 x 10^4 cells per well. Hepatocytes were preincubated with either small-molecule inhibitors in various combinations (see: Materials 3.4) or the respective vehicle as a negative control in 400 µl preincubation medium for one hour (see: Table 4). Following the preincubation 100 µl pulse medium, containing different combinations of alkyne-labeled and native fatty acids (see: Table 4) was added. After one hour of incubation (pulse) the cells were washed once with cold adhesion medium (see: Table 3). The second washing step was done with either ice cold 1xPBS or ice cold 100 mM ammonium acetate, depending on the lipid extraction procedure. 1xPBS was used in the extraction protocol prior to TLC while ammonium acetate was used in the extraction procedure prior to quantitative lipidomic MS. After the last washing step, as much liquid was removed as possible, and the plates were either stored at -80ºC until the lipid extraction procedure or extracted directly.

Table 4: Media used for pulse experiments. Inhibitor and fatty acid concentrations are stated as final assay concentrations.

Name	Basic composition	Inhibitors / Fatty acids
Preincubation Medium	Williams Medium E, supplemented with: 10 % (v/v) fetal calf serum 1 % (v/v) penicillin/streptomycin solution 1 % (v/v) 200 mM L-glutamine solution	- 50 µM Eto in ddH_2O - 3 µM D1 in DMSO - 15 µM D2 in DMSO - 5 µM PFD1 in DMSO - 5 µM PFD2 in ddH_2O - 10, 20, 50 µM Teglicar in DMSO
Pulse Medium	Williams Medium E, supplemented with: 10 % (v/v) fetal calf serum 1 % (v/v) penicillin/streptomycin solution 1 % (v/v) 200 mM L-glutamine solution	- 50 µM C11 - 50 µM C17:2 - 50 µM C19 - 50 µM C10

4.3.2. Pulse-chase experiments

In order to analyze the dynamics of the hepatic lipid metabolism with a special focus on the DGAT1-dependent incorporation of medium chain fatty acids into TAG, a pulse-chase experiment (Hou et al., 2013) with alkyne palmitate as a lipid tracer was carried out.

The experiments were performed in 24-well plates with 7.5 x 10^4 cells per well. The cells were preincubated with either a DGAT1-inhibitor, Etomoxir, a combination of both inhibitors, and the respective vehicle as a negative control in 400 µl preincubation medium for one hour (see: Table 5). Then 100 µl pulse medium (see: Table 5) was added for two minutes. After the incubation, the pulse medium was discarded, and the cells washed rapidly with 500 µl prewarmed adhesion medium (see: Table 3). Then, 250 µl prewarmed Chase medium, containing unlabeled decanoic acid and the respective inhibitor combination (see: Table 5), was added to each well. Lipid metabolism was stopped after different time points by washing the cells once with ice cold adhesion medium and once with ice cold 100 mM ammonium acetate, taking care to remove as much liquid as possible after the last washing step. Cells were then frozen at -80ºC until the lipid extraction procedure.

Table 5: Media used for pulse-chase experiments. Inhibitor and fatty acid concentrations are stated as final assay concentrations.

Name	Basic composition	Inhibitors / Fatty acids
Preincubation Medium	Williams Medium E, supplemented with: 10 % (v/v) fetal calf serum 1 % (v/v) penicillin/streptomycin solution 1 % (v/v) 200 mM L-glutamine solution	- 50 µM Eto in ddH_2O - 3 µM D1 in DMSO
Pulse Medium	Williams Medium E, supplemented with: 10 % (v/v) fetal calf serum 1 % (v/v) penicillin/streptomycin solution 1 % (v/v) 200 mM L-glutamine solution	- 100 µM C17:2
Chase Medium	Williams Medium E, supplemented with: 10 % (v/v) fetal calf serum 1 % (v/v) penicillin/streptomycin solution 1 % (v/v) 200 mM L-glutamine solution	- 100 µM C10 - 50 µM Eto in ddH_2O - 3 µM D1 in DMSO

4.4. Lipid extraction and click reaction

All lipid extractions were done directly from the cell culture plates. The extraction procedures were adapted from a previously described, full lipid extraction method (Bligh and Dyer, 1959).

For detection, the alkyne labeled lipids were then reacted with azido-reporter molecules namely 3-azido-7-hydroxycoumarin for fluorescent detection on a TLC plate (see: Chapter 4.5.1.) or a newly developed set of azido-reporter molecules for multiplexed lipid MS (see: Chapter 4.5.2.).

4.4.1. Lipid extraction and click reaction for TLC

When frozen, the plates were thawed, and as much as possible of the remaining liquid was removed. Then 800 µl $CHCl_3$/MeOH (1/3) was added directly in each well. The plates were agitated gently for 30 seconds and the monophasic solution from each well was transferred into a sperate 1.5 ml reaction tube. Precipitated proteins were sedimented by centrifugation at 2 x 10^4 g for two minutes and the supernatant containing the extracted lipids was transferred into a new 1.5 ml reaction tube. Then 200 µl $CHCl_3$ and 600 µl 1% Acetic acid in ddH_2O was added to generate a biphasic solution. The mixture was vigorously vortexed for one minute and then centrifuged again for two minutes at 2 x 10^4 g resulting in a clear phase separation. The upper phase consisting of methanol and water contains all non-lipids and the lower phase consisting of chloroform containing the lipids. The chloroform phase was carefully transferred into a fresh 1.5 ml reaction tube. The chloroform phase was then evaporated in a vacuum concentrator at 45ºC for twenty minutes. The lipids were redissolved in 50 µl $CHCl_3$ and vortexed for 5 minutes. The click reaction was performed with 10 µl from the lipid extract. The remaining lipid extract was stored at -20ºC.

For the click reaction, 40 µl of 3-azido-7-hydroxycoumarin reaction mixture (see: Table 6) was added beforehand in a 1.5 ml reaction tube. Then 10 µl from the full lipid extract was added, the mixture was shortly centrifuged and incubated overnight at 43ºC in a heat block. As a standard, each 1 µl of a 50 µmol solution of synthetized alkyne labeled lipids in $CHCl_3$ was reacted directly in 30 µl click reaction mixture (for information on the internal standards see: (Thiele et al., 2012)).

Table 6: Composition of the click reaction mixture for TLC detection.

Name	Composition
3-azido-7-hydroxycoumarin Reaction Mixture	-10 µl 3-azido-7-hydroxycoumarin (2 mg/ml in ACN) - 250 µl 10 mM Cu(I)-TFB in ACN - in 850 µl 100% EtOH

4.4.2. Lipid extraction and click reaction for MS

The following procedure is also published in: (Thiele et al., 2019).

When frozen, the plates were thawed, and as much as possible of the remaining liquid was removed. Then 500 µl MeOH/$CHCl_3$ extraction mixture for MS (see: Table 7) was added in each well, using a gas tight Hamilton syringe. The entire plate was then sonicated for one minute in a bath sonicator. The monophasic extract from each well was transferred in a 1.5 ml Eppendorf reaction tube. Precipitated proteins were centrifuged down for 5 min at 2 x 10^4 g. The supernatant was transferred in a new 1.5 ml Eppendorf reaction tube. After addition of 300 $CHCl_3$ and 600 µl 1% LC-MS grade acetic acid in H_2O the samples were shaken for 30 seconds and centrifuged for 2 minutes at 2 x 10^4 g. Form the resulting biphasic solution, the lower organic phase was transferred in a new 1.5 ml Eppendorf reaction tube. The organic phase was evaporated in a vacuum centrifuge at 45ºC for 20 minutes. The Lipids were redissolved in 10 µl $CHCl_3$ and vortexed for 30 seconds. The samples were spun down and reacted with the respective azido reporter molecules for multiplexed MS. To each sample 40 µl of reaction mixture (see: Table 7) containing either the azido reporter C175-73, -75, -76 or -77 was added. All samples were sonicated for 5 minutes followed by incubation at 40ºC for 16 hours in a heat block.

Table 7: Compositions of buffers used for extraction and click reaction of alkyne labeled lipids for MS.

Name	Composition
Extraction Mixture For MS	For 36 samples: - 14.7 ml MeOH (LC-MS grade) - 2.94 ml $CHCl_3$ - 360 µl internal standard mixture for alkyne labeled lipids in $CHCl_3$/MeOH (1:1) containing 118 pmol TAG [48.3], 16.7 pmol DAG [32:2], 29 pmol CE [18:2], 8.4 pmol Cer [18:2],14 pmol PA [34:4],125 pmol PC [34:3], and 22.5 pmol double labeled TAG [51:5] per 10 µl
Click Reaction Mixture	- 10 µl 100 mM C175-73,-75,-76,-77 in 50 % MeOH - 100 µl 10 mM Cu(I)-TFB in acetonitrile - in 900 µl 100 % EtOH
Spray Buffer	- 16 ml isopropanol (LC-MS grade) - 10 ml MeOH (LC-MS grade) - 1720 µl H_2O (LC-MS grade) - 280 µl 1 M ammonium acetate in water

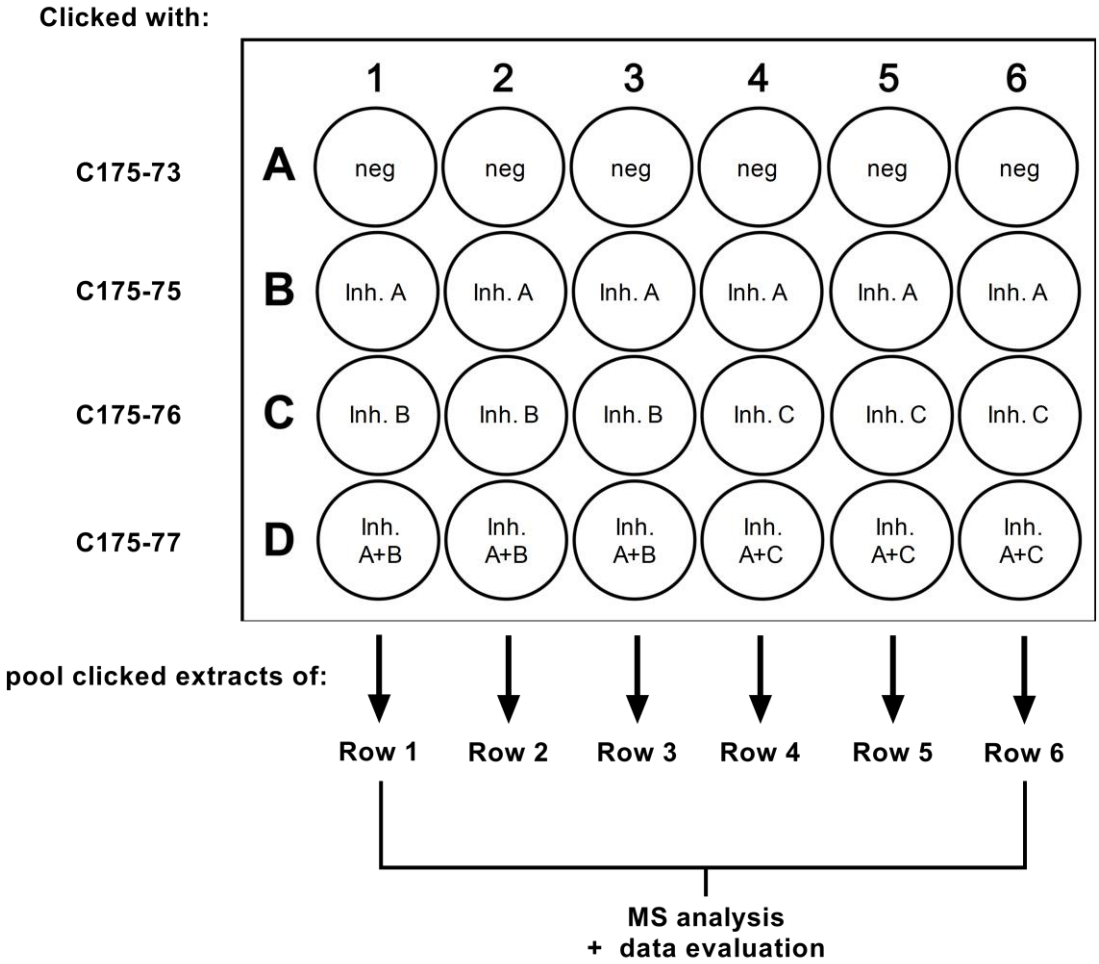

Figure 9: Schematic visualization of the experimental design, used in the pulse and pulse-chase experiments with alkyne labeled lipids, to analyze the effect of DGAT-inhibitors, Etomoxir and Teglicar on the incorporation of MCFA into hepatic TAGs, by multiplexed lipid MS in a 24 well setup. All experiments were done in triplicate determinations comprising a control group (neg, lane A) and three treatments consisting of different inhibitors and their combinations (Inh. A-C, lane B-D). After lipid extraction, samples from each lane were clicked to a different C175-XX azido reporter group. Samples from every row were then pooled, resulting in only 6 from the originally 24 samples. Finally, the pooled samples were analyzed by MS (see: Chapter 4.5.2.).

After incubation, 100 µl of $CHCl_3$ was added to each sample and the samples for multiplexing were pooled, as depicted in Figure 9. To the pooled samples 600 µl of LC-MS grade H_2O was added, the mixture briefly shaken for 30 seconds and centrifuged at 2 x 10^4 g for two minutes. This re-extraction step was done in order to reduce the copper ion concentration in the samples to a minimum, since the samples were sprayed directly into the mass spectrometer without any further HPLC method. The upper phase was removed, and the lower phase was evaporated at 45ºC for 20 min in a vacuum centrifuge. Each sample was redissolved in 800 µl spray buffer (see: Table 7), sonicated for five minutes and lipids were then analyzed by MS.

4.5. Detection methods for alkyne labeled Lipids

4.5.1. Detection of clicked alkyne labeled lipids by TLC

TLC is a separation method to analyze compositions of diverse sample mixtures. Separation is achieved on a stationary phase (in this case a silica gel) on which the analytes are separated due to their polarity differences in a solvent mixture as a mobile phase (Fuchs et al., 2011).

After the click reaction as described in chapter 4.4.1, the reaction tubes were centrifuged to collect the evaporated solvents condensed under the lid. The samples were then vortexed for 10 min. Meanwhile a TLC plate was prepared as follows: a line was drawn 2 cm from the bottom of the plate and spaces for lipid loading were marked. After the plate was prepared, the samples were centrifuged one again and the samples were loaded on the TLC plate using glass capillaries. The plate was then placed in a developing chamber, saturated with a solvent (Solvent Mixture I, see: Table 8) developed to separate polar and medium polar lipids (for example phospholipids). The plate was kept in the chamber for about 20 minutes until the front line reached a height of 10 cm measured from the line were the lipids were loaded.

The plate was then taken out, dried and placed in a second developing chamber saturated with a solvent (Solvent Mixture II, see: Table 8) developed to separate apolar lipids such as triacylglycerol or cholesteryl esters. In this step the plate was kept in the chamber until the solvent front line reached the near top of the plate. Finally, the plate was taken out, dried, soaked in 4 % Hünig's base solution (see: Table 8) and dried again.

Click labeled alkyne lipids were then detected using a laboratory intern system described in (Thiele et al., 2012). The fluorescent reporter clicked to the lipids was excited using a 420 nm LED lamp with a glass emission filter. Images were acquired with an EMCCD camera system equipped with a 494/20 (coumarin fluorescence signal) and 528/28 (noise signal) bandpass emission filter set. In each channel eight images were acquired with exposure times between 20 milliseconds and 5 seconds. For samples with a very low fluorescence signal, images form the 528-filter channel were subtracted from the 494-filter channel for background correction. Images were acquired and final quantification was done using the GelPro analyzer software. Fluorescence signals were saved as integrated optical density (IOD) values for further analyzation in any spreadsheet software. TAG signals were normalized by setting the sum of both TAG bands in the negative control, originating from either C11 or C19/C17:2 fatty acids, as 1. Changes upon inhibitor treatment were then calculated in for each TAG in relation to the negative control.

Table 8: Composition of solvents used for TLC development.

Name	Composition
Solvent Mixture I	- 65 (v/v) $CHCl_3$ - 25 (v/v) MeOH - 4 (v/v) H_2O - 1 (v/v) acetic acid (glacial)
Solvent Mixture II	- 1 (v/v) isohexane - 1 (v/v) ethyl acetate
Hünig's Base Solution	- 4 % (v/v) *N*,*N*-Diisopropylethylamine in isohexane

4.5.2. Multiplexed MS of reporter-labeled alkyne lipids

The following procedure is also published in: (Thiele et al., 2019).

The mass spectra were recorded on a Thermo Scientific Q Exactive Plus Hybrid quadrupole-orbitrap mass spectrometer. The device is equipped with an atmospheric pressure ion (API) source (Bruins, 1994), which is operating in the high-voltage electrospray ionization (HESI) modus (Banerjee and Mazumdar, 2012). The sample was directly injected using a gastight Hamiltion syringe operated by a syringe pump under the control of the Tune instrument software. The syringe port was connected directly to the HESI source with no additional connection tubings in order to minimize dead volume. The samples were sprayed at a flow rate of 10 µl/min in spray buffer (see: Table 7). The following parameters were used: sheath gas 4, aux gas 2, sweep gas 0, gas heating off, spray voltage positive mode 4.0 kV, ion transfer capillary temperature 280 ºC. Since the lipids clicked with the C175-XX reporter molecules result only in positive ions, the mass acquisition was done in positive ion mode. For all samples form cellular extracts, MS1 spectra were recorded in segmented overview scans with ranging mass to charge rations (m/z) from 300-1400 in 100 m/z windows for 1.2 minutes. This was followed by MS/MS (MS2) scans by data independent acquisition (DIA) (Alcoriza-Balaguer et al., 2019) for 16.8 minutes, using inclusion lists from m/z 305.373-1400.119 in intervals with m/z 1.0006 to reflect the typical mass defect of lipids at the respective masses. Scan parameters were as followed: for MS1: automatic gain control (AGC) target 3 x 10^6, maximum ion time 800 ms, resolution 280000, peak mode centroid, for MS2: automatic gain control (AGC) target 2 x 10^5, maximum ion time 700 ms, resolution 140000, no spectral multiplexing, dynamic first mass, isolation window m/z 1.0, stepped normalized collision energy (NCE) 10, 30, 35, spectrum data type centroid. In addition, a second scan for double charged species was performed in the scan range of m/z 300 - 700 with MS2 scans from m/z 300.8052 - 700.0648 at intervals of m/z 0.5002 and an isolation window of m/z 0.7. To identify the labeled lipids, the generated .raw files were first converted to .mzml files using the MSconvert program. Files were then analyzed using the program LipidXplorer (Herzog et al., 2011). For identification and quantification of labeled lipids,

molecular fragment query language (MFQL) scripts were written that identify the species by the presence of a peak corresponding to the expected masses of the labeled lipid class combined with the characteristic neutral loss. All MFQL scripts for the respective lipid classes can be found in the supplementary data (see: Supplements 10.5.). The .mzml files were first imported into LipidXplorer, then the associated MFQL scripts for the lipid classes to be analyzed were chosen and the program could be executed. As a data output a .csv file was written, which could be further analyzed by any spreadsheed software.

4.6. Live cell oxygen consumption rate (OCR) measurements

In order to measure the oxygen consumption in primary hepatocytes to investigate the influence of different small molecule inhibitors on the mitochondrial β-oxidation rate and cellular oxygen consumption in general, the Seahorse XF Analyzer (Agilent Technologies) in a 96 well format, was used. The assay was done as an adaption of the protocol for the Seahorse XF Flux Kit in a 96 well format. One day prior to the assay, the sensor cartridge was humidified in water at 37ºC in a non- carbonated incubator.

On the day of the assay, primary hepatocytes were isolated as described in chapter 4.2.2. Then 1000-2000 cells were plated in each well of a collagen coated (see: Chapter 4.2.1.) 96-well cell culture microplate for Seahorse XF Analyzer applications in 200 µl adhesion medium (see: Table 3). The cells were allowed to adhere for two hours, then the medium was changed by carefully adding 200 µl prewarmed assay medium (see: Table 9), then removing the same volume and repeating this step for three times. Finally, 40 µl was removed from each well, resulting in a final volume of 160 µl per plate. To avoid cooling, the plate was kept on a heater plate at 37ºC during this procedure. The plate was then placed in a non-carbonated incubator at 37ºC for at least one hour prior to the assay. During that time the injection ports of the sensor cartridge were loaded with inhibitor solutions in assay medium, as indicated in Table 9. As a negative control the respective vehicle was diluted in assay medium. The sensor cartridge was then incubated in Seahorse XF Assay calibrant (see: Table 9) and as well incubated at 37ºC in a non-carbonated incubator for at least one hour. Finally, the sensor cartridge was placed in the Seahorse XF Analyzer for instrument calibration. When calibration of the sensor cartridge was done, the experiment was started by placing the cell culture plate in the analyzer. The experimental setup was as followed: first baseline OCR measurement for 30 minutes, then injection of the inhibitor solutions, followed by 45 minutes of OCR measurements. The measurement cycles were set to measure every 5 minutes.

After the experiment was done, the data was exported from the instrument software (Wave 2.4) as an .xlsx file which could be further analyzed by any spreadsheet data.

Table 9: Composition of solvents used for Seahorse XF Analyzer experiments.

Name	Composition/ Catalogue Number
Seahorse XF Analyzer Calibrant	Cat. No.: 100840-000
Seahorse XF Analyzer Assay Medium	Agilent Seahorse XF RPMI Medium (Cat. No.: 103576-100) supplemented with: 10 % FCS (v/v) 1 % (v/v) penicillin/streptomycin solution 1 % (v/v) 200 mM L-glutamine solution
Inhibitor Solutions	As 10x concentrates in Seahorse XF Analyzer Assay Medium for following final assay concentrations: - 50 µM Etomoxir in ddH_2O - 50 µM Teglicar in DMSO - 3 µM A922500 (D1) in DMSO

4.7. Statistical analysis and data evaluation

If not otherwise stated, the data is presented as mean values ± standard deviation (SD). Within one biological replica, all values were raised from triplicate determinations. For all experimental sets at least 3 biological replicas were performed. Raw data analysis was executed using Microsoft Excel and final statistical analysis was done using the GraphPad software (Prism 6 or 7). For comparison of two groups an unpaired t-test was used. For comparisons of more than two groups within one experimental data set, an ordinary one-way ANOVA with Dunnetts's multiple comparison test (comparison of the mean values from the treatment group with the mean values from the control group (neg)) was applied. When multiple comparisons were done within two or more experimental data sets, an ordinary two-way ANOVA with Sidak's multiple comparison test (comparison of the mean values from the treatment group with the mean from the control group (neg) within one experimental data set) was applied. * stands for $p \leq 0.0332$, ** for $p \leq 0.0021$, *** for $p \leq 0.0002$, **** for $p \leq 0.0001$ and ns stands for not significant. All lipid signals from MS analysis were quantified by internal standardization with the standards shown in chapter 3.8. Absolute amounts are shown in pmol. Relative amounts (mol per mille) of each lipid class were calculated by multiplication of the pmol value from the respective lipid class times 1000, followed by dividing this value through the value of total labeled lipids (from aCE, aCer, aDAG, aPC, aPA and aTAG (in pmol)) within that sample. These values were used to calculate the "fold change concentration", which shows overall changes of the respective lipid class under experimental conditions in comparison to the negative control within one biological replica. To take advantage of the information provided by species resolution in our mass spectrometric methodology, changes from lipid species (namely TAG) upon treatment conditions within one lipid class were analyzed. However, a large variation of relative abundances form lipid species within its class and the change of total class abundance, often hinders a systematic evaluation of a lipid species spectra. To overcome that problem, the data from the aTAG species (in pmol), was first divided by the corresponding aTAG species from the respective negative control to obtain fold changes (FC). This normalizes for the relative abundance within the class. Individual FC values were then averaged to obtain the average FC of the lipid class. Next, individual FC were divided by the class average FC to obtain normalized FC values. These NFC arrays indicate the change of the species spectrum under experimental conditions of a class, independent of the changes in total abundance of the class and independent of the relative abundance of the species within the class.

5. Results

In the following, the hypothesis by Klizatie (Klizaite, 2017), regarding the MCFA preference of DGAT2 was tested by monitoring the C11-FA and C19-FA metabolism in hepatocytes under the influence of specific small molecule inhibitors against DGAT1 and DGAT2.

5.1. Analysis of C11-FA and C19-FA incorporation into TAGs upon DGAT inhibition

Freshly isolated hepatocytes were first preincubated with either 3 µM DGAT1 inhibitor (A922500 (D1)), 15 µM DGAT2 inhibitor (JNJ-DGAT2-A (D2)) or a combination of both inhibitors. As a negative control the cells were incubated with only the vehicle (in this case DMSO). After preincubation, cells were pulsed with 100 µM of either C11- or C19- alkyne fatty acid. The incorporation of both alkyne fatty acids into TAG was monitored through capturing the fluorescent signal of azido-coumarin reacted to the alkyne labeled lipids on a TLC plate. Changes under inhibitory conditions were quantified in comparison to the negative control.

These experiments revealed two main results. First, the incorporation of C11-FAs into TAG was far more reduced than of C19-FAs. The presence of both inhibitors resulted in a near total reduction of C11-TAG (Figure 10: A, C, in lanes/ filled red/blue bars labeled: D1/D2), whereas C19-TAGs were only slightly, but still significantly reduced (Figure 10: B, C, in lanes/ hatched red/blue bars labeled: D1/D2). Second, C11-FA incorporation into TAGs was already significantly reduced by about a half, when only the DGAT1 inhibitor was present (Figure 10: A, C, C11 TAG in lanes/ filled red bars labeled: D1). In contrary to our initial hypothesis, these results already indicated that not DGAT2, but DGAT1 might play a more important role in hepatic MCFA metabolism. A slight accumulation of 1,3 C19-DAG-, C19-PE- and C19-PC- bands were visible, when both inhibitors are present (Figure 10, B, lanes labeled D1/D2, data not quantified). On the opposite, these effects were not visible for the C11 fatty acid. Here, an inhibition of DGAT activity, resulted not only in a reduction of labeled TAG, but also in total reduction of alkyne labeled lipids (Figure 10, A, lanes labeled D1 and D1/D2, data not quantified).

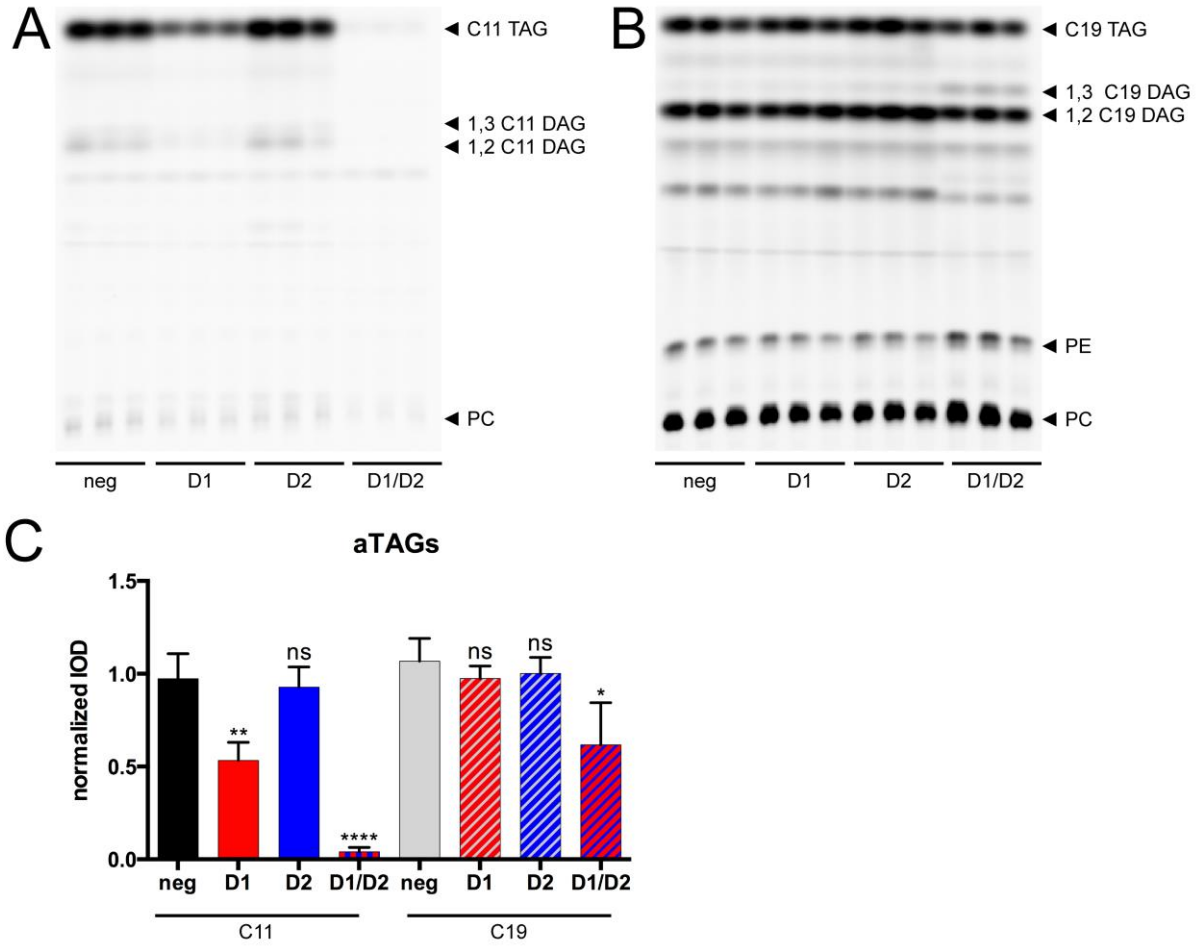

Figure 10: Analysis of aTAGs upon DGAT inhibition in primary hepatocytes, pulsed with either C11- or C19-fatty acids. After isolation, primary mouse liver hepatocytes were plated in 24 well plates with 7.5x10^4 cells per well. Cells were preincubated with either 3 µM DGAT1-Inhibitor (D1), 15 µM DGAT2-Inhibitor (D2) or a combination of both inhibitors (D1/D2) for 1 hour, in comparison to the respective vehicle as a negative control. Cells were then pulsed for 1 hour with either 100 µM C11- (A) or C19- (B) fatty acid. The cells were washed, lipids were extracted and click reaction for TLC was performed. Finally, lipids were separated on a TLC plate and the signal was captured by fluorescent imaging (panel A and B). Panel C illustrates the normalized quantification of fluorescent intensities from C11-TAG (filled bars) and C19-TAG (grey hatched bars) upon either D1- (red), D2- (blue) and a combination of both (blue/red) inhibitors, in comparison to the negative control (black: C11, grey: C19). The data represent mean ±SD for n=3 biological replicates. * stands for p≤0.0332, ** for p≤0.0021 and **** for p≤0.0001. Ns=not significant.

For further validation of these findings, 50 µM of C11- and C19- alkyne fatty acids were pulsed simultaneously under the same inhibitory conditions. As already shown by Klizaite (Klizaite, 2017), two groups of TAG species are formed, each originating from either C11- or C19 fatty acids. Conveniently, these can be detected as two distinct bands on the TLC plate (Figure 11, A, bands marked C19-TAG, C11-TAG). Under native conditions, both alkyne lipids got almost equally introduced into TAG, with a slightly higher concentration of C11-TAG (not significant (Figure 11, A: lanes marked as neg, B: black and grey bars, labeled as neg). Upon DGAT inhibition, C11 fatty acid metabolism, showed nearly the same phenotype in TAG concentrations, as when pulsed alone. When DGAT1 was inhibited, C11-TAG was significantly reduced by half, whereas a combination of both DGAT1- and DGAT2-inhibitors

resulted in a near total reduction of C11-TAG (Figure 11, A: lanes labeled D1 and D1/D2 (C11-TAG), B: filed bars C11 (D1 (red), D1/D2 (red/blue)).

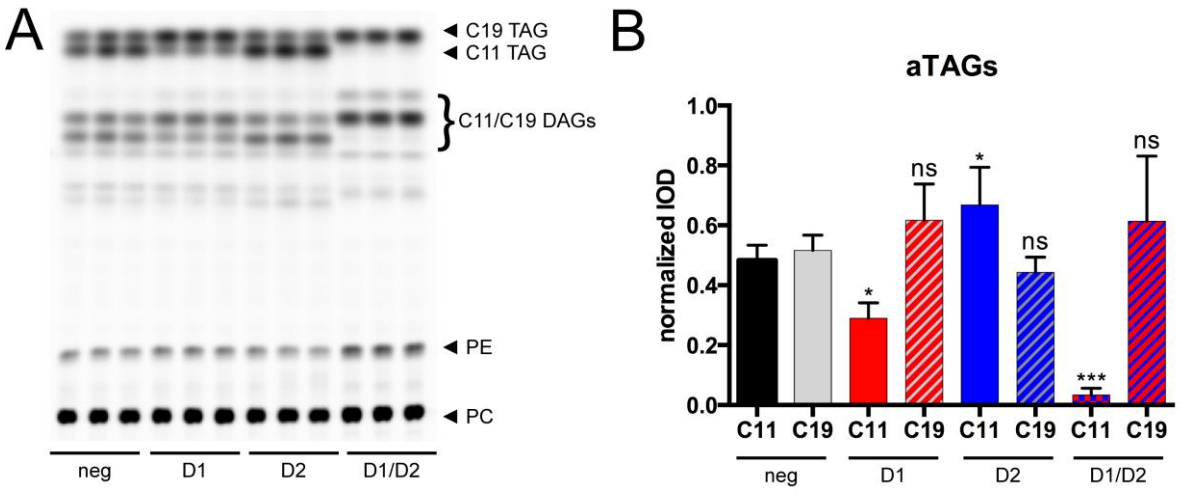

Figure 11: Analysis of aTAGs upon DGAT inhibition in primary hepatocytes, co-pulsed with C11- and C19-fatty acids. After isolation, primary mouse liver hepatocytes were plated in 24 well plates with $7.5x10^4$ cells per well. Cells were preincubated with either 3 µM DGAT1-Inhibitor (D1), 15 µM DGAT2-Inhibitor (D2) or a combination of both inhibitors (D1/D2) for 1 hour, in comparison to the respective vehicle as a negative control. Cells were then pulsed for 1 hour with a combination of 50 µM C11- and 50 µM C19-fatty acid. The cells were washed, lipids were extracted and click reaction for TLC was performed. Finally, lipids were separated on a TLC plate and the signal was captured by fluorescent imaging (A). Panel B illustrates the normalized quantification of fluorescent intensities from C11-TAG (filled bars) and C19-TAG (grey hatched bars) upon either D1 (red), D2 (blue) and a combination of both (blue/red) inhibitors, in comparison to the negative controls (black: C11, grey: C19). The data represent mean ±SD for n=3 biological replicates. * stands for p≤0.0332, ** for p≤0.0021 and *** for p≤0.0002. ns=not significant.

Upon DGAT2 inhibition the concentration of C11-TAG was slightly elevated in comparison to the negative control (Figure 11, B: filled blue bars labeled D2). The concentration of C19-TAG did not change significantly throughout all conditions (Figure 11, A: bands labeled C19-TAG, B: hatched bars labeled C19). Yet, an antiparallel effect on C11-TAG and C19-TAG levels was observable: Upon DGAT1 inhibition, C11-TAG was reduced, and C19-TAG was slightly (but not significantly) elevated and upon DGAT2 inhibition this effect was reversed. However, these changes were only significant for C11-TAG but not for C19-TAG. When both inhibitors were present, there was also an accumulation of DAG species observable (data not quantified). These should mainly consist of species labeled with C19-fatty acids, as the accumulating bands are those running higher on the plate due to their more hydrophobic nature (Figure 11, A: bands labeled as C11/C19 DAG). Since both alkyne fatty acids are metabolized in parallel, forming DAG species labeled with either one of the alkyne fatty acids, which could not be resolved via this TLC-detection method.

This was true for all other lipid species (except TAG in this case), thus making a specific quantification in this detection system unrealizable. However, the analysis of the two TAG classes and their response to the DGAT inhibitor treatment, indicated a metabolic

discrimination in between DGAT enzymes and their favored fatty acid substrates in terms of fatty acid chain length.

5.2. Etomoxir and a DGAT1-Inhibitor show similar effects on C11-TAG levels

Taking advantage to simultaneously trace the incorporation of C11- and C19-fatty acids into TAG via TLC analysis, this experimental setup was used next, to analyze the findings by Klizaite (Klizaite, 2017) regarding Etomoxir in greater detail.

Freshly isolated hepatocytes were treated with either 50 µM Etomoxir (Eto), 3 µM A922500 (D1) or a combination of both inhibitors for one hour and then co-pulsed with C11- and C19-fatty acid for one hour, and the TAG levels were analyzed as described before.

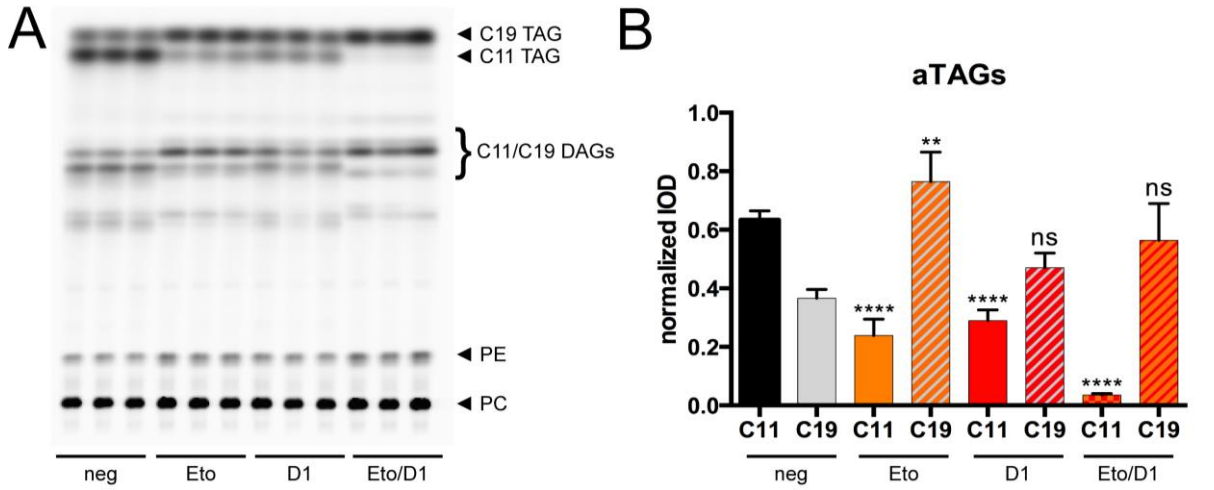

Figure 12: Analysis of aTAGs upon DGAT1 inhibitor-, and Etomoxir-treatment in primary hepatocytes, co-pulsed with C11- and C19-fatty acids. After isolation, primary mouse liver hepatocytes were plated in 24 well plates with $7.5x10^4$ cells per well. Cells were preincubated with either 3 µM DGAT1-Inhibitor (D1), 50 µM Etomoxir (Eto) or a combination of both inhibitors (D1/Eto) for one hour, in comparison to the respective vehicle as a negative control. Cells were then pulsed for 1 hour with a combination of 50 µM C11- and 50 µM C19-fatty acid. The cells were washed, lipids were extracted and click reaction for TLC was performed. Finally, lipids were separated on a TLC plate and the signal was captured by fluorescent imaging (A). Panel B illustrates the normalized quantification of fluorescent intensities from C11-TAG (filled bars) and C19-TAG (grey hatched bars) upon either D1 (red), Etomoxir (orange) and a combination of both (orange/red) inhibitors, in comparison to the negative controls (black: C11, grey: C19). The data represent mean ±SD for n=3 biological replicates. ** stands for p≤0.0021 and **** for p≤0.0001. ns=not significant.

As in the studies by Klizatie (Klizaite, 2017), the treatment with Etomoxir led to decreased C11-TAG levels, whereas the C19-TAG levels were signficantly elevated (Figure 12: A: bands named C19 TAG/C11-TAG in the lane labeled Eto, B: filled/hatched orange bars, labeled Eto). As shown before, treatment with the D1-inhibitor led to the same reduction of C11-TAG, with no altered levels of C19-TAG (Figure 12: A, lane D1, B: filled/hatched red bars). A combinaton of Etomoxir with the DGAT1-inhibitor led to the same phenotype as the combination of both DGAT-inhibitors. Here C11-TAG levels were strongly reduced, whereas

C19-TAG levels were slightly elevated (Figure 12: A, lane Eto/D1, B: filled/hatched orange/red bars). Triggered by these findings, similar pulse experiments were caried out, where Etomoxir was combined with the DGAT2-inhibitor.

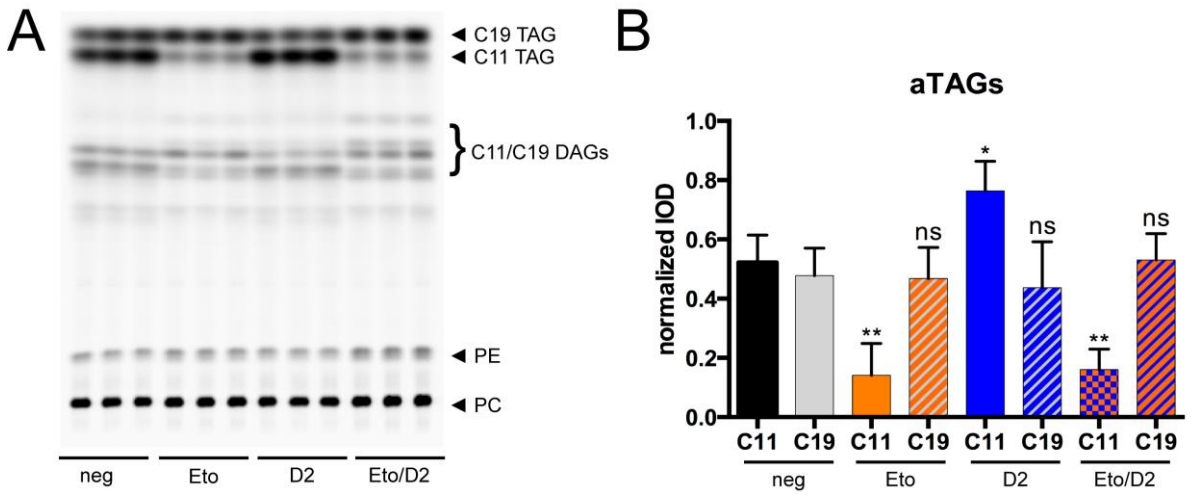

Figure 13: Analysis of aTAGs upon DGAT2 inhibitor-, and Etomoxir-treatment in primary hepatocytes, co-pulsed with C11- and C19-fatty acids. After isolation, primary mouse liver hepatocytes were plated in 24 well plates with $7.5x10^4$ cells per well. Cells were preincubated with either 15 µM DGAT2-Inhibitor (D2), 50 µM Etomoxir (Eto) or a combination of both inhibitors (D2/Eto) for one hour, in comparison to the respective vehicle as a negative control. Cells were then pulsed for 1 hour with a combination of 50 µM C11- and 50 µM C19-fatty acid. The cells were washed, lipids were extracted and click reaction for TLC was performed. Finally, lipids were separated on a TLC plate and the signal was captured by fluorescent imaging (A). Panel B illustrates the normalized quantification of fluorescent intensities from C11-TAG (filled bars) and C19-TAG (grey hatched bars) upon either D2 (blue), Etomoxir (orange) and a combination of both (orange/blue) inhibitors, in comparison to the negative controls (black: C11, grey: C19). The data represent mean ±SD for n=3 biological replicates. * stands for p≤0.0332 and ** for p≤0.0021. ns=not significant.

In this experimental setup, hepatocytes were preincubated with 50 µM Etomoxir, 15 µM JNJ-DGAT2-A (D2) or a combination of both inhibitors, followed by a co-pulse of C11- and C19-fatty acids.

Surprisingly, a combination of Etomoxir with the DGAT2-inhibitor did not lead to a complete reduction of C11-TAG (Figure 13, A: lanes labeled Eto/D2). Here the reduction was only as prominent as with Etomoxir alone (Fig 13, B: filled orange and orange/blue bars (Eto, Eto/D2)). However, the combination of both inhibitors led to a slightly stronger accumulation of DAG species, like in the experiments where both DGAT inhibitors were combined (Figure 13, A: lanes Eto/D2 C11/C19 DAGs (data not quantified)).

In order to verify the effects of the DGAT inhibitors and Etomoxir on TAG levels in hepatocytes, the experiments were repeated with a different set of DGAT inhibitors used in a study by Li and colleagues (Li et al., 2015).

Here, similar results could be observed, confirming these effects due to a DGAT1/2 specific inhibition. For more information on this matter, see Supplementary chapter 10.1.

Alkyne palmitate (C17:2) is another alkyne fatty acid, which is regularly used for lipid-tracing experiments in our group.

Since both C19- and C17:2-alkyne fatty acids have a different profile of lipid-classes and species in which they are incorporated (Thiele et al., 2012), it appeared reasonable to repeat the previously described experiments with a co-pulse of C11 and C17:2 under the same inhibitory conditions. In the following section, the results from these assays are illustrated.

First, freshly isolated hepatocytes were preincubated with a either Etomoxir, A922500 (D1) or a combination of both and afterwards co-pulsed with either 50 µM of C11 and C17:2.

As previously described (Thiele et al., 2012), hepatocytes incorporate more alkyne palmitate into PC and less into TAG, whereas alkyne oleate was preferably incorporated into TAG.

Likewise, this effect was visible in under these experimental conditions. In comparison to the C11/C19 pulse experiments, where C11- and C19-fatty acids were equally incorporated into TAG, C17:2 fatty acid was incorporated into TAG at only a quarter in comparison to C11-TAG levels under control conditions (Figure 14, A: lanes labeled as neg, B: black (C11) and grey (C17:2) bars).

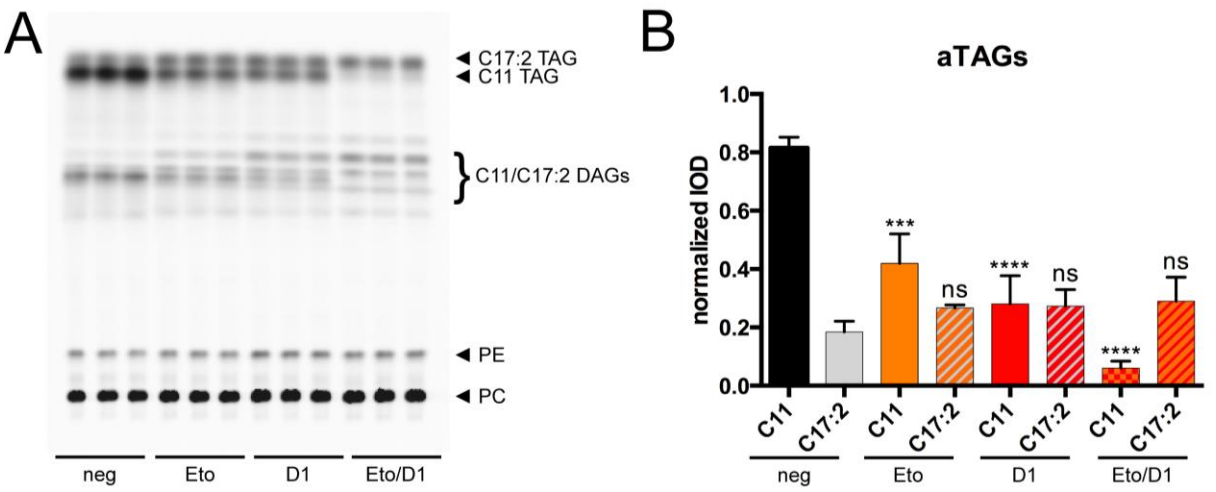

Figure 14: Analysis of aTAGs upon DGAT1 inhibitor-, and Etomoxir-treatment in primary hepatocytes, co-pulsed with C11- and C17:2-fatty acids. After isolation, primary mouse liver hepatocytes were plated in 24 well plates with $7.5x10^4$ cells per well. Cells were preincubated with either 3 µM DGAT1-Inhibitor (D1), 50 µM Etomoxir (Eto) or a combination of both inhibitors (D1/Eto) for one hour, in comparison to the respective vehicle as a negative control. Cells were then pulsed for 1 hour with a combination of 50 µM C11- and 50 µM C17:2-fatty acid. The cells were washed, lipids were extracted and click reaction for TLC was performed. Finally, lipids were separated on a TLC plate and the signal was captured by fluorescent imaging (A). Panel B illustrates the normalized quantification of fluorescent intensities from C11-TAG (filled bars) and C17:2-TAG (grey hatched bars) upon either D1 (red), Etomoxir (orange) and a combination of both (orange/red) inhibitors, in comparison to the negative controls (black: C11, grey: C17:2). The data represent mean ±SD for n=3 biological replicates. *** stands for p≤0.0002 and **** for p≤0.0001. ns=not significant.

The effects of Etomoxir and A922500 regarding C11-TAG levels, in relation to C17:2-TAG levels, however, were similar to those in C11/C19 co-pulse experiments. Here, C11-TAG levels showed the same response upon inhibitor treatment, whereas C17:2-TAG levels did not change significantly throughout all conditions (Figure 14, A: lanes labeled Eto, D1, Eto/D1, B: C11: filled bars, C17:2 hatched bars).

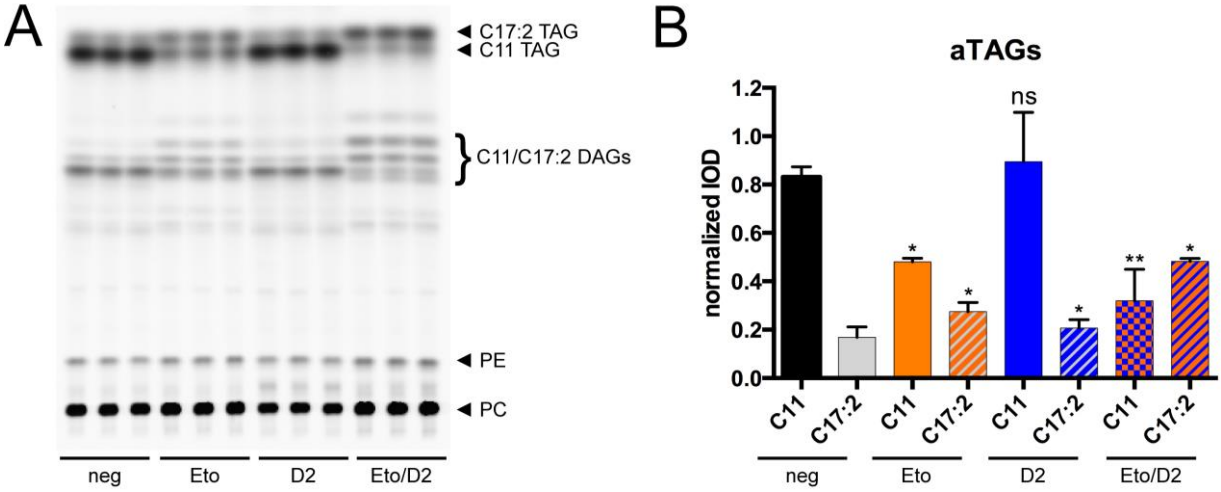

Figure 15: Analysis of aTAGs upon DGAT2 inhibitor-, and Etomoxir-treatment in primary hepatocytes, co-pulsed with C11- and C17:2-fatty acids. After isolation, primary mouse liver hepatocytes were plated in 24 well plates with $7.5x10^4$ cells per well. Cells were preincubated with either 15 µM DGAT2-Inhibitor (D2), 50 µM Etomoxir (Eto) or a combination of both inhibitors (D2/Eto) for one hour, in comparison to the respective vehicle as a negative control. Cells were then pulsed for 1 hour with a combination of 50 µM C11- and 50 µM C17:2-fatty acid. The cells were washed, lipids were extracted and click reaction for TLC was performed. Finally, lipids were separated on a TLC plate and the signal was captured by fluorescent imaging (A). Panel B illustrates the normalized quantification of fluorescent intensities from C11-TAG (filled bars) and C17:2-TAG (grey hatched bars) upon either D2 (blue), Etomoxir (orange) and combination of both (orange/blue) inhibitors, in comparison to the negative controls (black: C11, grey: C17:2). The data represent mean ±SD for n=3 biological replicates. * stands for p≤0.0332 and ** for p≤0.0021. ns=not significant.

Upon combination of Etomoxir with the D2 inhibitor JNJ-DGAT2-A, C17:2-TAG levels responded differently to the treatment with the D2 inhibitor in contrast to C19-TAG levels in the C11/C19 experiments. C17:2-TAG was significantly reduced when the D2 inhibitor was present, whereas in combination of both inhibitors, C17:2-TAG levels were significantly elevated (Figure 15, A: lanes labeled D2, Eto/D2, B: hatched bars labeled D2, Eto/D2).

Yet, C11-TAG levels were significantly reduced upon treatment with Etomoxir (Figure 15, B: filled bars). Because all inhibitors were added before the hepatocytes were treated with the fatty acids, in order to ensure an equal distribution within all cells another control experiment was done. Here, Etomoxir was co-pulsed with C11-fatty acid directly. Under these conditions, there were no significant reduction of C11-TAG levels visible (Figure 16).Since the active inhibitory form of Etomoxir is its CoA-ester, to which it needs to be converted first (Kiorpes et al., 1984), it seems likely that the effect is due to either a competition between C11-CoA and

the CoA-form of Etomoxir or an unspecific off-target effect. This matter, however, will be analyzed later in greater detail, using MS-based detection technology.

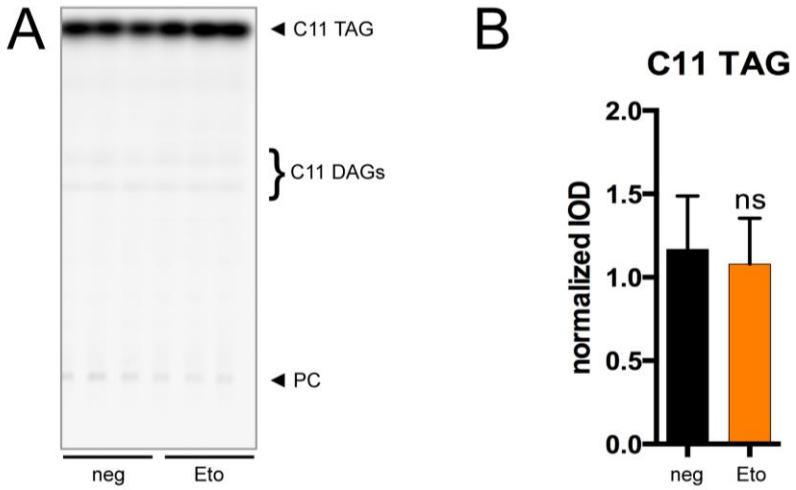

Figure 16: Analysis of C11-TAG in primary hepatocytes simultaneously co-pulsed with C11-fatty acid and Etomoxir. After isolation, primary mouse liver hepatocytes were plated in 24 well plates with $7.5x10^4$ cells per well. Cells were co-pulsed with 50 µM Etomoxir (Eto) and 100 µM C11-fatty acid for 1 hour. As a negative control only the C11-fatty acid was pulsed. The cells were washed, lipids were extracted and click reaction for TLC was performed. Finally, lipids were separated on a TLC plate and the signal was captured by fluorescent imaging (panel A). Panel B illustrates the normalized quantification of fluorescent intensities from C11 TAG upon Etomoxir treatment (orange bar), in comparison to the negative control (black bar). The data represent mean ±SD for n=3 biological replicates. ns=not significant.

Taken together, the results from the TLC experiments suggest that, in contrary to the hypothesis by Klitzaite (Klizaite, 2017), DGAT1 and not DGAT2 is the main enzyme responsible for the introduction of MCFA into TAG. The effects on the MCFA-TAG level upon Etomoxir treatment did resemble those caused by DGAT1 inhibition, and a combination of both inhibitors even led to a mutually increased effect, which might hint towards a direct interaction of Etomoxir with the DGAT enzymes, especially DGAT1.

However, these findings were restricted due to the TLC-based detection methodology to trace alkyne labeled lipids (see: Chapter 1.3), giving only lipid class resolution. Another limitation is the temporal resolution, only allowing an interpretation of the metabolic state after one hour of a continuous pulse of alkyne fatty acids. All the effects described above are due to an inhibition of DGAT enzymes via its respective small molecule inhibitors. Free fatty acids are introduced into DAG, followed by their DGAT-dependent conversion into TAG in a matter of minutes, due to the fast hepatic metabolism (Stein and Stein, 1967). Therefore, it would be interesting to conduct a pulse-chase experiment with a short pulse of an alkyne fatty acid, followed by several short chase time-points with an unlabeled MCFA. Here, one could directly monitor the DGAT-dependent introduction of the unlabeled MCFA into the labeled DAG pool. Given our newly established methodology for MS alkyne lipid tracing

(Thiele et al., 2019), it became possible to overcome both limitations mentioned above and conducting the detailed analysis of DGAT1-dependent MCFA metabolism.

5.3. DGAT1 acts as the main enzyme for MCFA incorporation into TAG

The results in this chapter investigate the role of DGAT1 in hepatic MCFA metabolism in more detail, with a focus on the role of Etomoxir as a possible DGAT inhibitor.

5.3.1. Pulse-chase experiments upon DGAT1 inhibition

In order to study the DGAT-dependent introduction of MCFA into TAG under the influence of either a DGAT1 inhibitor or Etomoxir, a pulse-chase experiment was conducted, followed by MS analysis of the alkyne labeled lipids.

Freshly isolated hepatocytes were first preincubated with either 3 µM A922500 (D1), 50 µM Etomoxir or a combination of both inhibitors. Then the cells were pulsed for 2 minutes with 100 µM alkyne-palmitate (C17:2) in order to generate a pool of alkyne labeled lipids via the glycerophospholipid-pathway. As already shown by our group, a 2-minute pulse time of the given concentration of the alkyne fatty acid, does not saturate the hepatic metabolism with the FA. Under this conditions the concentration of early onset metabolites such as PA and DAG is still high, while the endpoint metabolites like TAG and PC continue rising (Piotrowitz, 2016).

The cells were chased for several short time points (0, 1, 2, 5, 10 minutes) with 100 µM of the native MCFA decanoic acid (C10). The lipids were then extracted, clicked and analyzed according to the protocol for multiplexed MS analysis of alkyne labeled lipids described in the chapters 4.4.2 and 4.5.2.

First, the four lipid classes aTAG, aDAG, aPC, aPA were analyzed and are presented in Figure 17 as relative amounts in mol per mille, based on absolute amounts of aTAG, aDAG, aPA, aPC, aCE and aCer through internal standardization (see: Chapter 3.8. and 4.7.).

In accordance with the TLC-based pulse-chase data published by Piotrowitz (Piotrowitz, 2016) in our group, a fast introduction of alkyne lipids into aDAG, followed by the rise of labeled aTAG and aPC throughout the chase, could be measured (Figure 17, panels A-C (aTAG, aDAG, aPC) black lines labeled: neg). Also, the fast decline of labeled PA species within the short chase period agrees with this data (Figure 17, panel D (aPA), black line labeled: neg). These results from the negative controls provide evidence for the technical accuracy of the experiment.

Comparing the data from the negative controls with the respective values from the cells treated with the inhibitors, a major impact of both inhibitors on aTAG and aDAG levels could be observed. In line with the data acquired from the TLC-based pulse-experiments, both inhibitors significantly reduced the synthesis of aTAG species, decreasing even further when both inhibitors were combined (Figure 17, panel A, lines labeled Eto, D1 and Eto+D1).

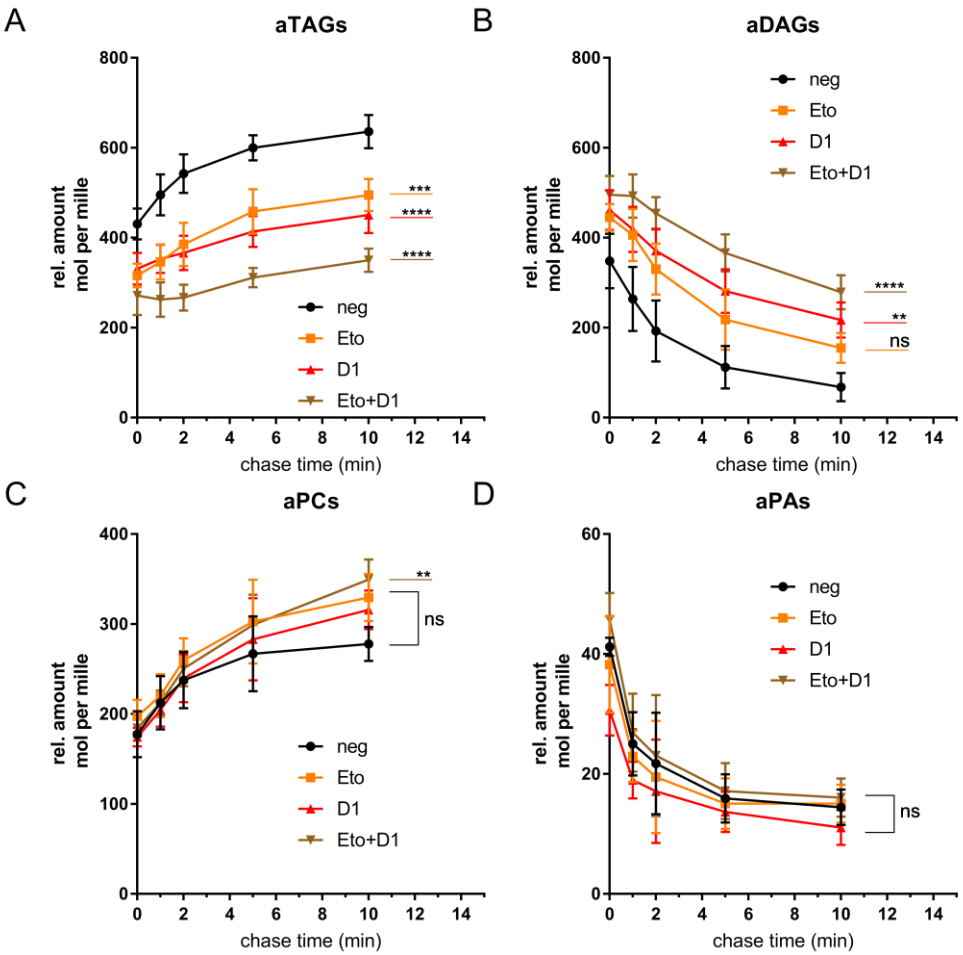

Figure 17: Relative amounts (mol per mille) of alkyne-labeled TAG (A), DAG (B), PC (C) and PA (D) species based on pmol from aTAG, aDAG, aPC, aPA, aCE and aCER, from primary hepatocytes, isolated from WT mice, treated with different inhibitor combinations, pulsed with alkyne-palmitate and chased with decanoic acid. After isolation, primary mouse liver hepatocytes were plated in 24 well plates with $7.5x10^4$ cells per well. Cells were preincubated with either 50 µM Etomoxir (Eto), 3 µM DGAT1-Inhibitor (D1) or a combination of both inhibitors (Eto+D1). Cells were then pulsed with 100 µM alkyne palmitate (C17:2) for 2 minutes and chased with 100 µM decanoic acid (C10) for either 0, 1, 2, 5 or 10 minutes in the presence of the respective inhibitor. Lipids were extracted with simultaneous addition of an internal standard mix for alkyne labeled lipids and click reaction with C175-XX reagents was performed. Multiplex samples were pooled and analyzed by MS. Mass signals were identified using LipidXplorer MFQL analysis with internal standard quantification for aTAG, aDAG, aPC, aPA, aCE and aCER. Relative concentrations are based on pmol from the internal standard quantifications and were calculated as described. The data represent mean ±SD for n=3 biological replicates. ** stands for p≤0.0021, *** for p≤0.0002 and **** for p≤0.0001. ns=not significant. Statistical significances are only indicated for the last timepoint (chase time 10 min).

Respectively, an accumulation of aDAG species could be observed (Figure 17, panel B). Etomoxir treatment did not lead to a significant increase in aDAG species, however there was an apparent tendency toward aDAG accumulation. The treatment with the DGAT1 inhibitor (D1) did lead to a visibe aDAG accumulation throughout every chase timepoint. This effect was even stronger when Etomoxir was combined with the DGAT1 inhibitor. Overall, aTAG species were decreased around 1.5 times upon treatment with A922500 and Etomoxir, respectively. When both inhibitors were combined aTAG levels decreased at about the half. aDAG levels corresponded with merley similar accumulation dynamics, as the aTAG decreased. No significant changes in aPA levels and only a significanct rise in aPC levels was observable when both inhibitors were present (Figure 17, panels C and D).

However, this data is shows basically the same changes in overall lipid levels in respond to the inhibitor treatment, as already obverved on the TLC experiments.

Since the MS-based detection method allows species resolution within all classes, one can directly analyze the DGAT-dependent introduction of C10 into aTAG. This effect should be clearly observable, since decanoic acid should not be present in the cells in detectable levels before adding the chase medium. LCFA-aTAG- and MCFA-aTAG levles should also correspond differently to the respective inhibitory treatments.

Indeed, when one observes the absolute amount (in pmol) of the most abundant alkyne labeled LCFA-TAG species, namely TAG [51:4], [51:3], [53:5] and [53:4], there was a strong reduction visible, solely in the presence of both inhibitors (Figure 18, panel B, brown line (Eto+D1). Treatment of either D1 or Etomoxir alone did not lead to a strong reduction of these species (Figure 18, panel B, orange line (Eto), red line (D1)).

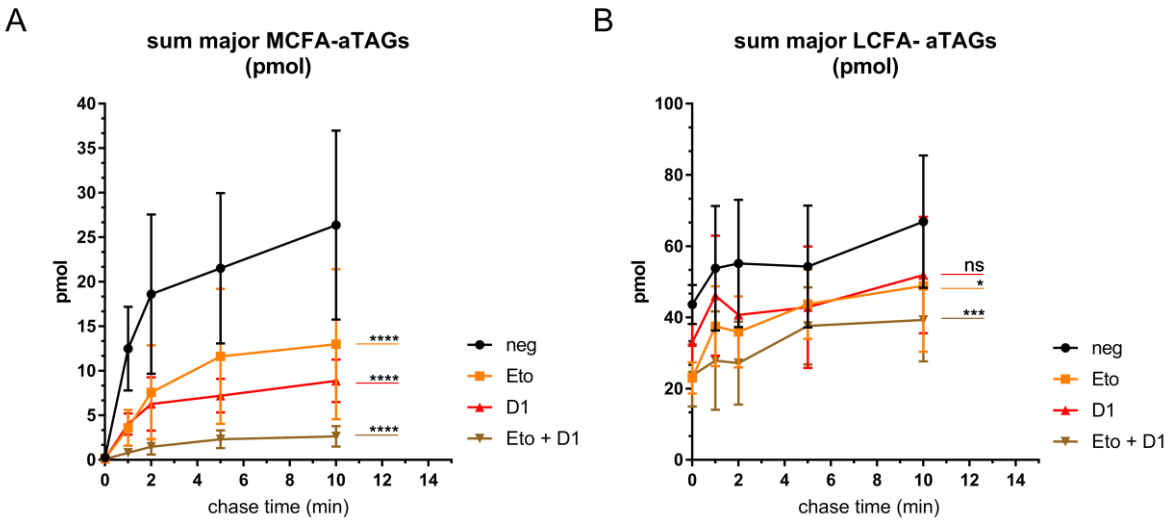

Figure 18: Absolute amounts of aTAG species isolated from WT mice, treated with different inhibitor combinations, pulsed with alkyne-palmitate and chased with decanoic acid. After isolation, primary mouse liver hepatocytes were plated in 24 well plates with $7.5x10^4$ cells per well. Cells were preincubated with either 50 µM Etomoxir (Eto), 3 µM DGAT1-Inhibitor (D1) or a combination of both inhibitors (Eto+D1). Cells were then pulsed with 100 µM alkyne palmitate (C17:2) for 2 minutes and chased with 100 µM decanoic acid (C10) for either 0, 1, 2, 5 or 10 minutes in the presence of the respective inhibitor. Lipids were extracted with simultaneous addition of an internal standard mix for alkyne labeled lipids and click reaction with C175-XX reagents was performed. Multiplex samples were pooled and analyzed by MS. Mass signals were identified using LipidXplorer MFQL analysis with internal standard quantification for aTAG, aDAG, aPC, aPA, aCE and aCER. Absolute amounts of the lipid species within the lipid classes of MCFA-aTAGs (A) (Σ of [43:3], [43:2], [45:4], [45:3]) and LCFA-aTAGs (B) (Σ of [51:4], [51:3], [53:5], [53:4]) are shown in pmol. The data represent mean ±SD for n=3 biological replicates. * stands for p≤0.0332, *** for p≤0.0002 and **** for p≤0.0001. ns=not significant.

When one observes the absolute amounts summed up from the four most abundant MCFA-aTAG species, namely TAG [43:3], [43:2], [45:4] and [45:3], the chase effect with the decanoic acid and the impact of both inhibitors becomes clearly observable.

These aTAG species increased during the chase period from no detectable value at 0 min chase up to 25 pmol (mean value) after 10 minutes chase (Figure 18, panel A, black line labeled neg). This dataset illustrates the direct DGAT-dependent introduction of the MCFA decanoic acid into a labeled DAG pool.

The treatment with the DGAT1 inhibitor and Etomoxir, both led to a significant decrease in the MCFA-aTAG levels, decreasing even further when both inhibitors were present (Figure 18, panel A, orange- (Eto), red- (D1) and brown line (Eto+D1)). With one of both inhibitors present, the analyzed MCFA-aTAG levels only reached about 10-15 pmol (mean values) after 10 minutes chase. With a combined Etomoxir- and A922500-treatment, MCFA-aTAG levels reached only 3 pmol (mean value) after a 10 min chase. For better visualization, both the aTAG and the corresponding aDAG species upon each inhibitor treatment are co-illustrated (Figure 19).

The analyzed aTAG species correspond to the four major aDAG species namely, [33:3], [33:2], [35:4] and [35:3] (Figure 19, panels A-D, dashed lines) to which decanoic acid (+10 more c-atoms) was introduced through the postulated DGAT1 activity, resulting in the four TAG species named above (Figure 19, panels A-D, solid lines). Panel E of figure 19 is a schematic illustration on the postulated DGAT1 activity, which is inhibited by either A922500 or Etomoxir.

After 2 minutes pulse time with alkyne palmitate, 18 aDAG species could be detected. However, the four aDAG species mentioned above, did comprise about 80 percent of the total amount of labeled DAG in the negative control groups (Supplementary figure 3). Therefore, the main corresponding aTAG species in which decanoic acid was incorporated, naturally originate from these four aDAG species.

Since the inhibition of DGAT1 does not only lead to the specific decrease of decanoic acid incorporation into aTAG, but also to a decreased incorporation of all fatty acids that belong to the spectrum of DGAT1, the accumulation effect of aDAG species should be observable in accordance to the data shown in figure 17. Indeed, the inhibition of MCFA-aTAG synthesis was paralleled by the accumulation of corresponding aDAG species (Figure 19, panels A-D, dashed lines).

Taken together this data illustrates not only the direct effect of reduced MCFA-incorporation upon DGAT1 inhibition, but also the systemic effect of DGAT1 inhibition on fatty acid incorporation into aTAG during the dynamics of a fatty acid pulse-chase experiment.

Furthermore, this data shows that treatment with Etomoxir does lead to decreased aTAG synthesis, similar to the specific inhibition of DGAT1 through the well characterized DGAT1 inhibitor A922500 (Qi et al., 2012). This dataset supports the hypothesis on the effects in reduced MCFA-TAG levels through Etomoxir, to be due to a DGAT1 inhibition as a possible off-target effect of Etomoxir, in contrary to the previously mentioned hypothesis by Klizaite (Klizaite, 2017).

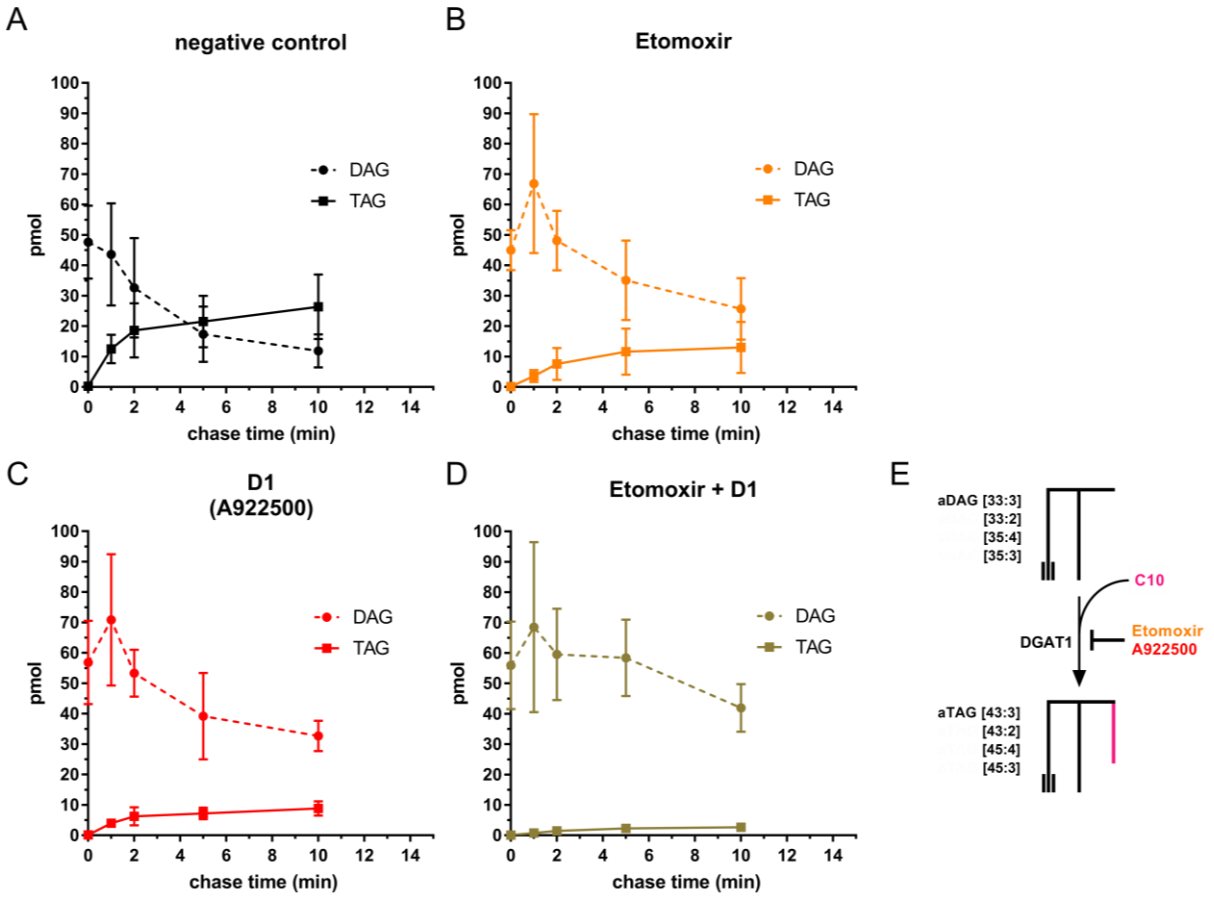

Figure 19: DGAT1-dependent incorporation of decanoic acid into aDAG species in hepatocytes, isolated from WT mice, treated with different inhibitor combinations, pulsed with alkyne-palmitate and chased with decanoic acid. After isolation, primary mouse liver hepatocytes were plated in 24 well plates with 7.5x10^4 cells per well. Cells were preincubated with either 50 µM Etomoxir (Eto), 3 µM DGAT1-Inhibitor (D1) or a combination of both inhibitors (Eto+D1). Cells were then pulsed with 100 µM alkyne palmitate (C17:2) for 2 minutes and chased with 100 µM decanoic acid (C10) for either 0, 1, 2, 5 or 10 minutes in the presence of the respective inhibitor. Lipids were extracted with simultaneous addition of an internal standard mix for alkyne labeled lipids and click reaction with C175-XX reagents was performed. Multiplex samples were pooled and analyzed by MS. Mass signals were identified using LipidXplorer MFQL analysis with internal standard quantification for aTAG, aDAG, aPC, aPA, aCE and aCER. Absolute amounts of the lipid species within the lipid classes of TAG (Σ of [43:3], [43:2], [45:4], [45:3]) and DAG (Σ of [33:3], [33:2], [35:4], [35:3]) are shown in pmol. Panels A-D show the direct incorporation of decanoic acid (C10) into the main DAG species (dashed lines) resulting in the respective TAG species (solid lines) over time, in the presence of Etomoxir (B), D1-Inhibitor (C), a combination of both Inhibitors (D) or the negative control (A). Panel E is a schematic visualization of this process. Note that in this scheme, the possible stereochemistry (sn1/sn3 or sn2) of DGAT1-dependent incorporation of the FFA is not considered. The data represent mean ±SD for n=3 biological replicates.

5.3.2. Analysis of the lipid profile in hepatocytes isolated form DGAT1$^{-/-}$ mice upon treatment with DGAT-specific inhibitors and Etomoxir

Through a cooperation with the group of Prof. Dr. Dagmar Kratky at the Medical University of Graz, Austria, it became possible to analyze the effects of Etomoxir and the DGAT inhibitors in hepatocytes isolated from DGAT1$^{-/-}$ mice (Smith et al., 2000). All experiments presented in this chapter (5.3.2.) are the result of this collaboration.

These experiments should firstly serve as a control for the effects seen the on hepatic aTAG metabolism upon DGAT inhibitor treatment. Second, in direct comparison to the respective WT hepatocytes, the hepatic DGAT1$^{-/-}$ lipid metabolism should give deeper insights into the putative role of DGAT1 in MCFA metabolism. And thirdly, the previously described off-target-effect of Etomoxir could be analyzed in greater detail.

In this collaborative project, pulse experiments, like in the TLC experiments described in chapter 5.1 and 5.2, were conducted.

All necessary consumables such as tissue culture plates and media were prepared at our lab, snap frozen and send to the Medical University of Graz on dry ice. There, the hepatocytes were isolated, treated with inhibitors and pulsed with alkyne fatty acids according to the protocol described in chapter 4.3.1. These procedures were handled by Christina Leopold (PhD) a postdoc in the lab of Prof. Dr. Dagmar Kratky. The cells were then directly frozen on the culture plates and shipped on dry ice back to our lab, were the lipid extraction followed by either MS- or TLC-analysis was done. In the figure legends of each data set in which the isolation and the pulse of the fatty acids were performed by Christina Leopold (CL) and the subsequent lipid extraction and MS analysis was done by Klaus Wunderling (KW), the respective part from each researcher will be stated as: Isolation of hepatocytes and fatty acid pulse was done by CL, lipid extraction and MS/TLC analysis were done by KW. For all experiments intended for MS analysis, hepatocytes were preincubated with different combinations of either DGAT inhibitors (3 µM A922500 (D1), 15 µM JNJ-DGAT2-A (D2)) or 50 µM Etomoxir and pulsed afterwards with a combination of 50 µM alkyne palmitate (C17:2) and 50 µM decanoic acid (C10). For the TLC experiments cells were preincubated with the inhibitors as described above and afterwards pulsed with a combination of 50 µM alkyne oleate (C19) and 50 µM alkyne decanoic acid (C11).

First, the lipid profile of DGAT1$^{-/-}$ hepatocytes under native conditions from the negative controls was analyzed in comparison to WT hepatocytes.

In the four major alkyne labeled lipid classes which were analyzed, only aPC was significantly elevated in DGAT1$^{-/-}$ hepatocytes (Figure 20, panels A,B,D (aTAG, aDAG, aPA) and panel C (aPC), bar graph labeled ΔDGAT1, values are displayed as absolute amounts in pmol).

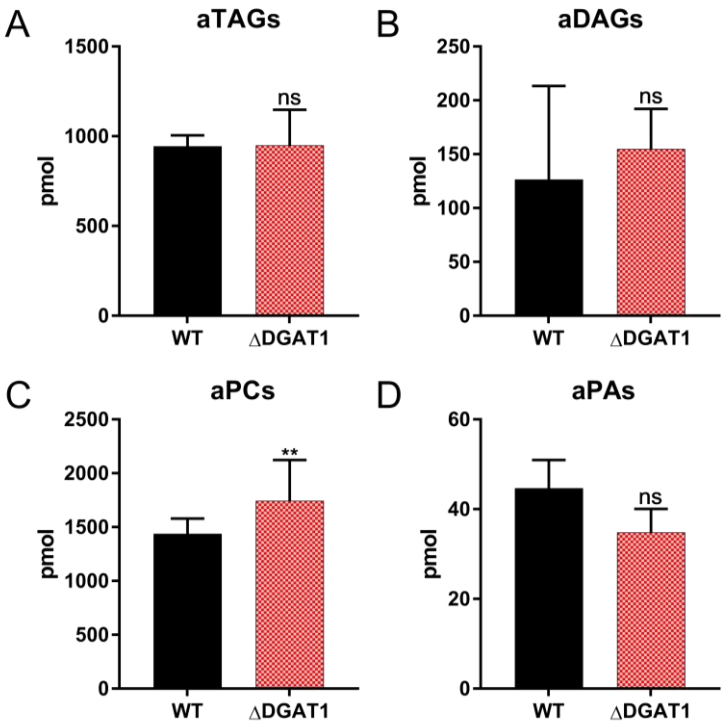

Figure 20: Absolute amounts of alkyne-labeled lipid classes from primary hepatocytes, isolated from wildtype mice (WT: black bars) or mice lacking DGAT1 (ΔDGAT1: red hatched bars), pulsed with alkyne-palmitate and decanoic acid. After isolation, primary mouse liver hepatocytes were plated in 24 well plates with 7.5x10^4 cells per well. Cells were co-pulsed with 50 µM alkyne palmitate (C17:2) and 50 µM decanoic acid (C10) for 1 hour. Lipids were extracted with simultaneous addition of an internal standard mix for alkyne labeled lipids and click reaction with C175-XX reagents was performed. Multiplex samples were pooled and analyzed by MS. Mass signals were identified using LipidXplorer MFQL analysis with internal standard quantification for aTAG, aDAG, aPC, aPA, aCE and aCER. Absolute amounts of the lipid classes aTAG (A), aDAG (B), aPC (C) and aPA (D) are shown in pmol. The data represent mean SD± for n=18 technical replicates in n=3 biological replicates. ** stands for p≤0.0021. ns=not significant. Isolation of hepatocytes and fatty acid pulse was done by CL, lipid extraction and MS/TLC analysis were done by KW.

However, the analysis of single species within the lipid classes, revealed some striking differences between DGAT1$^{-/-}$ and WT hepatocytes within the spectra of aTAG species (Figure 21, Heatmap array of mean values from white (0 pmol) to dark red (highest pmol value within each lipid class)).

Having nearly the same amount of labeled TAG, the DGAT1$^{-/-}$ hepatocytes had significantly lower amounts of shorter aTAG species compared to the WT hepatocytes (Figure 21, panel A, TAG [41:3] - [49:2]). This effect was compensated in these cells through the amount of aTAG species with longer acyl chains (Figure 21, panel A, TAG [51:7] - [57:5]). This outcome

was primarily visible within the main aTAG species in its carbon chain length class, namely TAG [43:3], [43:2], [45:4] and [45:3] representing the main MCFA-aTAG species and TAG [51:4], [51:3], [53:5] and [53:4] representing the major LCFA-aTAG species.

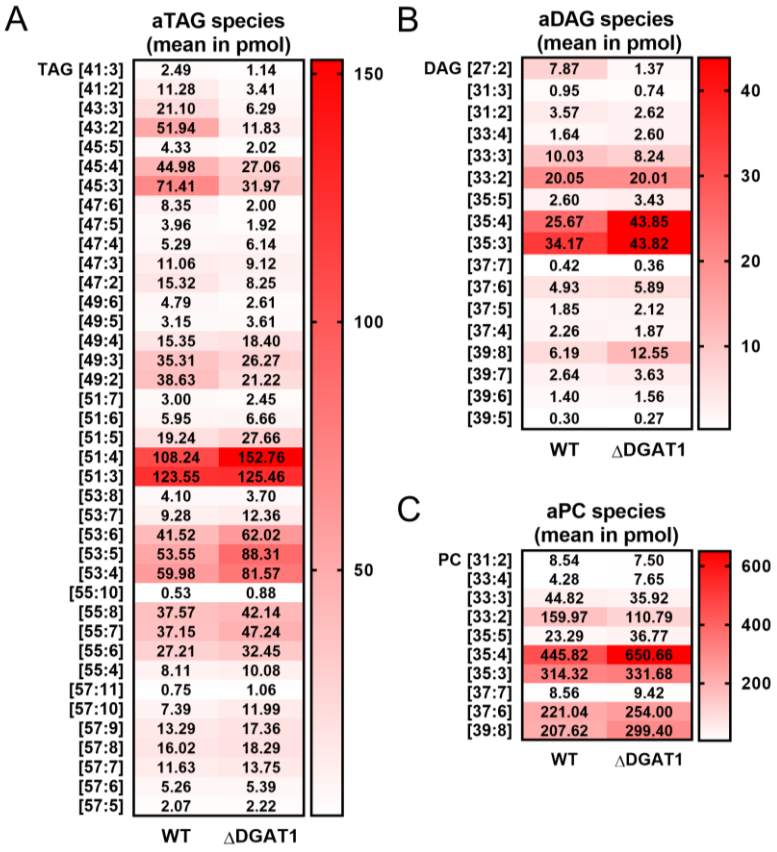

Figure 21: Absolute amounts of alkyne-labeled lipid species from primary hepatocytes, isolated from wildtype (WT) mice or mice lacking DGAT1 (ΔDGAT1), pulsed with alkyne-palmitate and decanoic acid. After isolation, primary mouse liver hepatocytes were plated in 24 well plates with $7.5x10^4$ cells per well. Cells were co-pulsed with 50 µM alkyne palmitate (C17:2) and 50 µM decanoic acid (C10) for 1 hour. Lipids were extracted with simultaneous addition of an internal standard mix for alkyne labeled lipids and click reaction with C175-XX reagents was performed. Multiplex samples were pooled and analyzed by MS. Mass signals were identified using LipidXplorer MFQL analysis with internal standard quantification for aTAG, aDAG, aPC, aPA, aCE and aCER. Absolute amounts of the lipid species within the lipid classes of aTAG (A), aDAG (B) and aPC (C) are shown in pmol. The data represent mean values for n=3 biological replicates. Isolation of hepatocytes and fatty acid pulse was done by CL, lipid extraction and MS/TLC analysis were done by KW.

On the side of the alkyne labeled DAG, only three species, namely DAG [35:4], [35:3] and [39:8] showed significantly higher concentrations in the $DGAT1^{-/-}$ hepatocytes, whereas all other species were either equally concentrated or slightly underrepresented (Figure 21, panel B (aDAG)). The overall significantly higher concentration of alkyne labeled PC in $DGAT1^{-/-}$ hepatocytes originated mainly from two species, namely PC [35:4] (over 200 pmol (mean value) more) and [39:8] (about 100 pmol (mean value) more) (Figure 21, panel C (aPC)).

On the side of the aTAG the effects in DGAT1$^{-/-}$ hepatocytes fit to those, observed in hepatocytes treated with a DGAT1 inhibitor, best seen in the effects described in the pulse experiments with C11- and C19-fatty acids upon D1 inhibitor treatment (Chapter 5.1, Figure 11). There, reverse effects, like those described in this experimental data, set could be observed.

Next, the influence of the treatment with DGAT inhibitors and Etomoxir within DGAT1$^{-/-}$ hepatocytes and the respective WT controls were investigated.

Overall effects on aTAG and aDAG levels in WT hepatocytes upon treatment of either DGAT1-, DGAT2-, or a combination of both inhibitors, were comparable to the results presented in chapter 5.1. These are summarized in Figure 22, visualized as fold changes upon inhibitory treatment, calculated from the relative concentrations (mol per mille) as described in chapter 4.7.

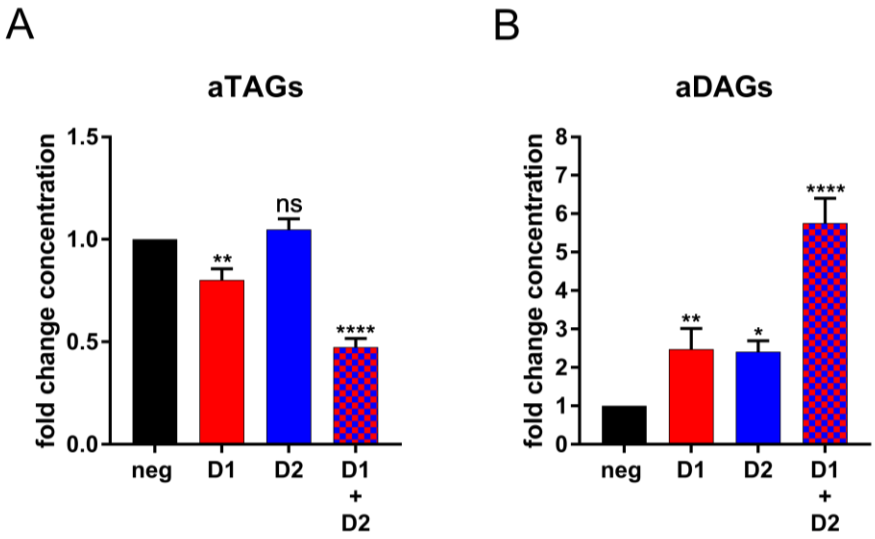

Figure 22: Fold change analysis of alkyne-labeled TAG (A) and DAG (B) based on relative amounts (mol per mile) from aTAG, aDAG, aPC, aPA, aCE and aCER, from primary hepatocytes, isolated from WT mice, treated with different inhibitor combinations, pulsed with alkyne-palmitate and decanoic acid. After isolation, primary mouse liver hepatocytes were plated in 24 well plates with 7.5x10^4 cells per well. Cells were preincubated with either 3 µM DGAT1-Inhibitor (D1), 15 µM DGAT2-Inhibitor (D2) or combinations of both inhibitors (D1+D2). Cells were then co-pulsed with 50 µM alkyne palmitate (C17:2) and 50 µM decanoic acid (C10) for 1 hour. Lipids were extracted with simultaneous addition of an internal standard mix for alkyne labeled lipids and click reaction with C175-XX reagents was performed. Multiplex samples were pooled and analyzed by MS. Mass signals were identified using LipidXplorer MFQL analysis with internal standard quantification for aTAG, aDAG, aPC, aPA, aCE and aCER. Fold changes (FC) in relative concentrations (from mol per mille) of each lipid species for each inhibitor treatment were calculated by normalization to the negative control. The data represent mean ±SD for n=3 biological replicates. * stands for p≤0.0332, ** for p≤0.0021 and **** for p≤0.0001. ns=not significant. Isolation of hepatocytes and fatty acid pulse was done by CL, lipid extraction and MS/TLC analysis were done by KW.

Upon treatment with D1 inhibitor alone, overall labeled TAG levels were significantly decreased and labeled DAG levels showed a signficant accumulation (Figure 22, panel A, B, red bar graphs (D1)). Treatment with D2 inhibitor alone did not show any significant changes in labebed TAG levels and a slight accumulation of labeled DAG species (Figure 22, panel A,

B, blue bar graphs (D2)). When both inhibitors were combined, overall aTAG levels decreased strongly (about a half reduced) and aDAG levels displayed increased fold changes of about 6 times (Figure 22, panel A, B, red/blue hatched bar graphs (D1+D2)). Following, the normalized fold changes (NFC) within every single aTAG species from the data set displayed in Figure 22 were analyzed. As described in chapter 4.7., this method enables the anaysis of changes from single lipid species within a class, independent of the changes in total abundance of the class itself and independent of the relative abundance of the species within the class.

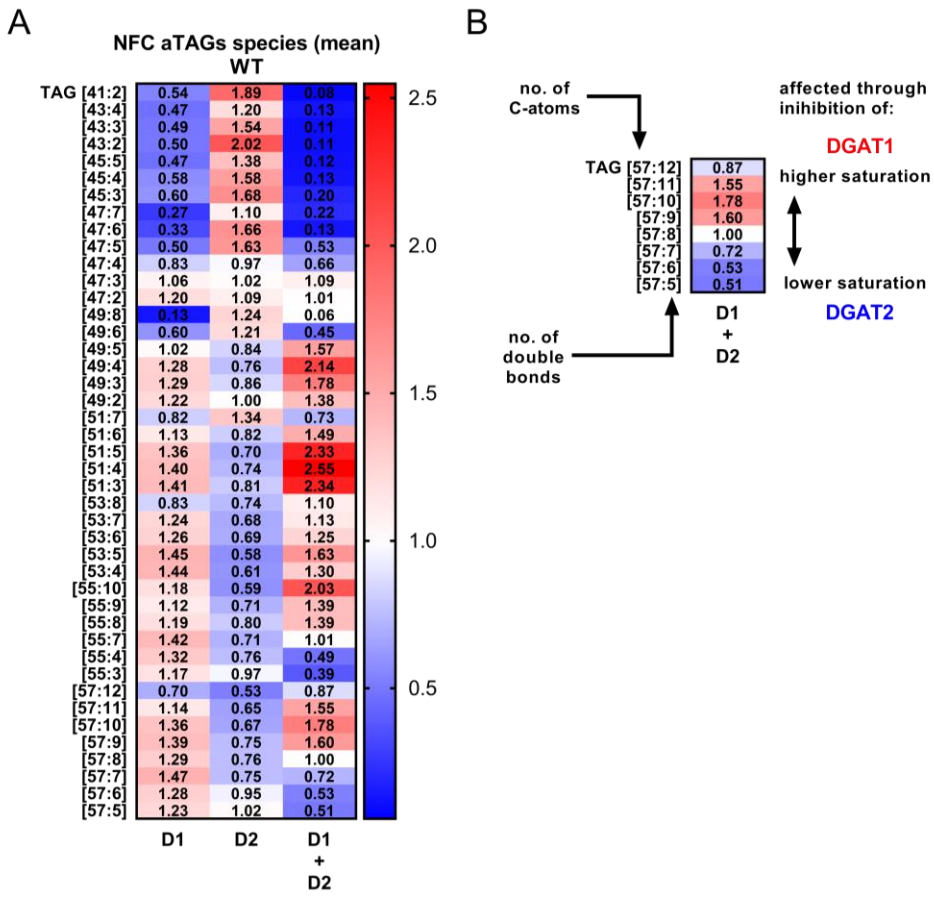

Figure 23: A: Detailed normalized fold change (NFC) analysis of alkyne-labeled TAG species from primary hepatocytes, isolated from WT mice, treated with inhibitor combinations and pulsed with alkyne-palmitate and decanoic acid. B: schematic representation of the fatty acid profile affected through either DGAT1 or DGAT2 inhibition. A: After isolation, primary mouse liver hepatocytes were plated in 24 well plates with $7.5x10^4$ cells per well. Cells were preincubated with either 3 µM DGAT1-Inhibitor (D1), 15 µM DGAT2-Inhibitor (D2) or a combination of both (D1+D2). Cells were then co-pulsed with 50 µM alkyne palmitate (C17:2) and 50 µM decanoic acid (C10) for 1 hour. Lipids were extracted with simultaneous addition of an internal standard mix for alkyne labeled lipids and click reaction with C175-XX reagents was performed. Multiplex samples were pooled and analyzed by MS. Mass signals were identified using LipidXplorer MFQL analysis with internal standard quantification for aTAG, aDAG, aPC, aPA, aCE and aCER. Normalized fold changes (NFC) in concentrations of each lipid species for each inhibitor treatment were calculated by normalization to the negative control and to the average class fold change. The data represent mean values for n=3 biological replicates. B: NFCs from TAGs with [57] c-atoms upon DGAT1 and DGAT2 inhibition with a schematic visualization of which fatty acids within one c-atom group are affected through either inhibition of DGAT1 or DGAT2. Isolation of hepatocytes and fatty acid pulse was done by CL, lipid extraction and MS/TLC analysis were done by KW.

While on the TLC plate MCFA- and LCFA-aTAGs were only represented through one band, here the change in the pattern can be visualized with 39 different aTAG species, which can be subdivided in the two groups responding to the inhibitor treatment. aTAG species ranging from 41 to 47 c-atoms can be classified as MCFA-aTAG, whereas all aTAG species with more than 47 c-atoms can be classified as LCFA-aTAG.

Changes upon treatment with D1, D2 and a combination of both inhibitors, can be displayed as a heatmap where a white-to-blue color pattern represents negative fold changes (decreased concentration in comparison to the negative control, all values below 1) and a white-to-red color pattern represents positive fold changes (increased concentration in comparison to the negative control, all values above 1). No change in the concentration of a species compared to the negative control is displayed as a 1 and is represented as a clear white color.

As well as in the TLC experiments, DGAT1 inhibition led to a decrease in the MCFA- aTAG species (Figure 23 A, lane labeled D1, TAG [41:2] - [47:4], displayed through a blue color pattern), while basically all other species had higher concentrations than the negative control, displayed through a red color pattern. An exception were five aTAG species, containing highly polyunsaturated fatty acids, namely TAG [49:6], [49:8], [51:7], [53:8] and [57:12]. These species were also downregulated, represented through a blue color pattern.

Upon DGAT2 inhibition, the aTAG species pattern showed opposite effects as upon DGAT1 inhibition. Here, MCFA-aTAG species (TAG 41-47) were upregulated, were all other aTAG with longer acyl chains were downregulated or had no change in their concentration (Figure 23 A, lane labeled D2). The species TAG [51:7] was as well an exception, as it was upregulated upon DGAT2 inhibition.

In line with the TLC-based pulse experiments, a combination of both inhibitors reduced the levels of MCFA-aTAGs even further (Figure 23 A, lane labeled D1+D2, TAG 41-47). Here, fold changes were always below 0.3, displaying a very strong downregulation of these species.

Fold changes of aTAGs with longer and polyunsaturated fatty acids however, revealed a complex pattern of up- or downregulated species. Figure 23 B gives a schematic visualization on the interpretation of changes within the LCFA species range due to either DGAT1- or DGAT2 inhibition.

For the range of aTAG 49-53, the NFC followed the pattern as upon DGAT1 inhibition alone, with even further up- or downregulation of the respective species. The species TAG [51:7], for example, was further downregulated and the three main species, namely TAG [51:5], [51:4] and [51:3], were the most upregulated with an NFC of 2,3-2,55. For aTAG species with 55 and more c-atoms, all species with lesser saturation in their group followed the pattern as

upon DGAT2 inhibition alone. With higher saturation within the acyl chains, the pattern changes towards the patters as observed upon DGAT1 inhibition alone.

In general, one could observe, that upon combination of both inhibitors the effects of the DGAT1 inhibitor were predominant over the changes upon DGAT2 inhibition, with a compensating effect on the main abundant species within the range of C49-C57.

This method of analysis as described in Figure 22 and 23 was now applied on experiments, in which hepatocytes, isolated form WT and DGAT1$^{-/-}$ mice, were treated with Etomoxir and the DGAT inhibitors in different combinations.

Overall effects on aTAG and aDAG levels of due to inhibitory treatment are displayed as fold changes from relative concentrations in Figure 24 (panel A (aTAG), panel B (aDAG)).

In WT hepatocytes, the treatment with Etomoxir showed the same reduction of labeled TAG and the associated increase of labeled DAG, as the treatment with the DGAT1 inhibitor (Figure 24, panel A (aTAG), B (aDAG), WT: lanes labeled Eto, D1).

A combination of Etomoxir with either one of the DGAT inhibitors decreased the amount of labeled TAG further, with a corresponding increase of aDAG levels (Figure 24, panels A (aTAG), B (aDAG), WT: lanes labeled Eto+D1, Eto+D2).

In DGAT1$^{-/-}$ hepatocytes, the treatment with Etomoxir only led to a minimal decrease in overall aTAG levels and no significant change in aDAG levels (Figure 24, panels A (aTAG), B (aDAG), ΔDGAT1: lanes labeled Eto). As expected, the treatment with DGAT1 inhibitor alone as well as the combination of the DGAT1 inhibitor with Etomoxir, had no significant effect (for D1 alone) or enhancing effects (for Eto+D1) on aTAG and aDAG levels in DGAT1$^{-/-}$ hepatocytes (Figure 24, panels A (aTAG), B (aDAG), ΔDGAT1: lanes labeled D1, Eto+D1). Treatment with the DGAT2 inhibitor alone, did lead to overall changes in aTAG and aDAG levels in DGAT1$^{-/-}$ hepatocytes (Figure 24, panels A (aTAG), B (aDAG), ΔDGAT1: lanes labeled D2), compared to those, where DGAT1 and 2 inhibitors were combined in WT hepatocytes (as previously described in Figure 22). The combination of Etomoxir with the DGAT2 inhibitor, did not further decrease aTAG levels or increase aDAG levels within the DGAT1$^{-/-}$ hepatocytes (Figure 24, panels A (aTAG), B (aDAG), ΔDGAT1, lanes labeled Eto+D2). Overall changes in levels of aPC and aPA upon inhibitor treatment were analyzed as well (Supplementary figure 9, panels A (aPC) and B (aPA)). aPA levels were significantly reduced upon either inhibitor treatment, both, in WT and DGAT1$^{-/-}$ hepatocytes. Overall aPC levels were significantly increased in WT cells only upon DGAT1 inhibition whereas in DGAT1$^{-/-}$ hepatocytes only upon DGAT2 inhibition.

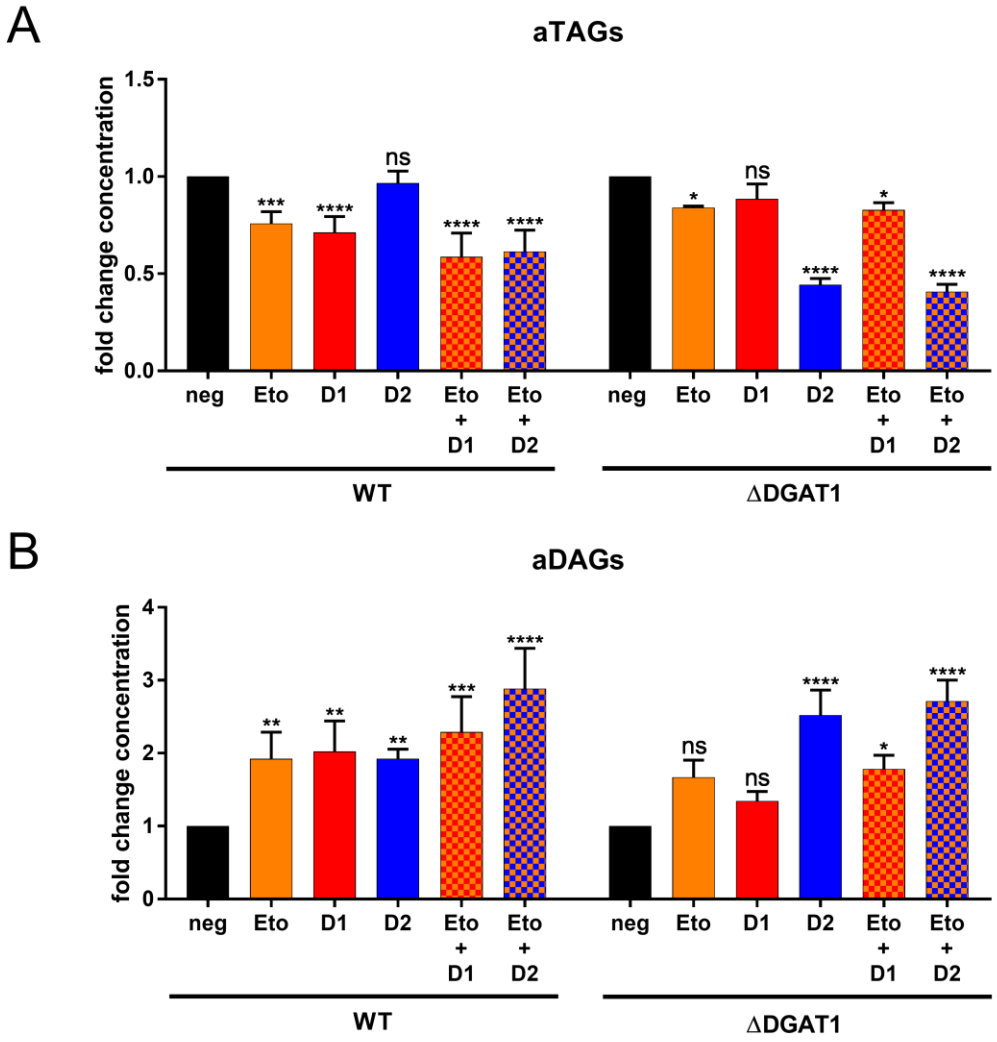

Figure 24: Fold change analysis of alkyne-labeled TAG (A) and DAG (B) based on relative amounts (mol per mile) from aTAG, aDAG, aPC, aPA, aCE and aCER, from primary hepatocytes, isolated from wildtype mice (WT) or mice lacking DGAT1 (ΔDGAT1), treated with different inhibitor combinations, pulsed with alkyne-palmitate and decanoic acid. After isolation, primary mouse liver hepatocytes were plated in 24 well plates with $7.5x10^4$ cells per well. Cells were preincubated with either 50 µM Etomoxir (Eto), 3 µM DGAT1-Inhibitor (D1), 15 µM DGAT2-Inhibitor (D2) or combinations of Etomoxir with each DGAT-inhibitor (Eto+D1, Eto+D2). Cells were then co-pulsed with 50 µM alkyne palmitate (C17:2) and 50 µM decanoic acid (C10) for 1 hour. Lipids were extracted with simultaneous addition of an internal standard mix for alkyne labeled lipids and click reaction with C175-XX reagents was performed. Multiplex samples were pooled and analyzed by MS. Mass signals were identified using LipidXplorer MFQL analysis with internal standard quantification for aTAG, aDAG, aPC, aPA, aCE and aCER. Fold changes (FC) in relative concentrations (from mol per mille) of alkyne TAGs and DAGs for each inhibitor treatment were calculated by normalization to the negative control. The data represent mean ±SD for n=3 biological replicates. * stands for p≤0.0332, ** for p≤0.0021, *** for p≤0.0002 and **** for p≤0.0001. ns=not significant. Isolation of hepatocytes and fatty acid pulse was done by CL, lipid extraction and MS/TLC analysis were done by KW.

Next, the normalized fold change array analysis was applied to the data derived from the data set described in Figure 24.

Strikingly, the NFC pattern from aTAG species in WT mice upon Etomoxir treatment, did resemble the pattern upon DGAT1 inhibition (Figure 25, panel A, lanes labeled Eto, D1).

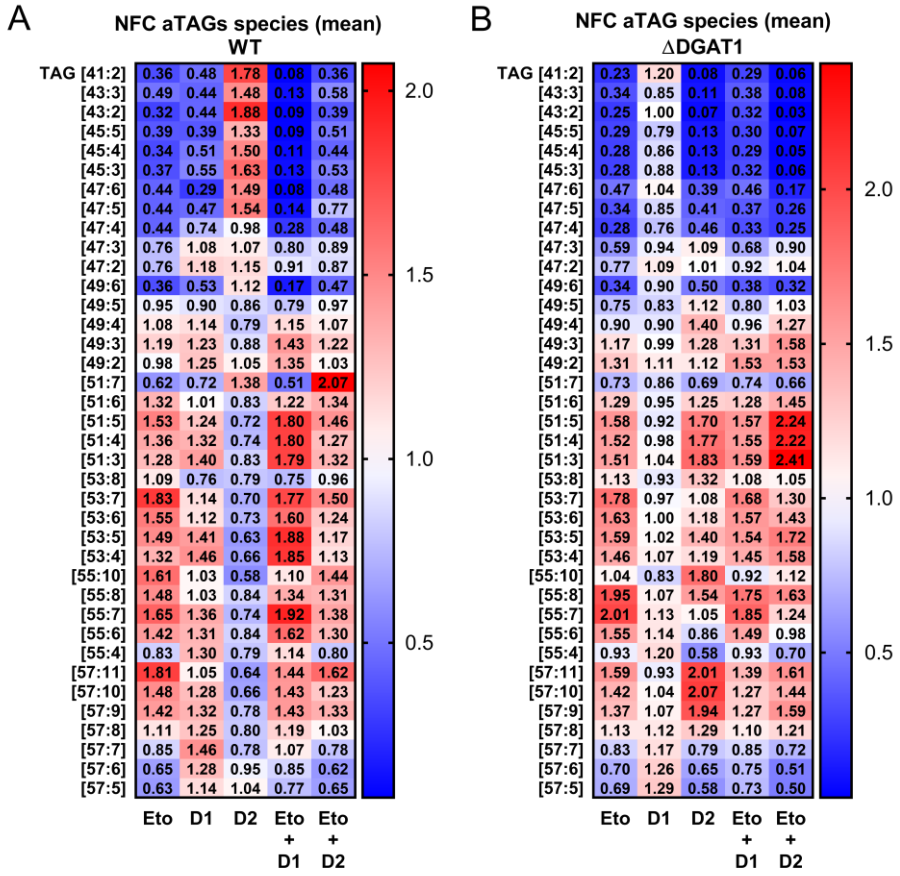

Figure 25: Detailed normalized fold change (NFC) analysis of alkyne-labeled TAG species from primary hepatocytes, isolated from wildtype mice (A: WT) or mice lacking DGAT1 (B: ΔDGAT1), treated with inhibitor combinations and pulsed with alkyne-palmitate and decanoic acid. After isolation, primary mouse liver hepatocytes were plated in 24 well plates with 7.5x10^4 cells per well. Cells were preincubated with either 50 µM Etomoxir (Eto), 3 µM DGAT1-Inhibitor (D1), 15 µM DGAT2-Inhibitor (D2) or combinations of Etomoxir with each DGAT-inhibitor (Eto+D1, Eto+D2). Cells were then co-pulsed with 50 µM alkyne palmitate (C17:2) and 50 µM decanoic acid (C10) for 1 hour. Lipids were extracted with simultaneous addition of an internal standard mix for alkyne labeled lipids and click reaction with C175-XX reagents was performed. Multiplex samples were pooled and analyzed by MS. Mass signals were identified using LipidXplorer MFQL analysis with internal standard quantification for aTAG, aDAG, aPC, aPA, aCE and aCER. Normalized fold changes (NFC) in concentrations of each lipid species for each inhibitor treatment were calculated by normalization to the negative control and to the average class fold change. The data represent mean values for n=3 biological replicates. Isolation of hepatocytes and fatty acid pulse was done by CL, lipid extraction and MS/TLC analysis were done by KW.

As seen in the TLC- and pulse-chase-experiments, the MCFA-aTAG levels (C41-47) were downregulated in the same way as upon treatment with the DGAT1 inhibitor (Figure 25, panel A, lanes Eto, D1).

A combination of both inhibitors led to an even stronger downregulation of these species, which additionally confirms the previous experiments (Figure 25, panel A, lanes Eto+D1). Overall, Etomoxir treatment did increase the effects of the DGAT1 inhibitor. When combined with the DGAT2 inhibitor, the resembling effect of Etomoxir as an DGAT1 inhibitor was not as prominent as if the DGAT1 inhibitor would act upon combination with the other inhibitor.

Surprisingly, in the DGAT1$^{-/-}$ hepatocytes, Etomoxir treatment alone led to a comparable NFC pattern as in the WT controls (Figure 25, panel B, lane labeled Eto). The MCFA-aTAG species (C41-47) were as well downregulated with values in between 0.23 – 0.77. The species with longer acyl chains were as well regulated in a similar manner as in the WT hepatocytes. As expected, the DGAT1 inhibitor showed little effect on the aTAG pattern compared to the negative control, as all values are located around 1 (Figure 25, panel B, lane labeled D1). Upon DGAT2 inhibition, the MCFA-aTAG pattern showed the same strong downregulation as when both DGAT inhibitors were combined in the WT controls (Figure 25, panel B, lane labeled D2). However, in DGAT1$^{-/-}$ hepatocytes absolute amounts of the main aMCTs were about half the concentration as in WT cells within the negative control (Supplementary figure 10). The aTAG species pattern with longer acyl chains did as well resemble the pattern as the one in WT hepatocytes treated with both inhibitors. As expected, the NFC pattern of Etomoxir combined with the DGAT1 inhibitor resembled the one as upon Etomoxir treatment alone (Figure 25, panel B, lane labeled Eto+D1). The combination of Etomoxir with the D2 inhibitor did increase the effects of the D2 inhibitor (Figure 25, panel B, lane labeled Eto+D2). This is best seen within the NFC pattern of the MCFA-aTAGs (C41-47), which showed a strong downregulation with values between 0.03-0.25 and stronger upregulation within the main aTAGs [51:5-3], with values over 2.2. This may be due to an over-compensatory effect of the remaining DGAT2 activity.

For better visualization of the described effects, the NFC pattern of the MCFA-aTAG species [41:2] – [45:3] are presented as floating bars (min to max with the line indicating the mean) (Figure 26). Bars below the dashed line indicate a downregulation, bars above the line an upregulation of aTAG levels. The effects throughout the species pattern within one inhibitory group were consistent in both, the WT control (Figure 26, panel A) and DGAT1$^{-/-}$ hepatocytes (Figure 26, panel B), especially upon downregulation. The bars cover a small area and the mean lines from each species within one group are nearly aligned. Two main effects are observable within this visualization. First, the downregulation pattern upon Etomoxir treatment within WT- and DGAT1$^{-/-}$-hepatocytes showed similar levels in all MCFA-aTAG species. And secondly, in WT hepatocytes, DGAT2 inhibition led to a significant upregulation of all MCFA species compared to all other inhibitory conditions (Figure 26, panel A), whereas in DGAT1$^{-/-}$ hepatocytes, all inhibitory conditions (except DGAT1 inhibition) led to a

significant downregulation of MCFA-aTAGs (in comparison to the levels upon DGAT1 inhibition (Figure 26, panel B)).

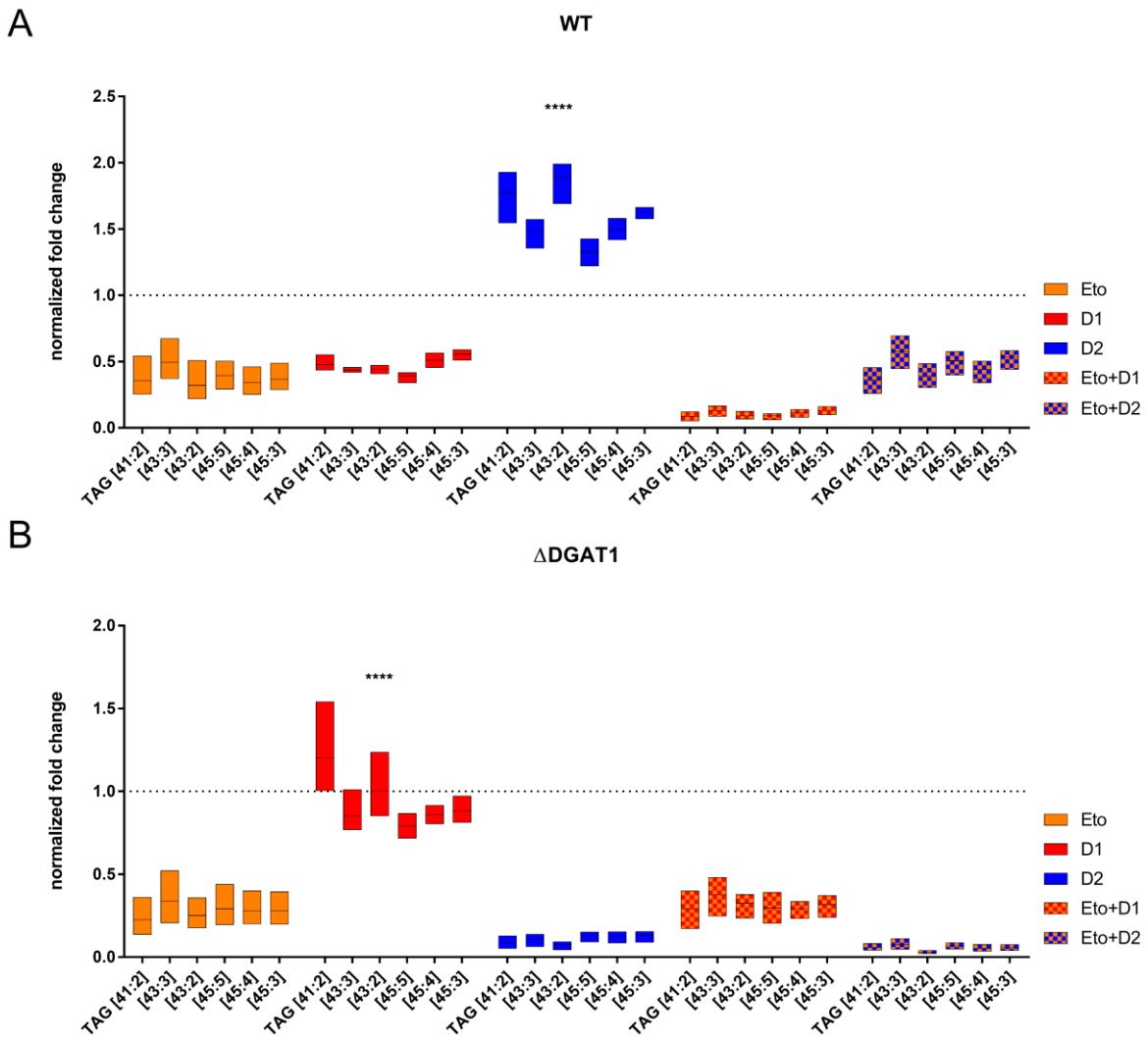

Figure 26: Detailed normalized fold change (NFC) analysis of short chain (C41-C45) alkyne-labeled TAG species from primary hepatocytes, isolated from wildtype mice (A: WT) or mice lacking DGAT1 (B: ΔDGAT1), treated with inhibitor combinations and pulsed with alkyne-palmitate and decanoic acid. After isolation, primary mouse liver hepatocytes were plated in 24 well plates with 7.5x10^4 cells per well. Cells were preincubated with either 50 µM Etomoxir (Eto), 3 µM DGAT1-Inhibitor (D1), 15 µM DGAT2-Inhibitor (D2) or combinations of Etomoxir with each DGAT-inhibitor (Eto+D1, Eto+D2). Cells were then co-pulsed with 50 µM alkyne palmitate (C17:2) and 50 µM decanoic acid (C10) for 1 hour. Lipids were extracted with simultaneous addition of an internal standard mix for alkyne labeled lipids and click reaction with C175-XX reagents was performed. Multiplex samples were pooled and analyzed by MS. Mass signals were identified using LipidXplorer MFQL analysis with internal standard quantification for aTAG, aDAG, aPC, aPA, aCE and aCER. Normalized fold changes (NFC) in concentrations of each lipid species for each inhibitor treatment were calculated by normalization to the negative control and to the average class fold change. The data is represented as floating bars (min to max) with the line indicating the mean value. n=3 biological replicates. **** stands for p≤0.0001. Isolation of hepatocytes and fatty acid pulse was done by CL, lipid extraction and MS/TLC analysis were done by KW.

Additionally, co-pulse experiments with C19- and C11-fatty acids were carried out, similar to the experiments described in the chapters 5.1 and 5.2.

Here, the inhibitory effects of Etomoxir and JNJ-DGAT2-A (D2) in DGAT1$^{-/-}$ hepatocytes were observable as well. Like in the WT hepatocytes, Etomoxir treatment alone, reduced C11-TAG levels significantly, whereas C19-TAG levels were not changed (Figure 27, panels A, B, lanes labeled Eto).

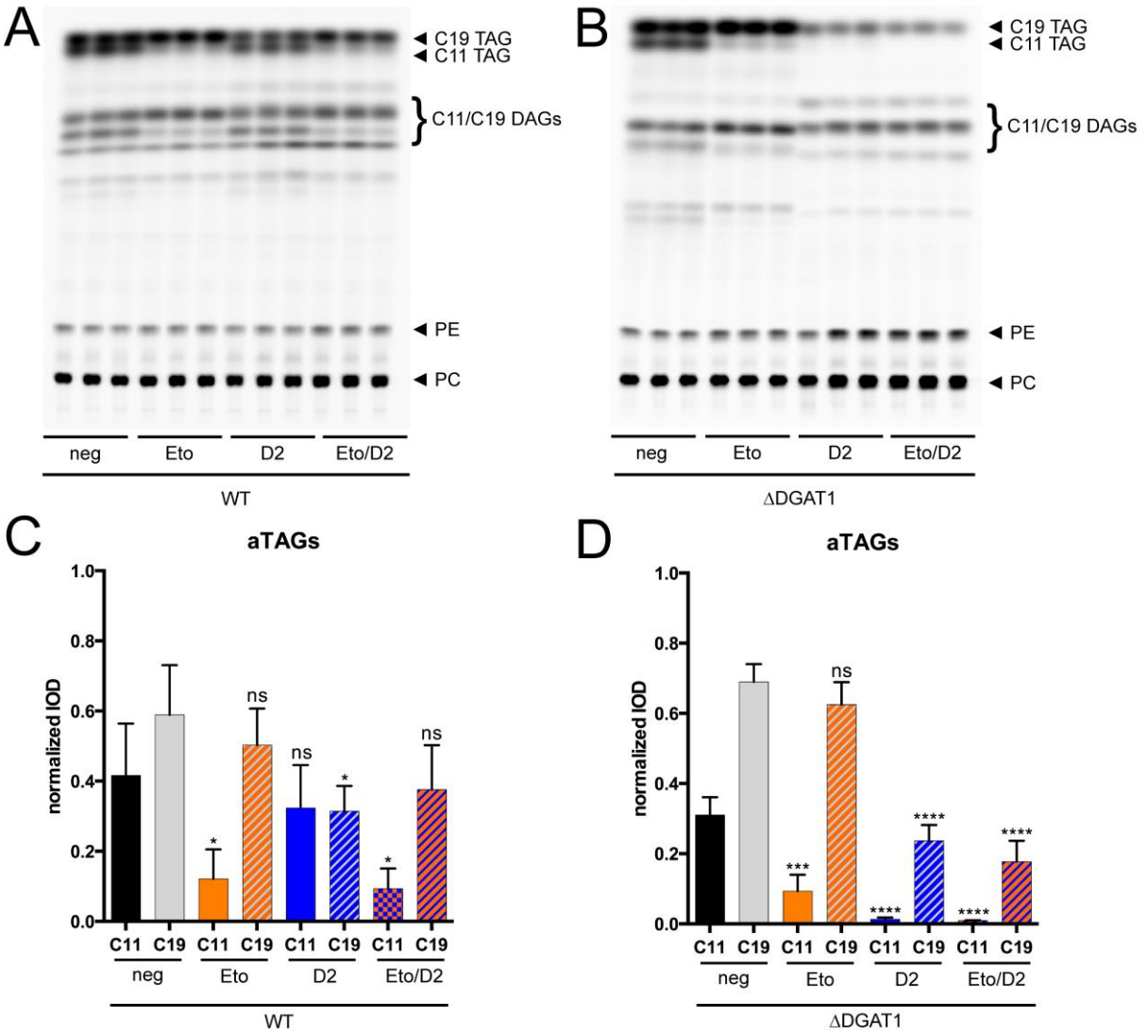

Figure 27: Analysis of aTAGs upon DGAT2 inhibitor-, and Etomoxir-treatment in primary hepatocytes from wildtype mice (A: WT) and mice lacking DGAT1 (B: ΔDGAT1), co-pulsed with C11- and C19-fatty acids. After isolation, primary mouse liver hepatocytes were plated in 24 well plates with 7.5x10^4 cells per well. Cells were preincubated with either 15 µM DGAT2-Inhibitor (D2), 50 µM Etomoxir (Eto) or a combination of both inhibitors (D2/Eto) for one hour, in comparison to the respective vehicle as a negative control. Cells were then pulsed for 1 hour with a combination of 50 µM C11- and 50 µM C19-fatty acid. The cells were washed, lipids were extracted and click reaction for TLC was performed. Finally, lipids were separated on a TLC plate and the signal was captured by fluorescent imaging (A, B). Panels C (WT) and D (ΔDGAT1) illustrate the normalized quantification of fluorescent intensities from C11 TAG (filled bars) and C19 TAG (grey hatched bars) upon either D2 (blue), Etomoxir (orange) and combination of both (orange/blue) inhibitors, in comparison to the negative controls (black: C11, grey: C19). The data represent mean ±SD for n=3 biological replicates. * stands for p≤0.0332, *** for p≤0.0002 and **** for p≤0.0001. ns=not significant. Isolation of hepatocytes and fatty acid pulse was done by CL, lipid extraction and MS/TLC analysis were done by KW.

In DGAT1$^{-/-}$ hepatocytes, DGAT2 inhibition alone significantly reduced both, C11-TAG and C19-TAG levels, which decreased even further in combination with Etomoxir (Figure 27, panel B, lanes labeled D2, Eto/D2).

Absolute amounts of overall labeled lipids upon all treatment conditions in DGAT1$^{-/-}$ hepatocytes were comparatively analyzed to those within the WT controls (Supplementary figure 8). Here any effects on the lipid levels other than the inhibitory treatment could be ruled out.

Altogether, these experiments further solidify the hypothesis that DGAT1 is the key player in hepatic MCFA metabolism and that Etomoxir inhibits DGAT activity as a prominent off-target effect. This latter shall be elaborated within the discussion of this thesis.

Also, for final clarification on the “Etomoxir-effect”, experiments with another liver-specific CPT1 inhibitor were conducted (see: Chapter 5.5).

5.4. DGAT inhibition during a short time *in vivo* LPS-stimulation

Previous studies within the community and our group showed that an acute short time *in vivo* LPS stimulation in mice can induce a NAFLD-like, pro-steatotic phenotype, which is mediated via the TLR4 signaling pathway (Park et al., 2009) of Kupffer cells (Baffy, 2009). One of the key morphologic features of this pathological state, is the accumulation of TAG in hepatocytes (Baffy, 2009; Soares et al., 2010; Berlanga et al., 2014). In the following, previous results on this matter are expanded, by conducting DGAT specific inhibitory experiments on hepatocytes isolated from LPS induced mice, using alkyne lipid tracing followed by MS analysis.

For that, mice were induced *in vivo* with 15 mg/kg LPS according to their respective body weight. 1.5 hours after the stimulation, hepatocytes were isolated by liver perfusion, seeded on 24 well plates and allowed to adhere for 2 hours. Then the hepatocytes were preincubated with a different combination of DGAT inhibitors (3 µM A922500 (D1), 15 µM JNJ-DGAT2-A (D2)) or Etomoxir, followed by a pulse with alkyne palmitate (C17:2) and decanoic acid (C10). The aim here was, not only to study the overall lipid composition, but to trigger as well the MCFA metabolism under the influence of an LPS induced pro-steatotic phenotype.

First, the lipid profiles form hepatocytes, isolated from LPS stimulated mice, in comparison to the respective negative control, were analyzed.

In three of the four major lipid classes which were analyzed, namely aTAG, aPA and aPC, significant changes in the absolute amount of all labeled lipids per class upon LPS-stimulation could be observed. All three of the lipid classes named above, showed at least one third higher amounts upon LPS stimulation than in the respective control (Figure 28, panels A, C, D, control: black bars, +LPS: red hatched bars). Only the labeled DAG showed no significant change in the absolute amount upon LPS stimulation (Figure 28, panel B, control: black bar, +LPS: red hatched bar).

These results are comparable to previous findings from our group, where alkyne lipids had been used for metabolic tracing in pulse-chase experiments with hepatocytes isolated form either *in vivo* stimulated mice or *in vitro* stimulated hepatocytes (Piotrowitz, 2016).

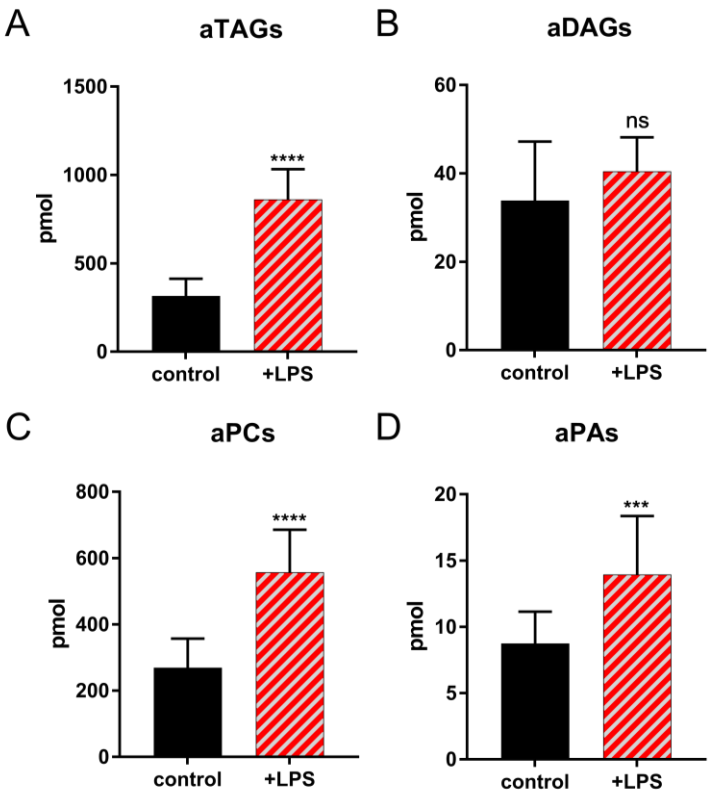

Figure 28: Absolute amounts of alkyne-labeled lipid classes from primary hepatocytes, isolated from unstimulated (control: black bars) mice or mice stimulated with 15 mg/kg LPS for 1.5 hours before hepatocyte isolation (+LPS: red hatched bars). Cells were pulsed with alkyne-palmitate and decanoic acid. After isolation, primary mouse liver hepatocytes were plated in 24 well plates with 7.5x10^4 cells per well. Cells were co-pulsed with 50 µM alkyne palmitate (C17:2) and 50 µM decanoic acid (C10) for 1 hour. Lipids were extracted with simultaneous addition of an internal standard mix for alkyne labeled lipids and click reaction with C175-XX reagents was performed. Multiplex samples were pooled and analyzed by MS. Mass signals were identified using LipidXplorer MFQL analysis with internal standard quantification for aTAG, aDAG, aPC, aPA, aCE and aCER. Absolute amounts of the lipid classes aTAG (A), aDAG (B), aPC (C) and aPA (D) are shown in pmol. The data represent mean SD± for n=18 technical replicates in n=3 biological replicates. *** stands for p≤0.0002 and **** for p≤0.0001. ns= not significant.

Next, using the advantage of alkyne lipid detection for MS, changes on species level upon LPS-stimulation within the classes of aTAG, aDAG and aPC were analyzed (Figure 29, panel A (aTAG), panel B (aDAG) and panel C (aPC) Heatmap array of mean values from white (0 pmol) to dark red (highest pmol value within each lipid class)).

Within the classes of aTAG and aPC, absolute amounts from all analyzed species were equally elevated upon LPS treatment in comparison to the unstimulated control. This effect can be observed predominantly within the main species form each class: for TAG [45:4] and [45:3], representing the MCFA-aTAG species, and [51:4], [51:3], [53:5] and [53:4] representing the LCFA-aTAG species and the main aPC species [35:4], [35:3] (Figure 29, panels A (aTAG and C (aPC)). There were no obvious changes observable throughout all labeled DAG species (Figure 29, panel B (aDAG)).

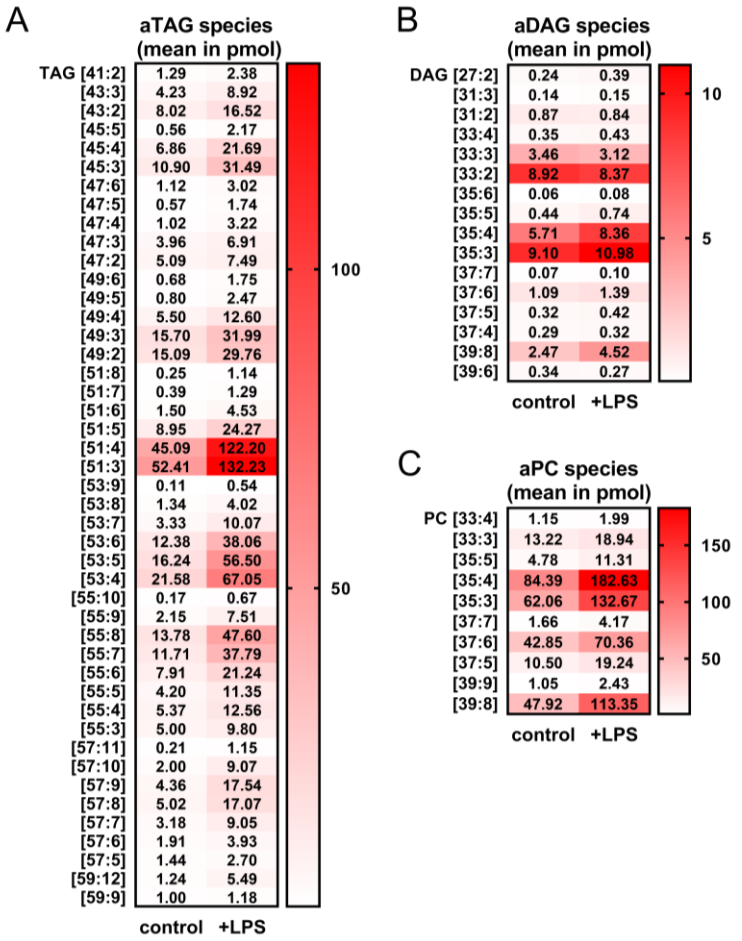

Figure 29: Absolute amounts of alkyne-labeled lipid species from primary hepatocytes, isolated from unstimulated mice (control) and mice treated with 15 mg/kg LPS for 1.5 hours before hepatocyte isolation (+LPS). Cells were pulsed with alkyne-palmitate and decanoic acid. After isolation, primary mouse liver hepatocytes were plated in 24 well plates with $7.5x10^4$ cells per well. Cells were co-pulsed with 50 µM alkyne palmitate (C17:2) and 50 µM decanoic acid (C10) for 1 hour. Lipids were extracted with simultaneous addition of an internal standard mix for alkyne labeled lipids and click reaction with C175-XX reagents was performed. Multiplex samples were pooled and analyzed by MS. Mass signals were identified using LipidXplorer MFQL analysis with internal standard quantification for aTAG, aDAG, aPC, aPA, aCE and aCER. Absolute amounts of the lipid species within the lipid classes of aTAG (A), aDAG (B) and aPC (C) are shown in pmol. The data represent mean values for n=3 biological replicates.

To analyze the effects of a DGAT inhibition during the LPS-induced prosteatotic phenotype experiments for MS analysis of alykne labeled lipids, similar to those described earlier, were performed. Fold changes in aTAG and aDAG levels upon different combinations of DGAT inhibitors and Etomoxir in hepatocytes isolated from either LPS-induced mice or the respective control mice, were analyzed (Figure 30, panel A (TaAG), panel B (aDAG)).

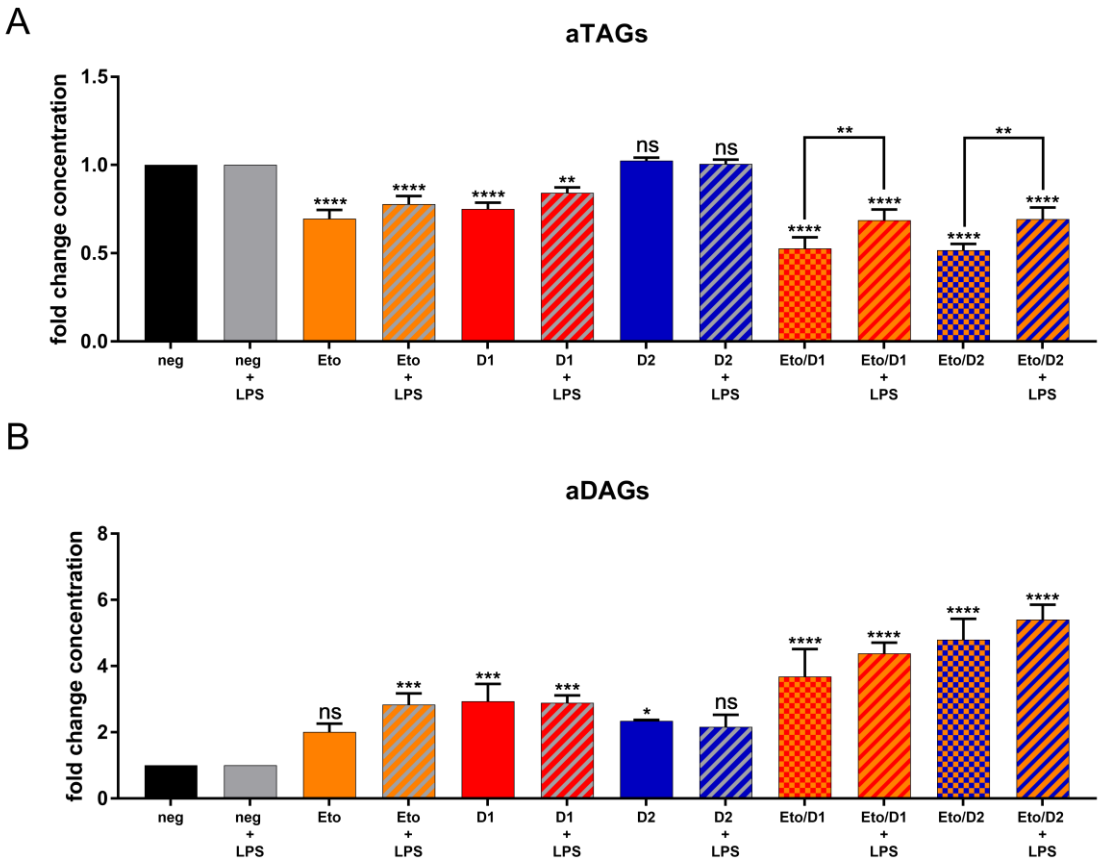

Figure 30: Fold change analysis alkyne-labeled TAG (A) and DAG (B) based on relative amounts (mol per mille) from aTAG, aDAG, aPC, aPA, aCE and aCER, from primary hepatocytes, isolated from unstimulated mice (filled bars) and mice treated with 15 mg/kg LPS for 1.5 hours before hepatocyte isolation (bars with dashed lines/ +LPS). Cells were treated with different inhibitor combinations and pulsed with alkyne-palmitate and decanoic acid. After isolation, primary mouse liver hepatocytes were plated in 24 well plates with $7.5x10^4$ cells per well. Cells were preincubated with either 50 µM Etomoxir (Eto), 3 µM DGAT1-Inhibitor (D1), 15 µM DGAT2-Inhibitor (D2) or combinations of Etomoxir with each DGAT-inhibitor (Eto+D1, Eto+D2). Cells were then co-pulsed with 50 µM alkyne palmitate (C17:2) and 50 µM decanoic acid (C10) for 1 hour. Lipids were extracted with simultaneous addition of an internal standard mix for alkyne labeled lipids and click reaction with C175-XX reagents was performed. Multiplex samples were pooled and analyzed by MS. Mass signals were identified using LipidXplorer MFQL analysis with internal standard quantification for aTAG, aDAG, aPC, aPA, aCE and aCER. Fold changes (FC) in relative concentrations (from mol per mille) of alkyne TAGs and DAGs for each inhibitor treatment were calculated by normalization to the negative control. The data represent mean ±SD for n=3 biological replicates. * stands for p≤0.0332, ** for p≤0.0021, *** for p≤0.0002 and **** for p≤0,0001. ns=not significant.

In general, aTAG and aDAG levels responded similar under both conditions upon the treatment with the combination of different inhibitors.

When treated with either D1 or Etomoxir alone, the decrease in aTAG levels in hepatocytes from LPS stimulated mice was nearly as high as in hepatocytes form control mice (Figure 30, panel A, bars labeled Eto/Eto+LPS (orange/hatched), D1/D1+LPS (red/hatched)). Inhibition through D2 alone did not lead to a significant decrease in overall aTAG levels under both conditions (Figure 30, panel A, bars labeled D2 (blue/hatched)). A combination of Etomoxir with either one of the both DGAT inhibitors led to a further decrease of aTAG upon both conditions. However, in hepatocytes form control mice, the decrease was significantly higher upon both inhibitor combinations (Figure 30, panel A, bars labeled Eto+D1/LPS, Eto+D2/+LPS).

Changes in aDAG levels in hepatocytes form LPS-stimulated mice upon inhibitory treatment, did as well resemble those from the control groups, with only minor differences observable.

Etomoxir treatment, only led to a significant accumulation of aDAG upon LPS stimulation (Figure 30, panel B, bars labeled Eto (orange hatched)), whereas DGAT2 inhibition significantly increased only aDAG levels in the unstimulated animals. The combination of Etomoxir with both DGAT inhibitors, did lead to the same accumulation of aDAG in both, the LPS-stimulated and the control animals (Figure 30, panel B, bars labeled Eto+D1/LPS and Eto+D2/LPS), despite the significantly different response in aTAG levels.

5.5. Comparison of two CPT1 inhibitors: Etomoxir and Teglicar

In the following chapter, the effects of Etomoxir on the hepatic TAG metabolism were experimentally compared with another CPT1 inhibitor, for further clarification on this matter. The small molecule inhibitor Teglicar (ST-1326) first described by R. Conti and colleagues in 2011 (Conti et al., 2011), was chosen to fulfill that purpose. Teglicar has been in various clinical trials for Type-2 *diabetes melitus* until their discontinuation in 2015. Fortunately, it is freely available for scientific purposes since early 2018.

As a first experimental setup, a co-pulse experiment with 50 µM of C11- and C19- alkyne fatty acid in hepatocytes, treated with either 50 µM Etomoxir, 10 µM Teglicar (Tegli) or a combination of both inhibitors, was done. The initial concentration of 10 µM for Teglicar was chosen according to the experiments done by R. Conti and colleagues in primary rat hepatocytes (Conti et al., 2011).

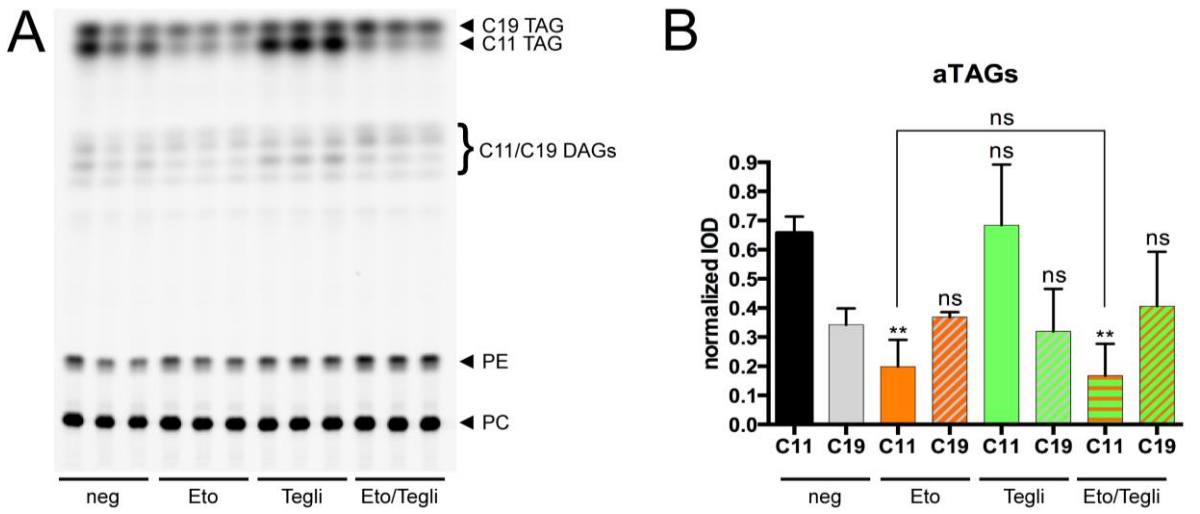

Figure 31: Analysis of aTAGs upon Etomoxir- and Teglicar-treatment in primary hepatocytes, co-pulsed with C11- and C19-fatty acids. After isolation, primary mouse liver hepatocytes were plated in 24 well plates with $7.5x10^4$ cells per well. Cells were preincubated with either 50 µM Etomoxir (Eto), 10 µM Teglicar (Tegli) or a combination of both inhibitors (Eto/Tegli) for one hour, in comparison to the respective vehicle as a negative control. Cells were then pulsed for 1 hour with a combination of 50 µM C11- and 50 µM C19-fatty acid. The cells were washed, lipids were extracted and click reaction for TLC was performed. Finally, lipids were separated on a TLC plate and the signal was captured by fluorescent imaging (A). Panel B illustrates the normalized quantification of fluorescent intensities from C11 TAG (filled bars) and C19 TAG (grey hatched bars) upon either Etomoxir (orange), Teglicar (mint) and combination of both (orange/mint) inhibitors, in comparison to the negative controls (black: C11, grey: C19). The data represent mean ±SD for n=3 biological replicates. ** stands for p≤0.0021. ns=not significant.

As shown previously, the treatment with Etomoxir led to a significant decrease in C11- TAG levels (Figure 31, panel A, lanes labeled Eto, panel B orange bar, labeled Eto/C11).
A treatment with Teglicar alone did not lead to a decrease in either C11- nor C19- TAG levels (Figure 31, panel A, lanes labeled Tegli, panel B green bars, labeled Tegli). The combination of Teglicar with Etomoxir did not increase the C11-TAG reduction, nor did it change C19-TAG levels (Figure 31, panel A lanes labeled Eto/Tegli, panel B, orange/green hatched bars labeled Eto/Tegli). For better comparison of both CPT1 inhibitors, pulse experiments for MS analysis of alkyne labeled lipids were done. Here, hepatocytes were pre-pulsed with 50 µM Etomoxir and either 10-, 20- or 50 µM Teglicar or a combination of both inhibitors and pulsed afterwards with a combination of 50 µM C17:2 and 50 µM C10.

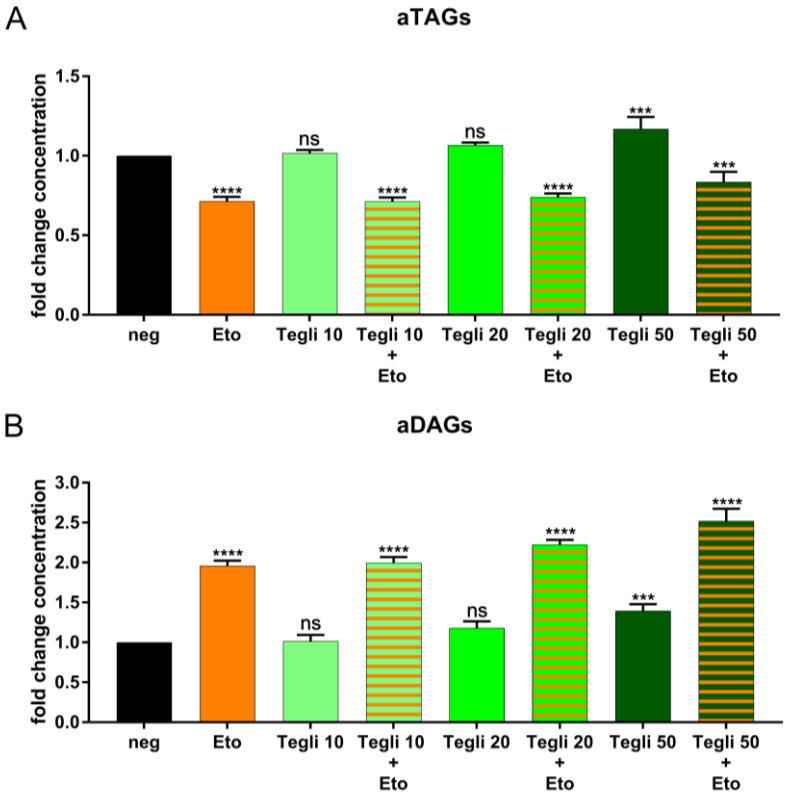

Figure 32: Fold change analysis of alkyne-labeled TAG (A) and DAG (B) based on relative amounts (mol per mille) from aTAG, aDAG, aPC, aPA, aCE and aCER, from primary hepatocytes, isolated from WT mice treated with different combinations of Etomoxir and Teglicar and pulsed with alkyne-palmitate and decanoic acid. After isolation, primary mouse liver hepatocytes were plated in 24 well plates with $7.5x10^4$ cells per well. Cells were preincubated with either 50 µM Etomoxir (Eto), 10 µM Teglicar (Tegli 10), 20 µM Teglicar (Tegli 20), 50 µM Teglicar (Tegli 50) or combinations of Etomoxir with each Teglicar concentration (Tegli XX + Eto). Cells were then co-pulsed with 50 µM alkyne palmitate (C17:2) and 50 µM decanoic acid (C10) for 1 hour. Lipids were extracted with simultaneous addition of an internal standard mix for alkyne labeled lipids and click reaction with C175-XX reagents was performed. Multiplex samples were pooled and analyzed by MS. Mass signals were identified using LipidXplorer MFQL analysis with internal standard quantification for aTAG, aDAG, aPC, aPA, aCE and aCER. Fold changes (FC) in relative concentrations (from mol per mille) of alkyne TAGs and DAGs for each inhibitor treatment were calculated by normalization to the negative control. The data represent mean ±SD for n=3 biological replicates. *** stands for p≤0.0002 and **** for p≤0.0001. ns=not significant.

FC analysis for overall aTAG and aDAG levels upon inhibitory treatment revealed striking differences in between both CPT1 inhibitors. Whereas 50 µM Etomoxir decreased overall aTAG levels (Figure 32, panel A, bar graph labeled Eto), Teglicar treatment resulted in an opposite effect.

Teglicar concentrations of 10- and 20 µM had no significant effect on overall aTAG levels (Figure 32, panel A, bar graphs labeled Tegli 10 and Tegli 20).

When hepatocytes were treated with 50 µM Teglicar alone, overall aDAG and especially aTAG levels increased significantly (Figure 32, panels A (aTAG) and B (aDAG), bar graphs labeled Tegli 50). aDAG accumulation upon Teglicar treatment was not as high as upon Etomoxir treatment (Etomoxir about 2-fold increase and Teglicar about 1.5-fold increase, (Figure 32, panel B, bar graphs labeled Eto, Tegli 50).

The combination of Etomoxir with 10- or 20 µM Teglicar only led to the same effects on aTAG levels, as with Etomoxir alone (Figure 32, panels A (aTAG), B (aDAG), bar graphs labeled Tegli 10/20 + Eto). The combinatorial treatment of both inhibitors did lead to a concentration-dependent increase in aDAG accumulation, with the highest values of 2.5-fold increase upon the combination of 50 µM Etomoxir and Teglicar each (Figure 32, panel B, bar graphs labeled Tegli 10/20/50 + Eto).

Overall, the impact of Etomoxir on decreasing aTAG levels was more prominent compared to the accumulative effect form Teglicar, as in equimolar concentrations of both inhibitors, aTAG levels were significantly decreased (Figure 32, panel A, bar graph labeled Tegli 50 + Eto).

FC analysis of overall aPA levels revealed no significant changes upon either treatment condition (Supplementary figure 11, panel B). Interestingly, FC analysis of overall aPC levels did show a reduction upon treatment with 50 µM Teglicar alone, which was equaled in the combinatorial treatment with Etomoxir (Supplementary figure 11, panel A).

In order to see, whether the accumulative effect on aTAG levels upon treatment with 50 µM Teglicar affected all labeled TAG species, absolute amounts within all aTAG species from the previous experiments were visualized together with absolute amounts from the samples treated with either Eto, Tegli 50 + Eto and the negative control (Figure 33, Heatmap array of mean values from white (0 pmol) to dark green (over 130 pmol)). This analysis revealed, that the accumulative effect of Teglicar, indeed, affected aTAG species of all chain lengths.

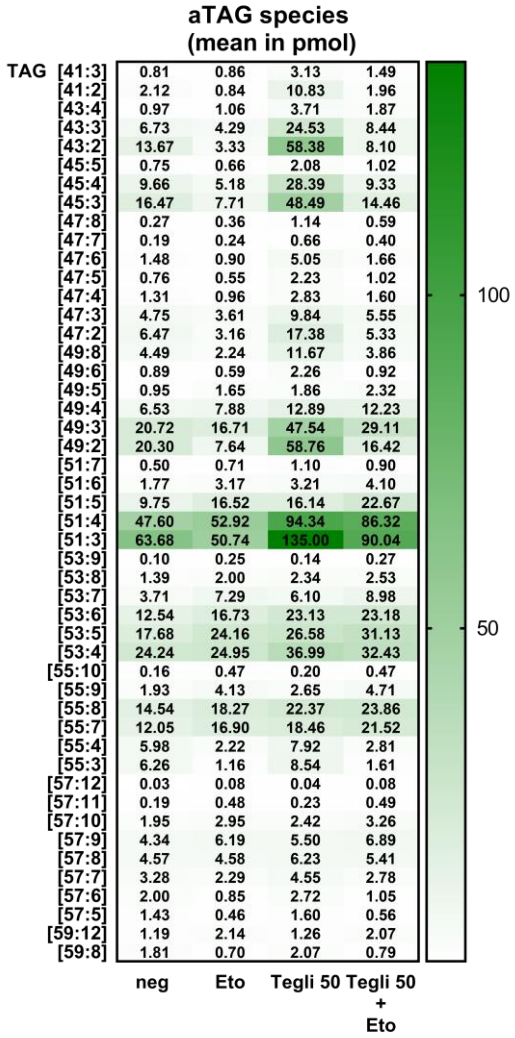

Figure 33: Absolute amounts of alkyne-labeled TAG species from primary hepatocytes, isolated from WT mice, treated with combinations of Etomoxir and Teglicar and pulsed with alkyne-palmitate and decanoic acid. After isolation, primary mouse liver hepatocytes were plated in 24 well plates with $7.5x10^4$ cells per well. Cells were preincubated with either 50 µM Etomoxir (Eto), 50 µM Teglicar (Tegli 50) or combinations of both inhibitors (Tegli 50 + Eto). Cells were co-pulsed with 50 µM alkyne palmitate (C17:2) and 50 µM decanoic acid (C10) for 1 hour. Lipids were extracted with simultaneous addition of an internal standard mix for alkyne labeled lipids and click reaction with C175-XX reagents was performed. Multiplex samples were pooled and analyzed by MS. Mass signals were identified using LipidXplorer MFQL analysis with internal standard quantification for aTAG, aDAG, aPC, aPA, aCE and aCER. Absolute amounts of the lipid species within the lipid class of aTAG are shown in pmol. The data represent mean values for n=3 biological replicates.

This is best observable within the main species of each sub-class (Summarized in Figure 34, panel A (major MCFA-aTAGs) and panel B (major LCFA-aTAGs)). One can also observe, that the inhibitory effect of Etomoxir which cannot be compensated through the opposite

effect of Teglicar, is mainly due to the reduction in MCFA-aTAG levels. Upon treatment with 50 µM Teglicar, absolute amounts from the four main MCFA-aTAG species were all significantly increased, whereas treatment with either Etomoxir alone or in combination with Teglicar, both strongly reduced these aTAG species (Figure 34, panel A).

The major LCFA-aTAGs on the other hand, were not so strongly affected by the treatment with Etomoxir. Therefore, the accumulative effect of Teglicar was still visible even in the presence of Etomoxir. This is best observed within the aTAG species [51:4] and [51:3], from which TAG [51:4] was significantly increased, both in the presence of Teglicar alone and upon combination with Etomoxir (Figure 34, panel B).

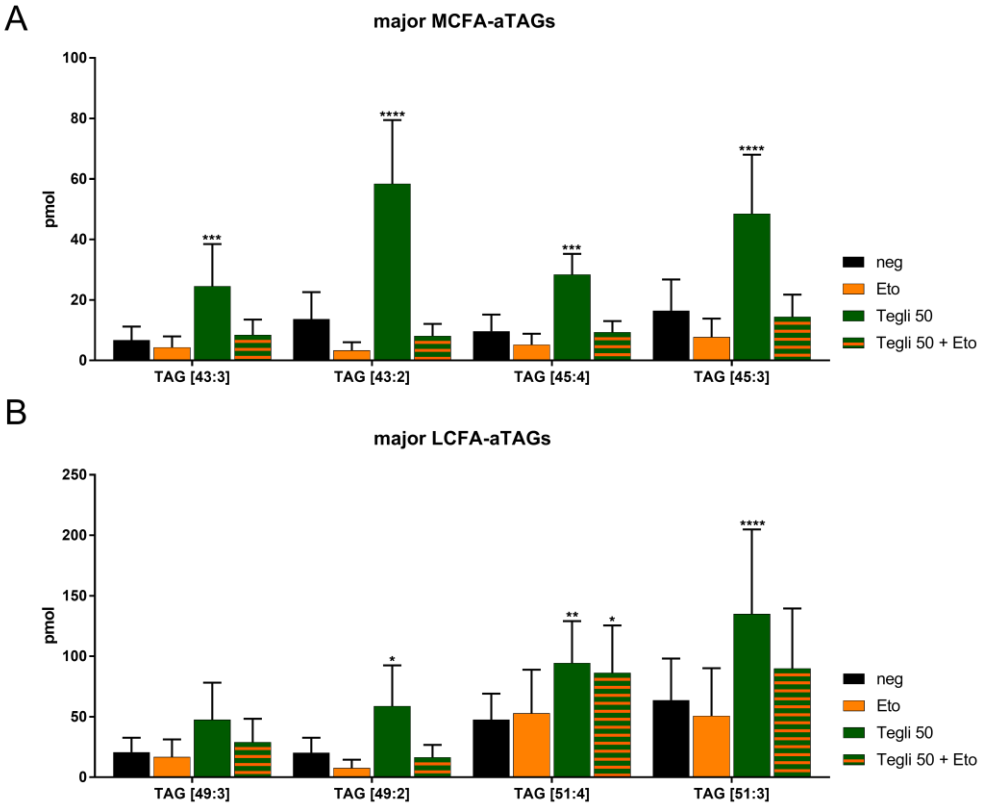

Figure 34: Absolute amounts of alkyne-labeled MCFA-aTAG (A) and LCFA-aTAG (B) species from primary hepatocytes, isolated from WT mice, treated with combinations of Etomoxir and Teglicar and pulsed with alkyne-palmitate and decanoic acid. After isolation, primary mouse liver hepatocytes were plated in 24 well plates with $7.5x10^4$ cells per well. Cells were preincubated with either 50 µM Etomoxir (Eto), 50 µM Teglicar (Tegli 50) or combinations of both inhibitors (Tegli 50 + Eto). Cells were co-pulsed with 50 µM alkyne palmitate (C17:2) and 50 µM decanoic acid (C10) for 1 hour. Lipids were extracted with simultaneous addition of an internal standard mix for alkyne labeled lipids and click reaction with C175-XX reagents was performed. Multiplex samples were pooled and analyzed by MS. Mass signals were identified using LipidXplorer MFQL analysis with internal standard quantification for aTAG, aDAG, aPC, aPA, aCE and aCER. Absolute amounts of the lipid species within the lipid class of aTAG are shown in pmol. The data represent mean ±SD for n=3 biological replicates. * stands for p≤0.0332, ** for p≤0.0021, *** for p≤0.0002 and **** for p≤0.0001.

Both, Etomoxir and Teglicar are inhibitors of CPT1 and therefore inhibit mitochondrial β-oxidation by hindering the transport of activated acyl-CoAs though the inner mitochondrial membrane towards the matrix, before entering the β-oxidation pathway (Turnbull et al., 1984; McGarry and Brown, 1997; Conti et al., 2011). This results in reduction of the cellular oxidation rate and should be therefore observable in a reduced OCR. In order to compare the ability of Etomoxir and Teglicar to inhibit hepatic CPT1 in equimolar concentrations, hepatocytes were treated with either 50 µM Etomoxir, 50 µM Teglicar as well as with 3 µM A922500 (D1) in addition to the respective negative control, followed by OCR measurement, using the Seahorse XF Analyzer Technology from Agilent.

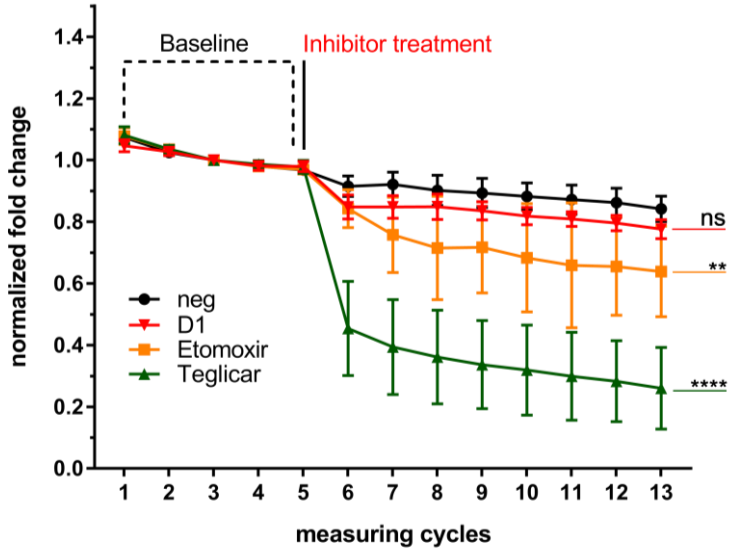

Figure 35: Normalized fold change analysis of live cell OCR measurement (pmol/min) in hepatocytes isolated from WT mice treated with Etomoxir, Teglicar or A922500 (D1). After isolation, primary mouse liver hepatocytes were plated in a Seahorse XF Analyzer 96 well plate with 1000 cells per well. Cells were allowed to adhere for two hours before the assay procedure was started (see: Chapter 3.6.). After 5 measuring cycles of baseline OCR measurement the inhibitors were injected, and the measurement was resumed for 8 more cycles. The inhibitors were used with the following final assay concentrations: D1 (red line): 3 µM, Etomoxir (orange line): 50 µM, Teglicar (dark green line), 50 µM and the negative control (neg/black line). Normalized fold changes were calculated for each well with the average value of all 5 baseline measurements set as 1. The data represent mean ±SD for n=2 biological replicates with 4 technical replicates. ** stands for p≤0.0021 and **** stands for p≤0.0001, ns=not significant. Results of the statistical analysis are only shown for the last measuring cycle (13).

As expected, treatment with the DGAT1 inhibitor A922500 did not lead to a reduced cellular oxygen consumption rate (Figure 35, red line (D1)). Treatment with Etomoxir or Teglicar did lead to a significant drop in the measured OCR, proofing that both molecules indeed reduce β-oxidation via CPT1 inhibition. However, treatment with Teglicar did lead to a more significant drop in the OCR after 8 measuring cycles than Etomoxir, even though both are used in the same concentration (Figure 35, orange (Etomoxir) and green line (Teglicar)). Upon treatment of hepatocytes with 5 µM Etomoxir, no drop in the OCR could be observed (Supplementary figure 12).

6. Discussion

6.1. DGAT1 primarily facilitates murine hepatic MCFA incorporation into TAG

Although DGAT1 and DGAT2 seem to have different physiological functions, which is reflected by the different phenotypes of their knockout mouse models, the ability of hepatic DGAT1 and DGAT2 to partially compensate for each other in TAG synthesis, has been shown in previous studies (Smith et al., 2000; Stone et al., 2004; Li et al., 2015). In this work, the compensating ability of DGAT enzymes was analyzed in more depth, focusing on the analysis of chain length and saturation preferences of each DGAT enzyme, using different DGAT inhibitors and the DGAT1$^{-/-}$ mouse model combined with MS-based alkyne lipid tracing with species resolution.

As already mentioned, there are various studies, dealing with acyl-chain length and saturation preferences from each DGAT enzyme. Studies working with mammalian and fungal DGAT enzymes proclaim a preference of DGAT2 for medium-chain CoAs, whereas in many plant species DGAT1 isoforms are associated with preference for medium-chain CoAs in seed oil production (Lardizabal et al., 2001; Aymé et al., 2015; Iskandarov et al., 2017; Klizaite, 2017). In the experiments presented in chapter 5.1 of this study using DGAT1 and DGAT2 inhibitors during an C19/C11-FA co-incubation, showed a drastic reduction of C11-FA incorporation into TAG upon DGAT1 inhibition, whereas C19-FA incorporation was slightly elevated (Figure 11). Upon DGAT2 inhibition, the vice versa effect could be observed, whereas a combination of both inhibitors nearly abolished MCT production with a corresponding accumulation of DAGs (Figure 11). These observations from the TLC experiments already suggested a DGAT1 preference for MCFA in hepatocytes.

Using the newly developed MS-based detection system for alkyne lipids, similar experiments were conducted, utilizing only C17:2 for tracing aTAG levels upon DGAT inhibitory treatment. For overall aTAG levels, the MS experiments did show comparable results to these obtained from TLC analysis (Figure 22 A, B). The detailed NFC array analysis, however, revealed a complex pattern of up- and downregulated aTAG species upon inhibitory treatment. The proposed acyl-chain length preference for both DGATs was confirmed, as all shorter chain aTAG species showed a strong downregulation upon DGAT1 inhibition and a strong upregulation upon DGAT2 inhibition (Figure 23). Additionally, this dataset shows a tendency towards saturation preferences of each DGAT enzyme. DGAT1 seems to prefer more saturated species in the LCFA-aTAGs, as upon inhibition, the most saturated members in this group were downregulated. A combination of both inhibitors led to an even further

downregulation of aMCTs with a few strongly upregulated aLCT species. The latter correspond to TAGs synthetized from the most abundant FA species in murine hepatocytes, namely palmitic acid (C16:0), palmitoleic acid (C16:1), stearic acid (C18:0) or oleic acid (C18:1) (Kindt et al., 2018). This may reflect a compensating effect of the remaining DGAT activity, maintaining FFA homeostasis by metabolizing DAGs which originate from remodeling of phospholipids, which contain mainly the FAs mentioned above.

In DGAT1$^{-/-}$ hepatocytes, slightly reduced aMCTs and increased aLCTs were observed while overall aTAG levels were similar (Figure 20 A, Figure 21 A, Supplementary figure 10, lanes labeled neg). As both cell types were fed with C17:2-FA and C10-FA, differences due to a lack of C10-CoA can be ruled out. The analogous TLC-experiments also showed slightly reduced C11-TAG levels in comparison to C19-TAG levels (Figure 26 B, data not quantified). Upon DGAT2 inhibition, a TAG phenotype like the one in WT hepatocytes where both DGATs were inhibited could be reproduced. aMCT levels were further reduced as well (Figure 24 B, 25 B, 26 B/D). As no DGAT1 was present, this suggests, that the compensating ability of DGAT2 for DGAT1 includes a certain flexibility in DGAT2's preference for acyl-CoAs, including those predominantly preferred by DGAT1. It is known, that DGAT2 locates both to the ER and LDs, whereas DGAT1 only locates to the ER (Kuerschner et al., 2008; Stone et al., 2009; Wurie et al., 2011). DGAT2 is also described to have a broader acyl-CoA specificity (Yen et al., 2008). The study of Li and colleagues suggests that the function of murine hepatic DGAT1 is mainly to channel FAs into TAG, which are then prone to be β-oxidized (Li et al., 2015). Altogether this may suggest, that hepatic DGAT1 acts mostly on MCFAs and that the DGAT2 population located at the ER is solely responsible for compensating the missing DGAT1 activity in DGAT1$^{-/-}$ hepatocytes. Thus, the pressure on the system created through additional DGAT2 inhibition may be reduced by direct oxidation of the acyl-CoAs without channeling them through a TAG pool first, resulting in further decrease of MCT levels. As hepatic β-oxidation of MCFAs was shown to be very abundant, the mechanisms mentioned above provide a possible explanation (Pégorier et al., 1988; Metges and Wolfram, 1991). Similar effects in DGAT1$^{-/-}$ hepatocytes were observed upon Etomoxir treatment, which are discussed in chapter 6.2.

Also, the pulse-chase experiments presented in chapter 5.3.1. showed an DGAT1-dependent incorporation of MCFAs into TAG. As these experiments were also including a comparison to Etomoxir-treatment, they are discussed in chapter 6.2.

In all experiments conducted with the DGAT inhibitors in WT hepatocytes, either within the TLC-based or the MS-based experiments, overall effects on aTAG levels were always more prominent upon DGAT1- rather than DGAT2-inhibition. A study in HepG2 cells, showed that DGAT1 is responsible for about 80% of overall TAG synthesis (Qi et al., 2012). This might serve as a possible explanation for the stronger overall effects on TAG levels upon DGAT1

inhibition, presented in this thesis. However, as the metabolic properties of HepG2 cells are not directly comparable to those of primary hepatocytes this interpretation should be considered with caution. It also has been proposed, that DGAT1 predominantly acts on FA from exogenous sources, whereas DGAT2 mainly utilizes FA from *de novo* synthesis (Villanueva et al., 2009; Qi et al., 2012). As the hepatocytes were always exogenously fed with fatty acids, one would expect a more drastic effect upon DGAT1 inhibition. However, as already mentioned, the experiments in DGAT1$^{-/-}$ hepatocytes, showed similar overall concentrations of aTAG. Also considering the fact that in DGAT1$^{-/-}$ hepatocytes, the overall labeled lipid concentrations were similar to those in WT controls (Supplementary figure 8), it may be postulated that DGAT2 can, at least in murine hepatocytes, fully compensate for the loss of DGAT1, to maintain the overall TAG levels.

Changes in levels of aPC and aPA upon inhibitor treatment were visible as well (Supplementary Figure 9). aPA levels were significantly reduced upon either inhibitor treatment, both in WT and DGAT1$^{-/-}$ hepatocytes. This may be due to a positive feedback loop from accumulating DAG, which triggers a faster channeling of PA to form PI and PG. As the reduced aPA was also visible upon DGAT1 inhibitory treatment in DGAT1$^{-/-}$ hepatocytes it may represent an off-target effect form the DGAT1 inhibitor affecting other enzymes upstream of PA. However, as aPC and aDAG levels were not altered significantly in DGAT1$^{-/-}$ hepatocytes upon DGAT1 inhibition (Figure 24 B, Supplementary Figure 9), it is not possible to proof this hypothesis. aPC levels were significantly increased in WT cells upon DGAT1 inhibition, but in DGAT1$^{-/-}$ hepatocytes only upon DGAT2 inhibition. This is most likely due to the highest increase of DAG levels upon the strongest DGAT inhibition in each condition, and therefore excess DAG is as well channeled into PC synthesis.

6.2. Etomoxir can act as a DGAT inhibitor, predominantly targeting DGAT1

Etomoxir has been first described as an irreversible inhibitor of mitochondrial LCFA β-oxidation by targeting CPT1 and therefore hindering the formation of acylcarnitine, which are necessary for the translocation of LCFA into the mitochondrial matrix (Kiorpes et al., 1984). Alongside other selective inhibitors of CPT1 like Perhexiline, it soon came into focus as a possible antidiabetic drug by shifting the cellular energy utilization from fatty acids to glucose, leading to hypoglycemia, hypoketonemia, and hypotriglyceridemia (Selby and Sherratt, 1989; Wolf, 1992; Ashrafian et al., 2007). However, it never was fully approved in clinical trials due to severe systemic side effects, such as hepatic hypertrophy, inducing cellular oxidative stress and activation of transcription factors like PPARα and nuclear factor kappaB (NF-κB) (Yotsumoto et al., 2000; Merrill et al., 2002; Cabrero et al., 2003; Carracedo et al., 2013).

With an increasing understanding of the role of FA oxidation in tumor growth and cancer metabolism in general, CPT1 and therefore its inhibitors have been most recently receiving rejuvenated attention as possible anti-cancer drugs (Qu et al., 2016). In a recent study, Etomoxir has been shown to suppress tumor progression and to induce cell cycle arrest via a PPARγ-mediated pathway in bladder cancer (Cheng et al., 2019). Also, an upregulated CPT1A activity in patients suffering from depression, has led to a recent study where the common antidepressant Escitalopram (SSRI) and Etomoxir have been comparatively analyzed on stress-induced depressed rats. Here, the blocking of FAO through the inhibition of CPT1 via Etomoxir has been shown to effectively reduce the stress-induced depression in the animals (Mørkholt et al., 2017). Through the renewed interest in Etomoxir as a candidate drug for various applications and the rising numbers of scientists from different fields dealing with the cellular effects of this drug in various cell types, more off-target effects of Etomoxir have been discovered. Many of these studies investigate off-target effects of Etomoxir in different immune cells, using relatively high concentrations between 40-200 µM (Raud et al., 2018). It has been shown that Etomoxir effectively inhibits FAO in BMDMs at a concentration of 3 µM but a concentration of 100 µM affects IL4-mediated macrophage polarization, independent of CPT1 activity by disrupting intracellular CoA levels (Divakaruni et al., 2018). In the same study it was also shown that Etomoxir inhibits the adenine nucleotide translocase (ANT), increasing mitochondrial membrane potential (Divakaruni et al., 2018). It has been shown as well, that high concentrations (above 100 µM) of Etomoxir induce severe oxidative stress in T-cells and alters T-cell proliferation and differentiation (O'Connor et al., 2018; Raud et al., 2018). As another off-target effect, it has been shown that at concentrations of 200 µM, Etomoxir inhibits Complex 1 of the respiratory chain (Yao et al., 2018). Importantly, Etomoxir inhibiting DGAT activity, as a side effect has been reported, in a study using in $H9_c2$ cells (Xu et al., 2003). In this study, $H9_c2$ cells were treated with 40 µM

Etomoxir, resulting in a reduced [1-14C] palmitic acid incorporation into TAG due to a diminished DGAT activity. Additionally, Etomoxiroyl-CoA inhibited DGAT activity *in vitro* (Xu et al., 2003). Still, this study did not determine specifically whether DGAT1 or DGAT2 was off targeted by Etomoxir and focused only on incorporation of palmitic acid without determination of species-specific differences in the TAG profile upon Etomoxir treatment. The experimental data in the present work describes the inhibition of DGAT enzymes in murine primary hepatocytes by Etomoxir and identifies DGAT1 as the predominantly targeted family member.

Interestingly, the present TLC analysis, did not show a reduced incorporation of alkyne palmitate (C17:2) upon Etomoxir treatment, but only a reduced incorporation of C11 into TAG (Figures 14, 15). This was also shown for alkyne oleate (C19) before (Klizaite, 2017).

In contrast, the data on C19 incorporation upon Etomoxir treatment presented here, showed slightly (but not significantly) elevated aTAG labeling (Figures 11, 13 and 26 A) or a significant increase (Figure 12).

Alike, an enhanced incorporation of [1-14C] oleic acid was observed in EL4 cells upon treatment with 100 µM Etomoxir (Boren and Brindle, 2012). Based on the findings above, an inhibition of DGAT1 by Etomoxir and DGAT2 compensating for DGAT1 appears the primary reason for the observed increase in LCTs, rather than an inhibition of CPT1, resulting in elevated acyl-CoAs through decreased oxidation. This hypothesis is supported by the data depicted in the NFC arrays, when hepatocytes were treated with Etomoxir and a D1 inhibitor (Figure 24 A). Both NFC arrays basically look the same in terms of up- and downregulated aTAG species, including the upregulated LCT species with either one or two molecules of oleic acid incorporated. The inhibition of DGAT1 by Etomoxir is best demonstrated by the diminished MCFA incorporation into TAGs or generally spoken the reduced levels of MCTs. Both, Etomoxir and the DGAT1 inhibitor show the same effects in TLC experiments, leading to decreased C11-TAG levels (Figures 12-15, 24 A). This finding was confirmed by extensive MS analysis. Here the effects on aMCTs could be observed by NFC array analysis showing a downregulation of the aMCT species TAG [41-47] upon action of Etomoxir and a D1 inhibitor (Figures 24 A, 25 A).

However, these experiments show a metabolic state after one hour of a constant pulse from the alkyne FA under inhibitory treatment. Thus, short term lipid remodeling of phospholipids or possible hydrolysis of TAGs via ATGL/HSL at LDs and subsequent re-esterification via DGAT2 (Eichmann and Lass, 2015), or TAG hydrolysis generating FFAs which are then catabolized through β-oxidation, may generate similar changes in lipid patterns, originating from different metabolic pathways. Also, the alkyne group of the C11-FA may influence the natural cellular metabolism of the FA, creating artifacts which lead to the discussed results.

These problems are overcome by conducting a pulse-chase analysis as presented in chapter 5.3.1. As it has been shown, that hepatocytes are able to synthetize TAGs within 2 minutes form incorporated pools of extracellular free fatty acids (Stein and Stein, 1967), a short pulse in combination with several short chase time points is necessary, in order to follow the direct biosynthesis of endpoint metabolites such as TAG and PC by incorporation of an unlabeled, native FA-CoA into alkyne labeled precursor metabolites such as PA and DAG. This is exactly what these experiments could show. Not only, that from the technical point of view the metabolites behaved as expected from previous studies in our laboratory and from the literature (Stein and Stein, 1967; Piotrowitz, 2016), but additionally these experiments could also show the DGAT1 dependent incorporation of native decanoic acid into a labeled DAG pool (Figures 17-19). Here, both the DGAT1-inhibitor and Etomoxir did decrease the incorporation of decanoic acid in the same manner, decreasing levels even further when combined. It is unlikely, that the effect is due to a DGAT2 inhibition by Etomoxir, as the changes in medium-chain aTAG levels were never observed upon solely a DGAT2 inhibition, when both DGATs were present. In this scenario, Etomoxir creates only effects as seen from the DGAT1 inhibitors.

Interestingly, in DGAT1$^{-/-}$ hepatocytes the treatment of Etomoxir did lead to the same NFC pattern change in aTAG levels. As expected, the DGAT1 inhibitor did not show any significant changes throughout all aTAG species (Figures 25 B, 26 B, 27 B). Nevertheless, even though Etomoxir creates nearly the same NFC pattern, absolute concentrations of the main aMCTs were about half the size as in WT cells in the neg control. Thus, the effects on aMCTs are not as prominent in DGAT1$^{-/-}$ hepatocytes in terms of absolute concentrations, even though they appear so in the NFC arrays. Generally, this effect can be explained with the compensating DGAT2 activity at the ER as mentioned before, presumably compensating for the loss of ER specific DGAT1 activity, which is then inhibited by Etomoxir. However, the overall effect on aTAG and aDAG levels by Etomoxir treatment was not as prominent in DGAT1$^{-/-}$ hepatocytes as in WT cells (Figure 27 A, B). Taken together this suggests that Etomoxir can act as a potent DGAT inhibitor which preferably inhibits DGAT1, but as well seems to partly inhibit DGAT2 activity which locates at the ER.

Teglicar, the small molecule inhibitor for the liver isoform of CPT1, served as a perfect control drug concerning the proposed off-target effects of Etomoxir on DGAT enzymes. Both, Teglicar and Etomoxir, did significantly reduce the cellular oxygen consumption rate in equimolar concentrations of 50 µM (Figure 35). However, they did cause opposite effects on aTAG levels. In accordance with the initial study by Conti and colleagues where Teglicar treatment was described to elevate liver TAG levels in healthy rats and *db/db* mice (Conti et al., 2011), significantly elevated aTAG levels in 50 µM Teglicar-treated hepatocytes could be observed (Figure 32, 33). This is exactly what one would expect, when CPT1 is inhibited.

Acyl-CoAs are no longer shuttled into the mitochondria and start accumulating within the cytoplasm. As a protective result against the toxic effects of high intracellular acyl-CoA levels the cells start to incorporate excessive acyl-CoAs into TAG (Aon et al., 2014). It has been shown that peroxisomal β-oxidation can serve as a backup system when the mitochondrial function is impaired and that Teglicar does not alter peroxisomal oxidation (Conti et al., 2011; Violante et al., 2013). However, the present data suggests, that murine hepatocytes also expediently cope with excess acyl-CoA through direct incorporation into TAG and storage in LDs. Upon Teglicar treatment (50 µM), the four main MCFA-aTAG species including decanoic acid (C10), TAG [43:3], [43:2], [45:4] and [45:3], were as well elevated to a great extend (Figure 33). This allows the conclusion, that CPT1-dependent conversion of MCFAs plays indeed a bigger part in mitochondrial β-oxidation, other than the proposed diffusion of MCFA-CoAs through the mitochondrial membrane, independent of the carnitine shuttle system (Bremer, 1983; Odle et al., 1991). However, all experiments were done in medium containing glucose. FAO is shown to be more active during fasting conditions (Guo et al., 2006). Hence, it would be interesting to repeat these experiments during glucose fasting conditions. Here, CPT1-dependent FAO would be higher and effects due to an inhibition of CPT1 could be stronger as well.

As expected, the combination of Etomoxir and Teglicar, lead to reduction of aTAG species according to the discussed DGAT1-dependent inhibition by Etomoxir, whereas the aTAG species which are not affected through inhibition still showed accumulative effects (Figures 33, 34). Through treatment of 50 µM Teglicar, a slight accumulation of aDAGs could be observed, likely via biosynthesis from elevated levels of acyl-CoAs and PA, as aPA levels were not elevated (Figure 32, Supplementary Figure 11 B). The treatment with 50 µM Teglicar alone, did lead to a reduction of overall aPC levels. This may be due to either an influence of Teglicar treatment on enhanced phospholipase C and/or enhanced sphingomyelin synthase activity at the ER and the plasma membrane. A shift form phospholipid synthesis to an enhanced TAG synthesis, dealing with the excess acyl-CoA levels due to reduced mitochondrial β-oxidation, could as well serve as an explanation.

As Etomoxir was always used at a concentration of 50 µM, one might also consider the possibility of different off-target effects, affecting different enzymatic pathways, thus creating these results. However, as hepatocytes have high metabolic rates in general, and pilot experiments performed with lower concentrations of Etomoxir did not show a drop in OCR (Supplementary figure 12), it is plausible that the inhibition of DGAT enzymes is an off-target effect of Etomoxir, which already manifests at low concentrations, where only CPT1 is also effectively inhibited. Many of the other off-target effects, mentioned above manifested at higher concentrations over 100 µM and were described in other cell types like different immune cells. Those cells are likely to have a lower metabolic capacity then hepatocytes.

Therefore, it is unlikely that the off-target effects shown in immune cells, manifest in hepatocytes at even lower concentrations. Nevertheless, this may be addressed in future studies. Additionally, treatment with the second CPT1 inhibitor Teglicar lead to a detectable change in lipid profiles at concentrations of 50 µM, whereas no changes were observable at lower concentrations. Taken together, this allows the conclusion that the inhibition of DGAT enzymes by Etomoxir is an off-target effect, which appears at rather low concentrations in the same range as the effective concentration for CPT1 inhibition.

6.3. DGAT inhibition upon an LPS-induced steatotic phenotype

It has been shown, that a diminished DGAT1 activity can protect mice from a high fat diet induced hepatic steatosis, due to reduced exogenous FA incorporation into TAG (Villanueva et al., 2009). Moreover, it has been shown, that DGAT1 expression is increased within humans with NAFLD (Kohjima et al., 2007). Hence, as it has been shown by our group and by other studies that a short term *in vivo* LPS injection, mimics a hepatocellular response comparable to a prosteatotic phenotype (Baffy, 2009; Berlanga et al., 2014; Piotrowitz, 2016), the intention was to investigate how inhibition of DGAT enzymes, especially DGAT1, influences the TAG profile upon these conditions. In accordance to the literature and previous findings from our group, overall lipid levels, especially aTAG and aPC (Figure 28), could be observed upon LPS-stimulation (Baffy, 2009; Berlanga et al., 2014; Piotrowitz, 2016). From the technical point of view, this proofs indeed a response in hepatic lipid metabolism to the *in vivo* LPS-stimulation, shifting towards a prosteatotic phenotype. Upon comparison of aTAG lipid species, one could observe that all species were elevated in the same ratio, compared to the controls (Figure 29, panel A). This was also true for aDAG and aPC species (Figure 29, panel B, C). For aTAG synthesis, this already hints towards an equally upregulated DGAT1 and DGAT2 activity upon LPS-stimulation, at least under these experimental conditions. And indeed, when one observes overall responses of aTAG and aDAG levels upon DGAT- and Etomoxir-treatment (Figure 30, panels A, B), all responses upon inhibitory treatment were merely comparable to those of the control groups. Exceptions were the combinations of Etomoxir with each DGAT inhibitor. Here aTAG levels were significantly lower in the control group compared to the LPS induced group (Figure 30, panel A). Nevertheless, at least under these conditions, there was no evident preference of one DGAT enzyme over the other upon an LPS induced prosteatotic phenotype. In order to evaluate this matter further, more time resolved pulse-chase experiments and the inclusion of DGAT1$^{-/-}$ hepatocytes into the experimental setup would be beneficial.

6.4. Concluding hypothesis

Based on the experimental data presented in this thesis in relation to what is known from the literature, a working model for hepatic DGAT1-dependent MCFA metabolism is introduced and summarized in Figure 36. The data from this thesis allows the conclusion, that murine hepatic DGAT1 acts predominantly on MCFA-CoA incorporation into TAGs. This MCFA-TAG pool might be then mostly used for catabolic processes, which appears logical, as MCFAs can be efficiently β-oxidized by hepatocytes (Pégorier et al., 1988; Metges and Wolfram, 1991). When DGAT1 activity is diminished either through inhibition or in DGAT1$^{-/-}$ mice, the DGAT2 pool located on the ER can compensate for the lacking DGAT1 activity with a certain flexibility towards the acyl-CoA spectrum predominantly preferred by DGAT1.

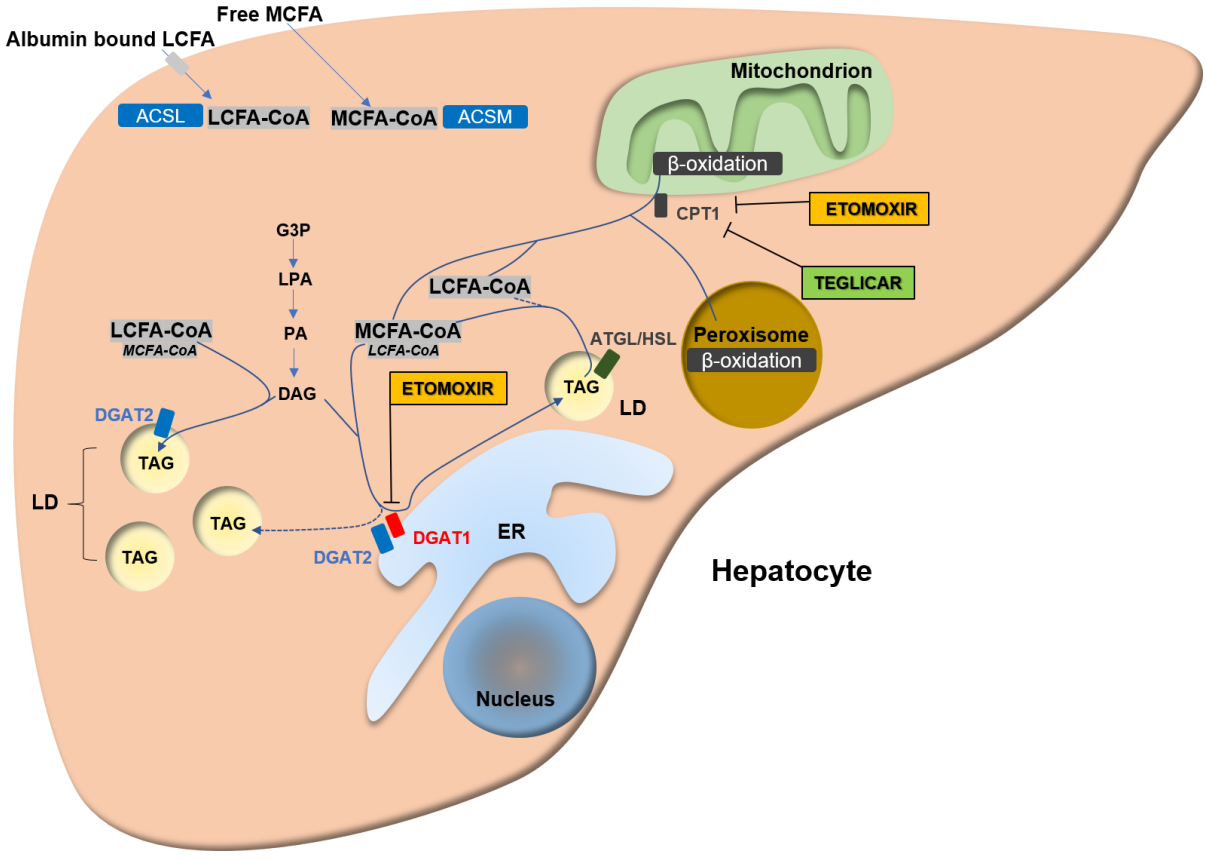

Figure 36: Proposed functional model of DGAT1 and DGAT2 in metabolizing MCFAs and LCFAs in murine hepatocytes. Activated MCFA-CoAs are predominantly incorporated by DGAT1 at the ER into a TAG pool, which is mainly used for catabolic processes via mitochondrial or peroxisomal β-oxidation. The DGAT2 pool, located at the ER can compensate for the loss or reduction of DGAT1 activity. The CPT1 inhibitor Etomoxir, inhibits mostly DGAT1 and to some extent DGAT2 at the ER as a prominent off-target effect, thus reducing the TAG pool created by DGAT1. Teglicar, another CPT1 inhibitor, does not show this off-target effect. TAG levels are elevated upon treatment, due to increased acyl-CoA incorporation, as the FAO of acyl-CoAs is efficiently impaired.

In the literature, mammalian DGAT2 has been proposed to have a broader substrate specificity and might also favor MFCA-CoAs (Lardizabal et al., 2001; Cases et al., 2001), whereas in several plant species, DGAT1 isoforms have been shown to act predominantly on

MCFA-CoA incorporation, forming MCTs rich seed oils (Iskandarov et al., 2017; Rigouin et al., 2018). Newer studies proposed, at least for murine hepatocytes, that DGAT1 channels TAG synthesis for intracellular energy utilization, whereas DGAT2 channels TAGs for VLDL synthesis (Li et al., 2015; McLaren et al., 2018). The hypothesis based on the experimental data from this thesis supports evidence for hepatic DGAT1 to act predominantly on MCFAs.

Apart from its various other published site effects, the CPT1 inhibitor Etomoxir does also efficiently inhibit DGAT activity, mostly acting on DGAT1 when both DGATs are present. In the case of a loss in DGAT1 activity, Etomoxir does as well inhibit DGAT2, creating similar NFC patterns in aTAG levels. This suggest the presence of a specialized DGAT2 pool also acting on the FA-CoA species normally metabolized by DGAT1. Upon an LPS-induced steatotic phenotype, activity from both DGAT enzymes seem to be upregulated in the same manner, as inhibitory treatments did not lead to any other effects as in the unstimulated control groups.

As a control, Teglicar, another specific inhibitor for the liver isoform of CPT1, was used to compare its effects to those of Etomoxir. The effects of Teglicar did not show any inhibition of DGAT activity. Instead Teglicar treatment did only lead to effects which can be correlated to an efficient CPT1 inhibition, like reduced OCR and increase of aTAG levels.

In conclusion, this work gives novel insights into the differing functions of hepatic DGAT1 and DGAT2, suggesting DGAT1 to function predominantly on MCFAs. Additionally, this work describes the inhibition of both DGAT enzymes through Etomoxir as a prominent off-target effect of this drug. Etomoxir is still widely used as a CPT1 inhibitor in various research fields, even though many other off-target effects were published over the past years. This thesis now adds more detail to the mentioned study form Xu and colleagues (Xu et al., 2003), by further defining the off-target effect of Etomoxir in murine hepatocytes. Hence, future studies should now carefully consider the use of Etomoxir as a CPT1 inhibitor, as it also acts on many other enzymes, including DGAT1 and DGAT2.

7. Outlook

As the hypothesis for the role of DGAT1 in hepatic MFCA metabolism is solely based on *ex vivo* experiments in murine hepatocytes there are several important experiments, which should be addressed in future studies in order to support this hypothesis as a general model in mice, but also in order to transfer it to higher mammal species. There are recent studies which propose that DGATs function differently in other mammals. It has been shown for higher mammals (rhesus primates), that DGAT2 does not have a controlling role in hepatic TAG synthesis which leads to VLDL secretion, even though it has been shown to do so in rodents (Li et al., 2015; McLaren et al., 2018). DGAT2 has also shown to channel *de novo* synthesized FA into a TAG pool for rapid β-oxidation in brown adipocytes, comparable to the proclaimed DGAT1 activity in hepatocytes (Irshad et al., 2017). Also, expression pattern of both DGAT enzymes can differ between organs from mice and humans. DGAT1 is the predominant enzyme in the human intestine, with a practically absence of DGAT2, whereas in rodents DGAT2 is highly expressed in the intestine (Haas et al., 2012).

Taking this to account, firstly *in vivo* studies in WT and DGAT1$^{-/-}$ mice should be performed, preferably feeding the mice labeled MCTs and LCTs followed by MS-based analysis of organ samples, in order to follow the natural metabolism as such in different organs. This experimental setup may as well include cohorts of mice treated with combinations DGAT- and other selective inhibitors targeting different enzymes in lipid metabolism.

Also, pulse-chase experiments should be done, including DGAT1$^{-/-}$ hepatocytes, as well as selective inhibition of DGAT2 and the addition of several unlabeled fatty acids, differing in chain length and saturation. It would also be helpful if one would separate intracellular LDs and ER bound VLDL fractions via gradient ultracentrifugation, followed by a subsequent analysis of labeled TAGs in those fractions. With such an experiment one could distinguish between spatially separated DGAT activities. Here, the presence of TAG pools differing in acyl-chain length and saturation degrees could be experimentally confirmed.

Whether the results obtained from the murine model can be applied to higher mammals and ultimately to humans, still needs to be confirmed. Here, a cooperation with clinics dealing with liver related diseases would be beneficial, as one might get the opportunity to conduct similar studies with primary hepatocytes obtained from liver biopsies. A cooperation with the scientists supervising the clinical study with patients lacking DGAT1 in the intestine (van Rijn et al., 2018) would also be very interesting, as one might get the chance to apply our alkyne lipid tracing technology on their patient-derived organoid cultures.

8. References

Alcoriza-Balaguer, M. I., J. C. García-Cañaveras, A. López, I. Conde, O. Juan, J. Carretero, and A. Lahoz. 2019. LipidMS: An R Package for Lipid Annotation in Untargeted Liquid Chromatography-Data Independent Acquisition-Mass Spectrometry Lipidomics. *Anal. Chem.* 91(1):836–845. doi:10.1021/acs.analchem.8b03409.

Aon, M. A., N. Bhatt, and S. C. Cortassa. 2014. Mitochondrial and cellular mechanisms for managing lipid excess. *Frontiers in physiology* 5:282. doi:10.3389/fphys.2014.00282.

Ashrafian, H., J. D. Horowitz, and M. P. Frenneaux. 2007. Perhexiline. *Cardiovascular drug reviews* 25(1):76–97. doi:10.1111/j.1527-3466.2007.00006.x.

Aymé, L., P. Jolivet, J.-M. Nicaud, and T. Chardot. 2015. Molecular Characterization of the Elaeis guineensis Medium-Chain Fatty Acid Diacylglycerol Acyltransferase DGAT1-1 by Heterologous Expression in Yarrowia lipolytica. *PLoS ONE* 10(11):e0143113. doi:10.1371/journal.pone.0143113.

Bach, A. C., and V. K. Babayan. 1982. Medium-chain triglycerides: an update. *The American journal of clinical nutrition* 36(5):950–962. doi:10.1093/ajcn/36.5.950.

Bach, A. C., Y. Ingenbleek, and A. Frey. 1996. The usefulness of dietary medium-chain triglycerides in body weight control: fact or fancy? *Journal of lipid research* 37(4):708–726.

Baffy, G. 2009. Kupffer cells in non-alcoholic fatty liver disease: the emerging view. *Journal of hepatology* 51(1):212–223. doi:10.1016/j.jhep.2009.03.008.

Banerjee, S., and S. Mazumdar. 2012. Electrospray ionization mass spectrometry: a technique to access the information beyond the molecular weight of the analyte. *International journal of analytical chemistry* 2012:282574. doi:10.1155/2012/282574.

Berlanga, A., E. Guiu-Jurado, J. A. Porras, and T. Auguet. 2014. Molecular pathways in non-alcoholic fatty liver disease. *Clinical and experimental gastroenterology* 7:221–239. doi:10.2147/CEG.S62831.

Berry, M. N. 1969. HIGH-YIELD PREPARATION OF ISOLATED RAT LIVER PARENCHYMAL CELLS: A Biochemical and Fine Structural Study. *The Journal of Cell Biology* 43(3):506–520. doi:10.1083/jcb.43.3.506.

Bligh, E. G., and W. J. Dyer. 1959. A RAPID METHOD OF TOTAL LIPID EXTRACTION AND PURIFICATION. *Can. J. Biochem. Physiol.* 37(8):911–917. doi:10.1139/o59-099.

Boren, J., and K. M. Brindle. 2012. Apoptosis-induced mitochondrial dysfunction causes cytoplasmic lipid droplet formation. *Cell death and differentiation* 19(9):1561–1570. doi:10.1038/cdd.2012.34.

Botchlett, R., and C. Wu. 2018. Diet Composition for the Management of Obesity and Obesity-related Disorders. *Journal of diabetes mellitus and metabolic syndrome* 3:10–25. doi:10.28967/jdmms.2018.01.18002.

Brandes, R., N. Mayorek, E. Berry, R. Arad, and J. Bar-Tana. 1985. The specificity of triacylglycerol synthesis for medium-chain fatty acids in rat and human adipose preparations. *Biochimica et biophysica acta* 836(1):63–66. doi:10.1016/0005-2760(85)90220-6.

Bremer, J. 1983. Carnitine--metabolism and functions. *Physiological reviews* 63(4):1420–1480. doi:10.1152/physrev.1983.63.4.1420.

Brügger, B. 2014. Lipidomics: analysis of the lipid composition of cells and subcellular organelles by electrospray ionization mass spectrometry. *Annual review of biochemistry* 83:79–98. doi:10.1146/annurev-biochem-060713-035324.

Brügger, B., G. Erben, R. Sandhoff, F. T. Wieland, and W. D. Lehmann. 1997. Quantitative analysis of biological membrane lipids at the low picomole level by nano-electrospray ionization tandem mass spectrometry. *Proceedings of the National Academy of Sciences of the United States of America* 94(6):2339–2344. doi:10.1073/pnas.94.6.2339.

Bruins, A. P. 1994. Atmospheric-pressure-ionization mass spectrometry. *TrAC Trends in Analytical Chemistry* 13(1):37–43. doi:10.1016/0165-9936(94)85057-7.

Bruss, M. L. 2008. Lipids and Ketones. In Clinical Biochemistry of Domestic Animals. Elsevier. 81–115.

Buhman, K. K., S. J. Smith, S. J. Stone, J. J. Repa, J. S. Wong, F. F. Knapp, B. J. Burri, R. L. Hamilton, N. A. Abumrad, and R. V. Farese. 2002. DGAT1 is not essential for intestinal triacylglycerol absorption or chylomicron synthesis. *The Journal of biological chemistry* 277(28):25474–25479. doi:10.1074/jbc.M202013200.

Cabrero, A., M. Merlos, J. C. Laguna, and M. V. Carrera. 2003. Down-regulation of acyl-CoA oxidase gene expression and increased NF-kappaB activity in etomoxir-induced cardiac hypertrophy. *J. Lipid Res.* 44(2):388–398. doi:10.1194/jlr.M200294-JLR200.

Cao, J., L. Cheng, and Y. Shi. 2007. Catalytic properties of MGAT3, a putative triacylgycerol synthase. *J. Lipid Res.* 48(3):583–591. doi:10.1194/jlr.M600331-JLR200.

Cao, J., J. Lockwood, P. Burn, and Y. Shi. 2003. Cloning and functional characterization of a mouse intestinal acyl-CoA:monoacylglycerol acyltransferase, MGAT2. *The Journal of biological chemistry* 278(16):13860–13866. doi:10.1074/jbc.M300139200.

Carracedo, A., L. C. Cantley, and P. P. Pandolfi. 2013. Cancer metabolism: fatty acid oxidation in the limelight. *Nature reviews. Cancer* 13(4):227–232. doi:10.1038/nrc3483.

Cases, S., S. J. Smith, Y. W. Zheng, H. M. Myers, S. R. Lear, E. Sande, S. Novak, C. Collins, C. B. Welch, A. J. Lusis, S. K. Erickson, and R. V. Farese. 1998. Identification of a gene encoding an acyl CoA:diacylglycerol acyltransferase, a key enzyme in triacylglycerol

synthesis. *Proceedings of the National Academy of Sciences of the United States of America* 95(22):13018–13023. doi:10.1073/pnas.95.22.13018.

Cases, S., S. J. Stone, P. Zhou, E. Yen, B. Tow, K. D. Lardizabal, T. Voelker, and R. V. Farese. 2001. Cloning of DGAT2, a second mammalian diacylglycerol acyltransferase, and related family members. *The Journal of biological chemistry* 276(42):38870–38876. doi:10.1074/jbc.M106219200.

Chen, H. C., S. J. Smith, Z. Ladha, D. R. Jensen, L. D. Ferreira, L. K. Pulawa, J. G. McGuire, R. E. Pitas, R. H. Eckel, and R. V. Farese. 2002. Increased insulin and leptin sensitivity in mice lacking acyl CoA:diacylglycerol acyltransferase 1. *The Journal of clinical investigation* 109(8):1049–1055. doi:10.1172/JCI14672.

Cheng, D., T. C. Nelson, J. Chen, S. G. Walker, J. Wardwell-Swanson, R. Meegalla, R. Taub, J. T. Billheimer, M. Ramaker, and J. N. Feder. 2003. Identification of acyl coenzyme A:monoacylglycerol acyltransferase 3, an intestinal specific enzyme implicated in dietary fat absorption. *The Journal of biological chemistry* 278(16):13611–13614. doi:10.1074/jbc.C300042200.

Cheng, S., G. Wang, Y. Wang, L. Cai, K. Qian, L. Ju, X. Liu, Y. Xiao, and X. Wang. 2019. Fatty acid oxidation inhibitor etomoxir suppresses tumor progression and induces cell cycle arrest via PPARγ-mediated pathway in bladder cancer. *Clinical science (London, England 1979)* 133(15):1745–1758. doi:10.1042/CS20190587.

Choi, C. S., D. B. Savage, A. Kulkarni, X. X. Yu, Z.-X. Liu, K. Morino, S. Kim, A. Distefano, V. T. Samuel, S. Neschen, D. Zhang, A. Wang, X.-M. Zhang, M. Kahn, G. W. Cline, S. K. Pandey, J. G. Geisler, S. Bhanot, B. P. Monia, and G. I. Shulman. 2007. Suppression of diacylglycerol acyltransferase-2 (DGAT2), but not DGAT1, with antisense oligonucleotides reverses diet-induced hepatic steatosis and insulin resistance. *The Journal of biological chemistry* 282(31):22678–22688. doi:10.1074/jbc.M704213200.

Coleman, R. A., and D. G. Mashek. 2011. Mammalian Triacylglycerol Metabolism: Synthesis, Lipolysis, and Signaling. *Chem. Rev.* 111(10):6359–6386. doi:10.1021/cr100404w.

Conti, R., E. Mannucci, P. Pessotto, E. Tassoni, P. Carminati, F. Giannessi, and A. Arduini. 2011. Selective reversible inhibition of liver carnitine palmitoyl-transferase 1 by teglicar reduces gluconeogenesis and improves glucose homeostasis. *Diabetes* 60(2):644–651. doi:10.2337/db10-0346.

Divakaruni, A. S., W. Y. Hsieh, L. Minarrieta, T. N. Duong, K. K. O. Kim, B. R. Desousa, A. Y. Andreyev, C. E. Bowman, K. Caradonna, B. P. Dranka, D. A. Ferrick, M. Liesa, L. Stiles, G. W. Rogers, D. Braas, T. P. Ciaraldi, M. J. Wolfgang, T. Sparwasser, L. Berod, S. J. Bensinger, and A. N. Murphy. 2018. Etomoxir Inhibits Macrophage Polarization by Disrupting CoA Homeostasis. *Cell metabolism* 28(3):490-503.e7. doi:10.1016/j.cmet.2018.06.001.

Doege, H., and A. Stahl. 2006. Protein-mediated fatty acid uptake: novel insights from in vivo models. *Physiology (Bethesda, Md.)* 21:259–268. doi:10.1152/physiol.00014.2006.

Eberhardt, C., P. W. Gray, and L. W. Tjoelker. 1999. cDNA cloning, expression and chromosomal localization of two human lysophosphatidic acid acyltransferases. *Advances in experimental medicine and biology* 469:351–356. doi:10.1007/978-1-4615-4793-8_51.

Eichmann, T. O., M. Kumari, J. T. Haas, R. V. Farese, R. Zimmermann, A. Lass, and R. Zechner. 2012. Studies on the substrate and stereo/regioselectivity of adipose triglyceride lipase, hormone-sensitive lipase, and diacylglycerol-O-acyltransferases. *The Journal of biological chemistry* 287(49):41446–41457. doi:10.1074/jbc.M112.400416.

Eichmann, T. O., and A. Lass. 2015. DAG tales: the multiple faces of diacylglycerol--stereochemistry, metabolism, and signaling. *Cell. Mol. Life Sci.* 72(20):3931–3952. doi:10.1007/s00018-015-1982-3.

Ejsing, C. S., J. L. Sampaio, V. Surendranath, E. Duchoslav, K. Ekroos, R. W. Klemm, K. Simons, and A. Shevchenko. 2009. Global analysis of the yeast lipidome by quantitative shotgun mass spectrometry. *Proceedings of the National Academy of Sciences of the United States of America* 106(7):2136–2141. doi:10.1073/pnas.0811700106.

Fenn, J. B., M. Mann, C. K. Meng, S. F. Wong, and C. M. Whitehouse. 1989. Electrospray ionization for mass spectrometry of large biomolecules. *Science (New York, N.Y.)* 246(4926):64–71. doi:10.1126/science.2675315.

Fuchs, B., R. Süß, K. Teuber, M. Eibisch, and J. Schiller. 2011. Lipid analysis by thin-layer chromatography—A review of the current state. *Journal of Chromatography A* 1218(19):2754–2774. doi:10.1016/j.chroma.2010.11.066.

Gaebler, A., R. Milan, L. Straub, D. Hoelper, L. Kuerschner, and C. Thiele. 2013. Alkyne lipids as substrates for click chemistry-based in vitro enzymatic assays. *Journal of lipid research* 54(8):2282–2290. doi:10.1194/jlr.D038653.

Gaebler, A., A. Penno, L. Kuerschner, and C. Thiele. 2016. A highly sensitive protocol for microscopy of alkyne lipids and fluorescently tagged or immunostained proteins. *Journal of lipid research* 57(10):1934–1947. doi:10.1194/jlr.D070565.

Gao, D., C. Pararasa, C. R. Dunston, C. J. Bailey, and H. R. Griffiths. 2012. Palmitate promotes monocyte atherogenicity via de novo ceramide synthesis. *Free radical biology & medicine* 53(4):796–806. doi:10.1016/j.freeradbiomed.2012.05.026.

Gomez-Muñoz, A., E. H. Hamza, and D. N. Brindley. 1992. Effects of sphingosine, albumin and unsaturated fatty acids on the activation and translocation of phosphatidate phosphohydrolases in rat hepatocytes. *Biochimica et biophysica acta* 1127(1):49–56. doi:10.1016/0005-2760(92)90200-f.

Grasselli, E., A. Voci, I. Demori, G. Vecchione, A. D. Compalati, G. Gallo, F. Goglia, R. de Matteis, E. Silvestri, and L. Vergani. 2015. Triglyceride Mobilization from Lipid Droplets Sustains the Anti-Steatotic Action of Iodothyronines in Cultured Rat Hepatocytes. *Frontiers in physiology* 6:418. doi:10.3389/fphys.2015.00418.

Grevengoed, T. J., E. L. Klett, and R. A. Coleman. 2014. Acyl-CoA Metabolism and Partitioning. *Annu. Rev. Nutr.* 34(1):1–30. doi:10.1146/annurev-nutr-071813-105541.

Gu, M., G. Cosenza, I. Nicolae, A. Bota, Y. Guo, L. Di Stasio, and A. Pauciullo. 2017. Transcript analysis at DGAT1 reveals different mRNA profiles in river buffaloes with extreme phenotypes for milk fat. *Journal of dairy science* 100(10):8265–8276. doi:10.3168/jds.2017-12771.

Guo, W., W. Xie, and J. Han. 2006. Modulation of adipocyte lipogenesis by octanoate: involvement of reactive oxygen species. *Nutrition & metabolism* 3:30. doi:10.1186/1743-7075-3-30.

Haas, J. T., H. S. Winter, E. Lim, A. Kirby, B. Blumenstiel, M. DeFelice, S. Gabriel, C. Jalas, D. Branski, C. A. Grueter, M. S. Toporovski, T. C. Walther, M. J. Daly, and R. V. Farese. 2012. DGAT1 mutation is linked to a congenital diarrheal disorder. *The Journal of clinical investigation* 122(12):4680–4684. doi:10.1172/JCI64873.

Han, X., and R. W. Gross. 2005. Shotgun lipidomics: multidimensional MS analysis of cellular lipidomes. *Expert review of proteomics* 2(2):253–264. doi:10.1586/14789450.2.2.253.

Harris, T. E., T. A. Huffman, A. Chi, J. Shabanowitz, D. F. Hunt, A. Kumar, and J. C. Lawrence. 2007. Insulin controls subcellular localization and multisite phosphorylation of the phosphatidic acid phosphatase, lipin 1. *The Journal of biological chemistry* 282(1):277–286. doi:10.1074/jbc.M609537200.

Hecker, M., N. Sommer, H. Voigtmann, O. Pak, A. Mohr, M. Wolf, I. Vadász, S. Herold, N. Weissmann, R. E. Morty, W. Seeger, and K. Mayer. 2014. Impact of short- and medium-chain fatty acids on mitochondrial function in severe inflammation. *JPEN. Journal of parenteral and enteral nutrition* 38(5):587–594. doi:10.1177/0148607113489833.

Herzog, R., D. Schwudke, K. Schuhmann, J. L. Sampaio, S. R. Bornstein, M. Schroeder, and A. Shevchenko. 2011. A novel informatics concept for high-throughput shotgun lipidomics based on the molecular fragmentation query language. *Genome Biology* 12(1):R8. doi:10.1186/gb-2011-12-1-r8.

Hill, J. O., J. C. Peters, D. Yang, T. Sharp, M. Kaler, N. N. Abumrad, and H. L. Greene. 1989. Thermogenesis in humans during overfeeding with medium-chain triglycerides. *Metabolism: clinical and experimental* 38(7):641–648. doi:10.1016/0026-0495(89)90101-7.

Hiramine, Y., and T. Tanabe. 2011. Characterization of acyl-coenzyme A:diacylglycerol acyltransferase (DGAT) enzyme of human small intestine. *Journal of physiology and biochemistry* 67(2):259–264. doi:10.1007/s13105-010-0071-1.

Hou, T., C. H. Rinderknecht, A. V. Hadjinicolaou, R. Busch, and E. Mellins. 2013. Pulse–Chase Analysis for Studies of MHC Class II Biosynthesis, Maturation, and Peptide Loading. In Antigen Processing. P. van Endert, editor. Humana Press, Totowa, NJ. 411–432.

Houten, S. M., and R. J. A. Wanders. 2010. A general introduction to the biochemistry of mitochondrial fatty acid β-oxidation. *Journal of inherited metabolic disease* 33(5):469–477. doi:10.1007/s10545-010-9061-2.

Huisgen, R. 1963. Kinetics and Mechanism of 1,3-Dipolr Cycloadditions. *Angew. Chem. Int. Ed. Engl.* 2(11):633–645. doi:10.1002/anie.196306331.

Ipsen, D. H., J. Lykkesfeldt, and P. Tveden-Nyborg. 2018. Molecular mechanisms of hepatic lipid accumulation in non-alcoholic fatty liver disease. *Cell. Mol. Life Sci.* 75(18):3313–3327. doi:10.1007/s00018-018-2860-6.

Irshad, Z., F. Dimitri, M. Christian, and V. A. Zammit. 2017. Diacylglycerol acyltransferase 2 links glucose utilization to fatty acid oxidation in the brown adipocytes. *J. Lipid Res.* 58(1):15–30. doi:10.1194/jlr.M068197.

Iskandarov, U., J. E. Silva, H. J. Kim, M. Andersson, R. E. Cahoon, K. Mockaitis, and E. B. Cahoon. 2017. A Specialized Diacylglycerol Acyltransferase Contributes to the Extreme Medium-Chain Fatty Acid Content of Cuphea Seed Oil. *Plant physiology* 174(1):97–109. doi:10.1104/pp.16.01894.

Jornayvaz, F. R., and G. I. Shulman. 2012. Diacylglycerol activation of protein kinase Cε and hepatic insulin resistance. *Cell metabolism* 15(5):574–584. doi:10.1016/j.cmet.2012.03.005.

Kalhan, S. C., S. Mahajan, E. Burkett, L. Reshef, and R. W. Hanson. 2001. Glyceroneogenesis and the source of glycerol for hepatic triacylglycerol synthesis in humans. *The Journal of biological chemistry* 276(16):12928–12931. doi:10.1074/jbc.M006186200.

Karlsson, M., J. A. Contreras, U. Hellman, H. Tornqvist, and C. Holm. 1997. cDNA cloning, tissue distribution, and identification of the catalytic triad of monoglyceride lipase. Evolutionary relationship to esterases, lysophospholipases, and haloperoxidases. *The Journal of biological chemistry* 272(43):27218–27223. doi:10.1074/jbc.272.43.27218.

Kaytor, E. N., H.-m. Shih, and H. C. Towle. 1997. Carbohydrate Regulation of Hepatic Gene Expression. *The Journal of biological chemistry* 272(11):7525–7531. doi:10.1074/jbc.272.11.7525.

Kindt, A., G. Liebisch, T. Clavel, D. Haller, G. Hörmannsperger, H. Yoon, D. Kolmeder, A. Sigruener, S. Krautbauer, C. Seeliger, A. Ganzha, S. Schweizer, R. Morisset, T. Strowig, H. Daniel, D. Helm, B. Küster, J. Krumsiek, and J. Ecker. 2018. The gut microbiota promotes hepatic fatty acid desaturation and elongation in mice. *Nature communications* 9(1):3760. doi:10.1038/s41467-018-05767-4.

King, A. J., J. A. Segreti, K. J. Larson, A. J. Souers, P. R. Kym, R. M. Reilly, C. A. Collins, M. J. Voorbach, G. Zhao, S. W. Mittelstadt, and B. F. Cox. 2010. In vivo efficacy of acyl CoA: diacylglycerol acyltransferase (DGAT) 1 inhibition in rodent models of postprandial hyperlipidemia. *European journal of pharmacology* 637(1-3):155–161. doi:10.1016/j.ejphar.2010.03.056.

Kiorpes, T. C., D. Hoerr, W. Ho, L. E. Weaner, M. G. Inman, and G. F. Tutwiler. 1984. Identification of 2-tetradecylglycidyl coenzyme A as the active form of methyl 2-tetradecylglycidate (methyl palmoxirate) and its characterization as an irreversible, active site-directed inhibitor of carnitine palmitoyltransferase A in isolated rat liver mitochondria. *The Journal of biological chemistry* 259(15):9750–9755.

Klizaite, K. 2017. Medium-chain fatty acid metabolism in hepatocytes and adipocytes. Universitäts- und Landesbibliothek Bonn, Bonn. Online-Ressource.

Kohjima, M., M. Enjoji, N. Higuchi, M. Kato, K. Kotoh, T. Yoshimoto, T. Fujino, M. Yada, R. Yada, N. Harada, R. Takayanagi, and M. Nakamuta. 2007. Re-evaluation of fatty acid metabolism-related gene expression in nonalcoholic fatty liver disease. *International journal of molecular medicine* 20(3):351–358.

Kraemer, F. B., and W.-J. Shen. 2002. Hormone-sensitive lipase: control of intracellular tri-(di-)acylglycerol and cholesteryl ester hydrolysis. *J. Lipid Res.* 43(10):1585–1594. doi:10.1194/jlr.R200009-JLR200.

Kuerschner, L., C. Moessinger, and C. Thiele. 2008. Imaging of lipid biosynthesis: how a neutral lipid enters lipid droplets. *Traffic (Copenhagen, Denmark)* 9(3):338–352. doi:10.1111/j.1600-0854.2007.00689.x.

Lardizabal, K. D., J. T. Mai, N. W. Wagner, A. Wyrick, T. Voelker, and D. J. Hawkins. 2001. DGAT2 is a new diacylglycerol acyltransferase gene family: purification, cloning, and expression in insect cells of two polypeptides from Mortierella ramanniana with diacylglycerol acyltransferase activity. *The Journal of biological chemistry* 276(42):38862–38869. doi:10.1074/jbc.M106168200.

Lass, A., R. Zimmermann, M. Oberer, and R. Zechner. 2011. Lipolysis - a highly regulated multi-enzyme complex mediates the catabolism of cellular fat stores. *Progress in lipid research* 50(1):14–27. doi:10.1016/j.plipres.2010.10.004.

Lee, B., A. M. Fast, J. Zhu, J.-X. Cheng, and K. K. Buhman. 2010. Intestine-specific expression of acyl CoA:diacylglycerol acyltransferase 1 reverses resistance to diet-

induced hepatic steatosis and obesity in Dgat1-/- mice. *J. Lipid Res.* 51(7):1770–1780. doi:10.1194/jlr.M002311.

Li, C., L. Li, J. Lian, R. Watts, R. Nelson, B. Goodwin, and R. Lehner. 2015. Roles of Acyl-CoA:Diacylglycerol Acyltransferases 1 and 2 in Triacylglycerol Synthesis and Secretion in Primary Hepatocytes. *Arteriosclerosis, thrombosis, and vascular biology* 35(5):1080–1091. doi:10.1161/ATVBAHA.114.304584.

Marten, B., M. Pfeuffer, and J. Schrezenmeir. 2006. Medium-chain triglycerides. *International Dairy Journal* 16(11):1374–1382. doi:10.1016/j.idairyj.2006.06.015.

Mayorek, N., and J. Bar-Tana. 1983. Medium chain fatty acids as specific substrates for diglyceride acyltransferase in cultured hepatocytes. *The Journal of biological chemistry* 258(11):6789–6792.

McCarty, M. F., and J. J. DiNicolantonio. 2016. Lauric acid-rich medium-chain triglycerides can substitute for other oils in cooking applications and may have limited pathogenicity. *Open heart* 3(2):e000467. doi:10.1136/openhrt-2016-000467.

McGarry, J. D., and N. F. Brown. 1997. The mitochondrial carnitine palmitoyltransferase system. From concept to molecular analysis. *European journal of biochemistry* 244(1):1–14. doi:10.1111/j.1432-1033.1997.00001.x.

McLaren, D. G., S. Han, B. A. Murphy, L. Wilsie, S. J. Stout, H. Zhou, T. P. Roddy, J. N. Gorski, D. E. Metzger, M. K. Shin, D. F. Reilly, H. H. Zhou, M. Tadin-Strapps, S. R. Bartz, A.-M. Cumiskey, T. H. Graham, D.-M. Shen, K. O. Akinsanya, S. F. Previs, J. E. Imbriglio, and S. Pinto. 2018. DGAT2 Inhibition Alters Aspects of Triglyceride Metabolism in Rodents but Not in Non-human Primates. *Cell metabolism* 27(6):1236-1248.e6. doi:10.1016/j.cmet.2018.04.004.

Merrill, C. L., H. Ni, L. W. Yoon, M. A. Tirmenstein, P. Narayanan, G. R. Benavides, M. J. Easton, D. R. Creech, C. X. Hu, D. C. McFarland, L. M. Hahn, H. C. Thomas, and K. T. Morgan. 2002. Etomoxir-induced oxidative stress in HepG2 cells detected by differential gene expression is confirmed biochemically. *Toxicological sciences an official journal of the Society of Toxicology* 68(1):93–101. doi:10.1093/toxsci/68.1.93.

Metges, C. C., and G. Wolfram. 1991. Medium- and long-chain triglycerides labeled with 13C: a comparison of oxidation after oral or parenteral administration in humans. *The Journal of nutrition* 121(1):31–36. doi:10.1093/jn/121.1.31.

Mørkholt, A. S., O. Wiborg, J. G. K. Nieland, S. Nielsen, and J. D. Nieland. 2017. Blocking of carnitine palmitoyl transferase 1 potently reduces stress-induced depression in rat highlighting a pivotal role of lipid metabolism. *Scientific reports* 7(1):2158. doi:10.1038/s41598-017-02343-6.

Mumme, K., and W. Stonehouse. 2015. Effects of medium-chain triglycerides on weight loss and body composition: a meta-analysis of randomized controlled trials. *Journal of the Academy of Nutrition and Dietetics* 115(2):249–263. doi:10.1016/j.jand.2014.10.022.

O'Connor, R. S., L. Guo, S. Ghassemi, N. W. Snyder, A. J. Worth, L. Weng, Y. Kam, B. Philipson, S. Trefely, S. Nunez-Cruz, I. A. Blair, C. H. June, and M. C. Milone. 2018. The CPT1a inhibitor, etomoxir induces severe oxidative stress at commonly used concentrations. *Scientific reports* 8(1):6289. doi:10.1038/s41598-018-24676-6.

Odle, J., N. J. Benevenga, and T. D. Crenshaw. 1991. Utilization of medium-chain triglycerides by neonatal piglets: chain length of even- and odd-carbon fatty acids and apparent digestion/absorption and hepatic metabolism. *The Journal of nutrition* 121(5):605–614. doi:10.1093/jn/121.5.605.

Pande, S. V. 1975. A mitochondrial carnitine acylcarnitine translocase system. *Proceedings of the National Academy of Sciences of the United States of America* 72(3):883–887. doi:10.1073/pnas.72.3.883.

Papamandjaris, A. A., D. E. MacDougall, and P. J. Jones. 1998. Medium chain fatty acid metabolism and energy expenditure: obesity treatment implications. *Life sciences* 62(14):1203–1215. doi:10.1016/s0024-3205(97)01143-0.

Park, B. S., D. H. Song, H. M. Kim, B.-S. Choi, H. Lee, and J.-O. Lee. 2009. The structural basis of lipopolysaccharide recognition by the TLR4-MD-2 complex. *Nature* 458(7242):1191–1195. doi:10.1038/nature07830.

Parks, E. J., and M. K. Hellerstein. 2006. Thematic review series: patient-oriented research. Recent advances in liver triacylglycerol and fatty acid metabolism using stable isotope labeling techniques. *Journal of lipid research* 47(8):1651–1660. doi:10.1194/jlr.R600018-JLR200.

Pégorier, J. P., P. H. Duée, C. Herbin, P. Y. Laulan, C. Bladé, J. Peret, and J. Girard. 1988. Fatty acid metabolism in hepatocytes isolated from rats adapted to high-fat diets containing long- or medium-chain triacylglycerols. *The Biochemical journal* 249(3):801–806. doi:10.1042/bj2490801.

Piotrowitz, K. 2016. Regulation des Lipidmetabolismus in Hepatozyten. Universitäts- und Landesbibliothek Bonn, Bonn.

Qi, J., W. Lang, J. G. Geisler, P. Wang, I. Petrounia, S. Mai, C. Smith, H. Askari, G. T. Struble, R. Williams, S. Bhanot, B. P. Monia, S. Bayoumy, E. Grant, G. W. Caldwell, M. J. Todd, Y. Liang, M. D. Gaul, K. T. Demarest, and M. A. Connelly. 2012. The use of stable isotope-labeled glycerol and oleic acid to differentiate the hepatic functions of DGAT1 and -2. *Journal of lipid research* 53(6):1106–1116. doi:10.1194/jlr.M020156.

Qi, J., W. Lang, E. Giardino, G. W. Caldwell, C. Smith, L. K. Minor, A. L. Darrow, G. Willemsens, K. Dewaepenaert, P. Roevens, J. T. M. Linders, Y. Liang, and M. A.

Connelly. 2010. High-content assays for evaluating cellular and hepatic diacylglycerol acyltransferase activity. *J. Lipid Res.* 51(12):3559–3567. doi:10.1194/jlr.D008029.

Qu, Q., F. Zeng, X. Liu, Q. J. Wang, and F. Deng. 2016. Fatty acid oxidation and carnitine palmitoyltransferase I: emerging therapeutic targets in cancer. *Cell death & disease* 7:e2226. doi:10.1038/cddis.2016.132.

Raud, B., D. G. Roy, A. S. Divakaruni, T. N. Tarasenko, R. Franke, E. H. Ma, B. Samborska, W. Y. Hsieh, A. H. Wong, P. Stüve, C. Arnold-Schrauf, M. Guderian, M. Lochner, S. Rampertaap, K. Romito, J. Monsale, M. Brönstrup, S. J. Bensinger, A. N. Murphy, P. J. McGuire, R. G. Jones, T. Sparwasser, and L. Berod. 2018. Etomoxir Actions on Regulatory and Memory T Cells Are Independent of Cpt1a-Mediated Fatty Acid Oxidation. *Cell metabolism* 28(3):504-515.e7. doi:10.1016/j.cmet.2018.06.002.

Reddy, J. K., and T. Hashimoto. 2001. Peroxisomal beta-oxidation and peroxisome proliferator-activated receptor alpha: an adaptive metabolic system. *Annu. Rev. Nutr.* 21:193–230. doi:10.1146/annurev.nutr.21.1.193.

Reue, K. 2009. The lipin family: mutations and metabolism. *Current opinion in lipidology* 20(3):165–170. doi:10.1097/MOL.0b013e32832adee5.

Rigouin, C., C. Croux, V. Borsenberger, M. Ben Khaled, T. Chardot, A. Marty, and F. Bordes. 2018. Increasing medium chain fatty acids production in Yarrowia lipolytica by metabolic engineering. *Microbial cell factories* 17(1):142. doi:10.1186/s12934-018-0989-5.

Rittenberg, D., and R. Schoenheimer. 1937. Deuterium as an indicator in the study of intermediary metabolism. 11. Further studies on the biological uptake of deuterium into organic substances, with special reference to fat and cholesterol formation. *The Journal of biological chemistry*(Vol. 121):pp.235-253.

Ross, P. L., Y. N. Huang, J. N. Marchese, B. Williamson, K. Parker, S. Hattan, N. Khainovski, S. Pillai, S. Dey, S. Daniels, S. Purkayastha, P. Juhasz, S. Martin, M. Bartlet-Jones, F. He, A. Jacobson, and D. J. Pappin. 2004. Multiplexed Protein Quantitation in Saccharomyces cerevisiae Using Amine-reactive Isobaric Tagging Reagents. *Mol Cell Proteomics* 3(12):1154–1169. doi:10.1074/mcp.M400129-MCP200.

Rostovtsev, V. V., L. G. Green, V. V. Fokin, and K. B. Sharpless. 2002. A Stepwise Huisgen Cycloaddition Process: Copper(I)-Catalyzed Regioselective “Ligation” of Azides and Terminal Alkynes. *Angew. Chem. Int. Ed. Engl.* 41(14):2596–2599. doi:10.1002/1521-3773(20020715)41:14<2596:AID-ANIE2596>3.0.CO;2-4.

Schwudke, D., K. Schuhmann, R. Herzog, S. R. Bornstein, and A. Shevchenko. 2011. Shotgun lipidomics on high resolution mass spectrometers. *Cold Spring Harbor perspectives in biology* 3(9):a004614. doi:10.1101/cshperspect.a004614.

Selby, P. L., and H.S. A. Sherratt. 1989. Substituted 2-oxiranecarboxylic acids: a new group of candidate hypoglycaemic drugs. *Trends in Pharmacological Sciences* 10(12):495–500. doi:10.1016/0165-6147(89)90049-7.

Shi, Y., and D. Cheng. 2009. Beyond triglyceride synthesis: the dynamic functional roles of MGAT and DGAT enzymes in energy metabolism. *American journal of physiology. Endocrinology and metabolism* 297(1):E10-8. doi:10.1152/ajpendo.90949.2008.

Sletten, E. M., and C. R. Bertozzi. 2009. Bioorthogonal chemistry: fishing for selectivity in a sea of functionality. *Angewandte Chemie (International ed. in English)* 48(38):6974–6998. doi:10.1002/anie.200900942.

Smith, S. J., S. Cases, D. R. Jensen, H. C. Chen, E. Sande, B. Tow, D. A. Sanan, J. Raber, R. H. Eckel, and R. V. Farese. 2000. Obesity resistance and multiple mechanisms of triglyceride synthesis in mice lacking Dgat. *Nature Genetics* 25(1):87–90. doi:10.1038/75651.

Soares, J.-B., P. Pimentel-Nunes, R. Roncon-Albuquerque, and A. Leite-Moreira. 2010. The role of lipopolysaccharide/toll-like receptor 4 signaling in chronic liver diseases. *Hepatology international* 4(4):659–672. doi:10.1007/s12072-010-9219-x.

Stein, O., and Y. Stein. 1967. Lipid synthesis, intracellular transport, storage, and secretion. I. Electron microscopic radioautographic study of liver after injection of tritiated palmitate or glycerol in fasted and ethanol-treated rats. *The Journal of Cell Biology* 33(2):319–339. doi:10.1083/jcb.33.2.319.

Stoeckman, A. K., and H. C. Towle. 2002. The Role of SREBP-1c in Nutritional Regulation of Lipogenic Enzyme Gene Expression. *The Journal of biological chemistry* 277(30):27029–27035. doi:10.1074/jbc.M202638200.

Stone, S. J., M. C. Levin, and R. V. Farese. 2006. Membrane topology and identification of key functional amino acid residues of murine acyl-CoA:diacylglycerol acyltransferase-2. *The Journal of biological chemistry* 281(52):40273–40282. doi:10.1074/jbc.M607986200.

Stone, S. J., M. C. Levin, P. Zhou, J. Han, T. C. Walther, and R. V. Farese. 2009. The endoplasmic reticulum enzyme DGAT2 is found in mitochondria-associated membranes and has a mitochondrial targeting signal that promotes its association with mitochondria. *The Journal of biological chemistry* 284(8):5352–5361. doi:10.1074/jbc.M805768200.

Stone, S. J., H. M. Myers, S. M. Watkins, B. E. Brown, K. R. Feingold, P. M. Elias, and R. V. Farese. 2004. Lipopenia and skin barrier abnormalities in DGAT2-deficient mice. *The Journal of biological chemistry* 279(12):11767–11776. doi:10.1074/jbc.M311000200.

Takeuchi, K., and K. Reue. 2009. Biochemistry, physiology, and genetics of GPAT, AGPAT, and lipin enzymes in triglyceride synthesis. *American journal of physiology. Endocrinology and metabolism* 296(6):E1195-209. doi:10.1152/ajpendo.90958.2008.

Thiele, C., C. Papan, D. Hoelper, K. Kusserow, A. Gaebler, M. Schoene, K. Piotrowitz, D. Lohmann, J. Spandl, A. Stevanovic, A. Shevchenko, and L. Kuerschner. 2012. Tracing fatty acid metabolism by click chemistry. *ACS chemical biology* 7(12):2004–2011. doi:10.1021/cb300414v.

Thiele, C., K. Wunderling, and P. Leyendecker. 2019. Multiplexed and single cell tracing of lipid metabolism. *Nat Methods* 7:2004. doi:10.1038/s41592-019-0593-6.

Thompson, A., J. Schäfer, K. Kuhn, S. Kienle, J. Schwarz, G. Schmidt, T. Neumann, and C. Hamon. 2003. Tandem Mass Tags: A Novel Quantification Strategy for Comparative Analysis of Complex Protein Mixtures by MS/MS. *Anal. Chem.* 75(8):1895–1904. doi:10.1021/ac0262560.

Tornøe, C. W., C. Christensen, and M. Meldal. 2002. Peptidotriazoles on solid phase: 1,2,3-triazoles by regiospecific copper(i)-catalyzed 1,3-dipolar cycloadditions of terminal alkynes to azides. *The Journal of organic chemistry* 67(9):3057–3064. doi:10.1021/jo011148j.

Turnbull, D. M., K. Bartlett, S. I.M. Younan, and H.S. A. Sherratt. 1984. The effects of 2{5(4-chlorophenyl) pentyl}oxirane-2-carbonyl-CoA on mitochondrial oxidations. *Biochemical Pharmacology* 33(3):475–481. doi:10.1016/0006-2952(84)90243-0.

Uchida, A., M. N. Slipchenko, T. Eustaquio, J. F. Leary, J.-X. Cheng, and K. K. Buhman. 2013. Intestinal acyl-CoA:diacylglycerol acyltransferase 2 overexpression enhances postprandial triglyceridemic response and exacerbates high fat diet-induced hepatic triacylglycerol storage. *Biochimica et biophysica acta* 1831(8):1377–1385. doi:10.1016/j.bbalip.2013.04.013.

Unger, R. H. 2002. Lipotoxic Diseases. *Annu. Rev. Med.* 53(1):319–336. doi:10.1146/annurev.med.53.082901.104057.

van Rijn, J. M., R. C. Ardy, Z. Kuloğlu, B. Härter, D. Y. van Haaften-Visser, H. P. J. van der Doef, M. van Hoesel, A. Kansu, A. H. M. van Vugt, M. Thian, F. T. M. Kokke, A. Krolo, M. K. Başaran, N. G. Kaya, A. Ü. Aksu, B. Dalgıç, F. Ozcay, Z. Baris, R. Kain, E. C. A. Stigter, K. D. Lichtenbelt, M. P. G. Massink, K. J. Duran, J. B. G. M. Verheij, D. Lugtenberg, P. G. J. Nikkels, H. G. F. Brouwer, H. J. Verkade, R. Scheenstra, B. Spee, E. E. S. Nieuwenhuis, P. J. Coffer, A. R. Janecke, G. van Haaften, R. H. J. Houwen, T. Müller, S. Middendorp, and K. Boztug. 2018. Intestinal Failure and Aberrant Lipid Metabolism in Patients With DGAT1 Deficiency. *Gastroenterology* 155(1):130-143.e15. doi:10.1053/j.gastro.2018.03.040.

Villanueva, C. J., M. Monetti, M. Shih, P. Zhou, S. M. Watkins, S. Bhanot, and R. V. Farese. 2009. Specific role for acyl CoA:Diacylglycerol acyltransferase 1 (Dgat1) in hepatic steatosis due to exogenous fatty acids. *Hepatology (Baltimore, Md.)* 50(2):434–442. doi:10.1002/hep.22980.

Violante, S., L. Ijlst, H. Te Brinke, J. Koster, I. Tavares de Almeida, R. J. A. Wanders, F. V. Ventura, and S. M. Houten. 2013. Peroxisomes contribute to the acylcarnitine production when the carnitine shuttle is deficient. *Biochimica et biophysica acta* 1831(9):1467–1474. doi:10.1016/j.bbalip.2013.06.007.

Watkins, P. A., D. Maiguel, Z. Jia, and J. Pevsner. 2007. Evidence for 26 distinct acyl-coenzyme A synthetase genes in the human genome. *J. Lipid Res.* 48(12):2736–2750. doi:10.1194/jlr.M700378-JLR200.

Watt, M. J., and G. R. Steinberg. 2008. Regulation and function of triacylglycerol lipases in cellular metabolism. *The Biochemical journal* 414(3):313–325. doi:10.1042/BJ20080305.

Wilfling, F., H. Wang, J. T. Haas, N. Krahmer, T. J. Gould, A. Uchida, J.-X. Cheng, M. Graham, R. Christiano, F. Fröhlich, X. Liu, K. K. Buhman, R. A. Coleman, J. Bewersdorf, R. V. Farese, and T. C. Walther. 2013. Triacylglycerol synthesis enzymes mediate lipid droplet growth by relocalizing from the ER to lipid droplets. *Developmental cell* 24(4):384–399. doi:10.1016/j.devcel.2013.01.013.

Wolf, H. P. 1992. Possible new therapeutic approach in diabetes mellitus by inhibition of carnitine palmitoyltransferase 1 (CPT1). *Hormone and metabolic research. Supplement series* 26:62–67.

Wurie, H. R., L. Buckett, and V. A. Zammit. 2011. Evidence that diacylglycerol acyltransferase 1 (DGAT1) has dual membrane topology in the endoplasmic reticulum of HepG2 cells. *The Journal of biological chemistry* 286(42):36238–36247. doi:10.1074/jbc.M111.251900.

Wurie, H. R., L. Buckett, and V. A. Zammit. 2012. Diacylglycerol acyltransferase 2 acts upstream of diacylglycerol acyltransferase 1 and utilizes nascent diglycerides and de novo synthesized fatty acids in HepG2 cells. *The FEBS journal* 279(17):3033–3047. doi:10.1111/j.1742-4658.2012.08684.x.

Xu, F. Y., W. A. Taylor, J. A. Hurd, and G. M. Hatch. 2003. Etomoxir mediates differential metabolic channeling of fatty acid and glycerol precursors into cardiolipin in H9c2 cells. *J. Lipid Res.* 44(2):415–423. doi:10.1194/jlr.M200335-JLR200.

Yamashita, A., Y. Hayashi, N. Matsumoto, Y. Nemoto-Sasaki, S. Oka, T. Tanikawa, and T. Sugiura. 2014. Glycerophosphate/Acylglycerophosphate acyltransferases. *Biology* 3(4):801–830. doi:10.3390/biology3040801.

Yao, C.-H., G.-Y. Liu, R. Wang, S. H. Moon, R. W. Gross, and G. J. Patti. 2018. Identifying off-target effects of etomoxir reveals that carnitine palmitoyltransferase I is essential for cancer cell proliferation independent of β-oxidation. *PLoS biology* 16(3):e2003782. doi:10.1371/journal.pbio.2003782.

Yao, Z., H. Zhou, D. Figeys, Y. Wang, and M. Sundaram. 2013. Microsome-associated lumenal lipid droplets in the regulation of lipoprotein secretion. *Current opinion in lipidology* 24(2):160–170. doi:10.1097/MOL.0b013e32835aebe7.

Yeaman, S. J. 1990. Hormone-sensitive lipase--a multipurpose enzyme in lipid metabolism. *Biochimica et biophysica acta* 1052(1):128–132. doi:10.1016/0167-4889(90)90067-n.

Yen, C.-L. E., C. H. Brown, M. Monetti, and R. V. Farese. 2005a. A human skin multifunctional O-acyltransferase that catalyzes the synthesis of acylglycerols, waxes, and retinyl esters. *J. Lipid Res.* 46(11):2388–2397. doi:10.1194/jlr.M500168-JLR200.

Yen, C.-L. E., M. Monetti, B. J. Burri, and R. V. Farese. 2005b. The triacylglycerol synthesis enzyme DGAT1 also catalyzes the synthesis of diacylglycerols, waxes, and retinyl esters. *J. Lipid Res.* 46(7):1502–1511. doi:10.1194/jlr.M500036-JLR200.

Yen, C.-L. E., D. W. Nelson, and M.-I. Yen. 2015. Intestinal triacylglycerol synthesis in fat absorption and systemic energy metabolism. *J. Lipid Res.* 56(3):489–501. doi:10.1194/jlr.R052902.

Yen, C.-L. E., S. J. Stone, S. Cases, P. Zhou, and R. V. Farese. 2002. Identification of a gene encoding MGAT1, a monoacylglycerol acyltransferase. *Proceedings of the National Academy of Sciences of the United States of America* 99(13):8512–8517. doi:10.1073/pnas.132274899.

Yen, C.-L. E., S. J. Stone, S. Koliwad, C. Harris, and R. V. Farese. 2008. Thematic review series: glycerolipids. DGAT enzymes and triacylglycerol biosynthesis. *Journal of lipid research* 49(11):2283–2301. doi:10.1194/jlr.R800018-JLR200.

Yotsumoto, T., T. Naitoh, M. Kitahara, and N. Tsuruzoe. 2000. Effects of carnitine palmitoyltransferase I inhibitors on hepatic hypertrophy. *European journal of pharmacology* 398(2):297–302. doi:10.1016/s0014-2999(00)00288-0.

You, Y.-Q. N., P.-R. Ling, J. Z. Qu, and B. R. Bistrian. 2008. Effects of medium-chain triglycerides, long-chain triglycerides, or 2-monododecanoin on fatty acid composition in the portal vein, intestinal lymph, and systemic circulation in rats. *JPEN. Journal of parenteral and enteral nutrition* 32(2):169–175. doi:10.1177/0148607108314758.

Yu, S., J. H. Choi, H. J. Kim, S. H. Park, G.-W. Go, and W. Kim. 2017. In Vitro Evidence of Anti-Inflammatory and Anti-Obesity Effects of Medium-Chain Fatty Acid-Diacylglycerols. *Journal of microbiology and biotechnology* 27(9):1617–1627. doi:10.4014/jmb.1703.03071.

Zhang, X.-d., J.-w. Yan, G.-r. Yan, X.-y. Sun, J. Ji, Y.-m. Li, Y.-h. Hu, and H.-y. Wang. 2010. Pharmacological inhibition of diacylglycerol acyltransferase 1 reduces body weight gain, hyperlipidemia, and hepatic steatosis in db/db mice. *Acta pharmacologica Sinica* 31(11):1470–1477. doi:10.1038/aps.2010.104.

Zimmermann, R., J. G. Strauss, G. Haemmerle, G. Schoiswohl, R. Birner-Gruenberger, M. Riederer, A. Lass, G. Neuberger, F. Eisenhaber, A. Hermetter, and R. Zechner. 2004. Fat mobilization in adipose tissue is promoted by adipose triglyceride lipase. *Science (New York, N.Y.)* 306(5700):1383–1386. doi:10.1126/science.1100747.

9. Table of figures

Figure 1: Schematic representation of the digestion and absorption process of dietary MCTs and LCTs ..... - 6 -

Figure 2: Schematic overview on the pathways involved in TAG synthesis..... - 12 -

Figure 3: Schematic visualization of the Cu(I) catalyzed click reaction. ..... - 14 -

Figure 4: Schematic visualization of the workflow used to trace lipid metabolism with alkyne labeled fatty acids ..... - 15 -

Figure 5: Structure, click reaction and fragmentation pattern of the compound C171. .. - 17 -

Figure 6: Structures (A) and biological application (B) of the isobarically labeled C171 compounds for multiplex analysis..... - 18 -

Figure 7: Structure of alkyne labeled lipids used for metabolic tracing..... - 25 -

Figure 8: Structure of triacylglycerol labeled with alkyne palmitate (C17:2)..... - 26 -

Figure 9: Schematic visualization of the experimental design, used in the pulse and pulse-chase experiments..... - 35 -

Figure 10: Analysis of aTAGs upon DGAT inhibition in primary hepatocytes, pulsed with either C11- or C19-fatty acids..... - 42 -

Figure 11: Analysis of aTAGs upon DGAT inhibition in primary hepatocytes, co-pulsed with C11- and C19-fatty acids..... - 43 -

Figure 12: Analysis of aTAGs upon DGAT1 inhibitor-, and Etomoxir-treatment in primary hepatocytes, co-pulsed with C11- and C19-fatty acids..... - 44 -

Figure 13: Analysis of aTAGs upon DGAT2 inhibitor-, and Etomoxir-treatment in primary hepatocytes, co-pulsed with C11- and C19-fatty acids..... - 45 -

Figure 14: Analysis of aTAGs upon DGAT1 inhibitor-, and Etomoxir-treatment in primary hepatocytes, co-pulsed with C11- and C17:2-fatty acids..... - 46 -

Figure 15: Analysis of aTAGs upon DGAT2 inhibitor-, and Etomoxir-treatment in primary hepatocytes, co-pulsed with C11- and C17:2-fatty acids..... - 47 -

Figure 16: Analysis of C11-TAG in primary hepatocytes simultaneously co-pulsed with C11-fatty acid and Etomoxir ..... - 48 -

Figure 17: Relative amounts (mol per mille) of alkyne-labeled TAG (A), DAG (B), PC (C) and PA (D) species..... - 50 -

Figure 18: Absolute amounts of aTAG species isolated from WT mice ..... - 52 -

Figure 19: DGAT1-dependent incorporation of decanoic acid into aDAG species in hepatocytes ..... - 54 -

Figure 20: Absolute amounts of alkyne-labeled lipid classes from primary hepatocytes ..... - 56 -

Figure 21: Absolute amounts of alkyne-labeled lipid species from primary hepatocytes ..... - 57 -

Figure 22: Fold change analysis of alkyne-labeled TAG (A) and DAG (B) based on relative amounts..... - 58 -

Figure 23: A: Detailed normalized fold change (NFC) analysis of alkyne-labeled TAG species..... - 59 -

Figure 24: Fold change analysis of alkyne-labeled TAG (A) and DAG (B) based on relative amounts ..... - 62 -

Figure 25: Detailed normalized fold change (NFC) analysis of alkyne-labeled TAG species from primary hepatocytes ..... - 63 -

Figure 26: Detailed normalized fold change (NFC) analysis of short chain (C41-C45) alkyne-labeled TAG species from primary hepatocytes ..... - 65 -

Figure 27: Analysis of aTAGs upon DGAT2 inhibitor-, and Etomoxir-treatment in primary hepatocytes from wildtype mice (A: WT) and mice lacking DGAT1 (B: ΔDGAT1) ..... - 66 -

Figure 28: Absolute amounts of alkyne-labeled lipid classes from primary hepatocytes, ... - 69 -

Figure 29: Absolute amounts of alkyne-labeled lipid species from primary hepatocytes ..... - 70 -

Figure 30: Fold change analysis alkyne-labeled TAG (A) and DAG (B) based on .... - 71 -

Figure 31: Analysis of aTAGs upon Etomoxir- and Teglicar-treatment in primary hepatocytes, co-pulsed with C11- and C19-fatty acids ..... - 73 -

Figure 32: Fold change analysis of alkyne-labeled TAG (A) and DAG (B) based on - 74 -

Figure 33: Absolute amounts of alkyne-labeled TAG species from primary hepatocytes ..... - 76 -

Figure 34: Absolute amounts of alkyne-labeled MCFA-aTAG (A) and LCFA-aTAG (B) species ..... - 77 -

Figure 35: Normalized fold change analysis of live cell OCR measurement..... - 78 -

Figure 36: Proposed functional model of DGAT1 and DGAT2 in metabolizing MCFAs .. - 87 -

10. Supplements

10.1. Validation of the MCFA-TAG effects with a different set of DGAT inhibitors

In a study on the roles of DGAT1 and 2 in primary hepatocytes on TAG synthesis and secretion, a different set of small-molecule DGAT inhibitors from the company Pfizer was used (Li et al., 2015) (see: Materials 3.4). In order to validate the effects of DGAT1 inhibition on MCFA-TAG levels, described in this study, some of the experiments were repeated with the inhibitor set from Pfizer, using the same concentrations as described in the mentioned study (Li et al., 2015).

In co-pulse experiments with C11- and C19-fatty acids for TLC detection, the DGAT1 inhibitor from Pfizer showed the same effect in accordance to the experiments done with the inhibitor A922500. Levels of C11-TAGs were significantly reduced with either the DGAT1 inhibitor alone, or even further reduced in combination with Etomoxir (Supplementary figure 1, B). Levels of C19-TAGs showed no significant changes upon the inhibitor treatments.

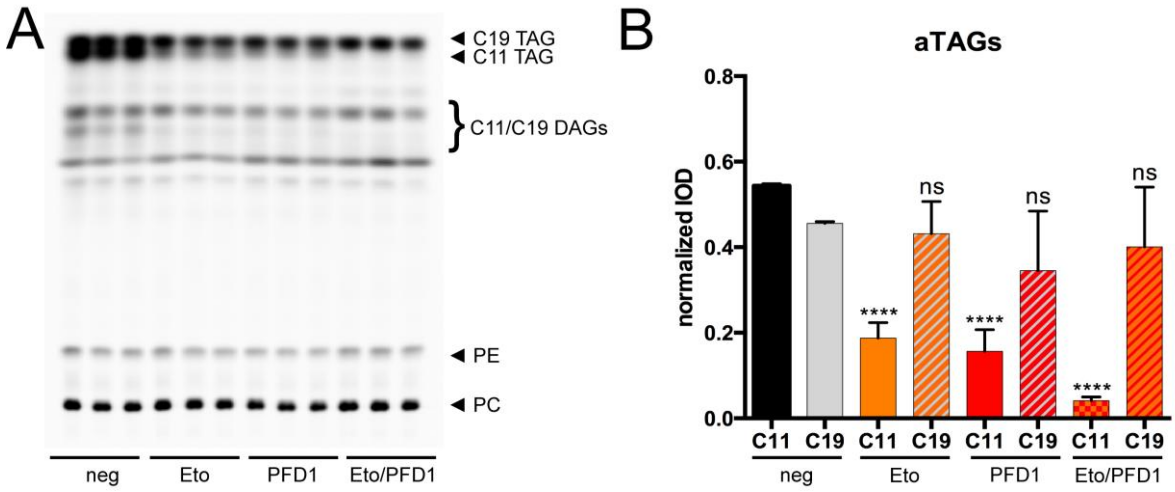

Supplementary figure 1: Analysis of aTAGs upon DGAT1 inhibitor- (from Pfizer), and Etomoxir-treatment in primary hepatocytes, co-pulsed with C11- and C19 fatty acids. After isolation, primary mouse liver hepatocytes were plated in 24 well plates with $7.5x10^4$ cells per well. Cells were preincubated with either 5 µM DGAT1-Inhibitor from Pfizer (PFD1), 50 µM Etomoxir (Eto) or a combination of both inhibitors (PFD1/Eto) for one hour, in comparison to the respective vehicle as a negative control. Cells were then pulsed for 1 hour with a combination of 50 µM C11- and 50 µM C19-fatty acid. The cells were washed, lipids were extracted and click reaction was performed. Finally, lipids were separated on a TLC plate and the signal was captured by fluorescent imaging (A). Panel B illustrates the normalized quantification of fluorescent intensities from C11 TAG (filled bars) and C19 TAG (hatched bars) upon either PFD1 (red), Etomoxir (orange) and combination of both (orange/red) inhibitors, in comparison to the negative controls (black: C11, grey: C19). The data represent mean ±SD for n=3 biological replicates. **** stands for p≤0.0001, ns=not significant.

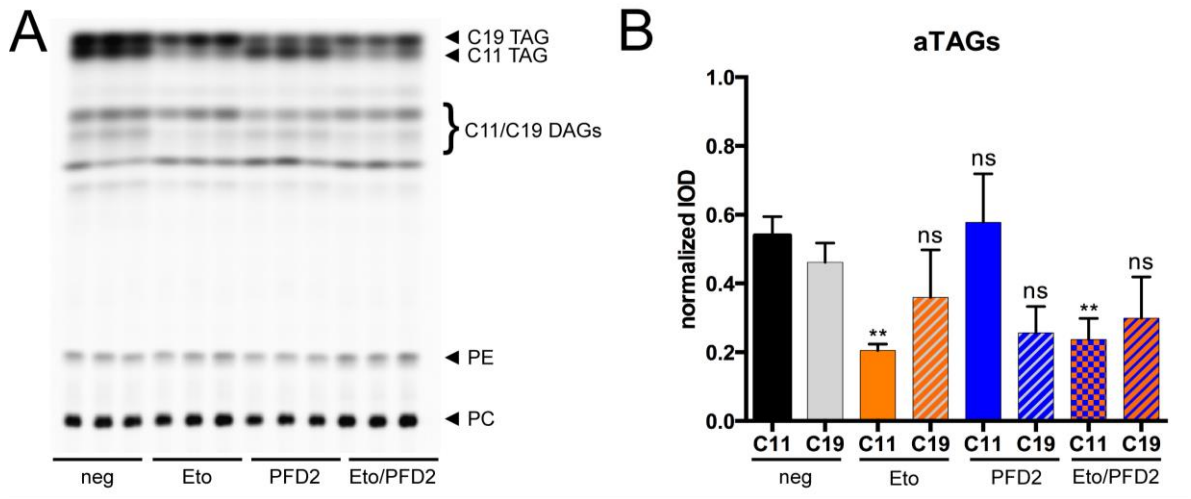

Supplementary figure 2: Analysis of aTAGs upon DGAT2 inhibitor- (from Pfizer), and Etomoxir-treatment in primary hepatocytes, co-pulsed with C11- and C19 fatty acids. After isolation, primary mouse liver hepatocytes were plated in 24 well plates with $7.5x10^4$ cells per well. Cells were preincubated with either 5 µM DGAT2-Inhibitor from Pfizer (PFD2), 50 µM Etomoxir (Eto) or a combination of both inhibitors (PFD2/Eto) for one hour, in comparison to the respective vehicle as a negative control. Cells were then pulsed for 1 hour with a combination of 50 µM C11- and 50 µM C19-fatty acid. The cells were washed, lipids were extracted and click reaction was performed. Finally, lipids were separated on a TLC plate and the signal was captured by fluorescent imaging (A). Panel B illustrates the normalized quantification of fluorescent intensities from C11 TAG (filled bars) and C19 TAG (hatched bars) upon either PFD2 (blue), Etomoxir (orange) and combination of both (orange/blue) inhibitors, in comparison to the negative controls (black: C11, grey: C19). The data represent mean ±SD for n=3 biological replicates. ** stands for p=0.0021, ns=not significant.

As in the experiments done with the DGAT2 inhibitor JNJ-DGAT2-A, a combination of the inhibitor PFD2 with Etomoxir in C11/C19 co-pulse experiments did not result in a complete reduction of C11-TAG levels (Supplementary figure 2).

These inhibitors were also used in a MS-based setup, like in the experiments shown in this thesis. Here, similar changes in the profile of aTAG and aDAG species upon inhibitor treatment, could be observed (data not shown).

The results from the experiments done with hepatocytes from DGAT1-K.O. mice are as well in favor of these findings. Here the DGAT1 inhibitor A922500 did not have any effect, while an inhibition of DGAT2 via the compound JNJ-DGAT-2-A alone, did lead to effects similar to those, were both inhibitors were combined. This was true for both MS and TLC experiments. This shows the immense substrate specificity of both inhibitors. Taken together, the validation using a different set of inhibitors against DGAT enzymes, leads to the conclusion, that the observed effects are indeed a result of the substrate specific inhibition of both DGAT1 and 2.

10.2. Supplementary data for chapter 5.3.1.

Supplementary figure 3 shows a lipid species resolution of all alkyne labeled DAGs after a 2-minute pulse of alkyne 100 µM alkyne palmitate. As already described in chapter 5.3.1, out of 18 detectable aDAG species, 79.4% of the whole class is formed from 4 major DAG species, consisting of alkyne palmitate (C17:2) in combination with either palmitic acid (C16:0), palmitoleic acid (C16:1), stearic acid (C18:0) or oleic acid (C18:1).

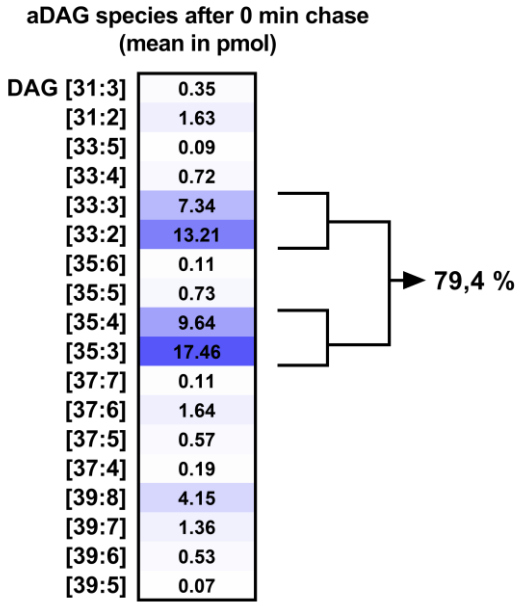

Supplementary figure 3: Absolute amounts of aDAG species isolated from WT mice, pulsed for 2 minutes with alkyne-palmitate. After isolation, primary mouse liver hepatocytes were plated in 24 well plates with $7.5x10^4$ cells per well. Cells were then pulsed with 100 µM alkyne palmitate (C17:2) for 2 minutes. Lipids were extracted with simultaneous addition of an internal standard mix for alkyne labeled lipids and click reaction with C175-XX reagents was performed. Multiplex samples were pooled and analyzed by MS. Mass signals were identified using LipidXplorer MFQL analysis with internal standard quantification for aTAG, aDAG, aPC, aPA, aCE and aCER. Absolute amounts of the lipid species are shown in pmol. The data represent mean ±SD for n=3 biological replicates. Percentage value of the four major aDAG species (DAG [33:3], [33:2], [35:4] and [35:3]) is presented as mean.

10.3. Double alkyne-labeled TAG

This chapter gives an overview on double alkyne-labeled triacylglycerol (dlTAG) species in comparison to their single-labeled counterparts. This is shown on the example of the dataset acquired form the DGAT1-K.O. mice (see: Chapter: 5.3.2.).

Supplementary figure 4 visualizes a double alkyne-palmitate (C17:2)-labeled triacylglycerol molecule.

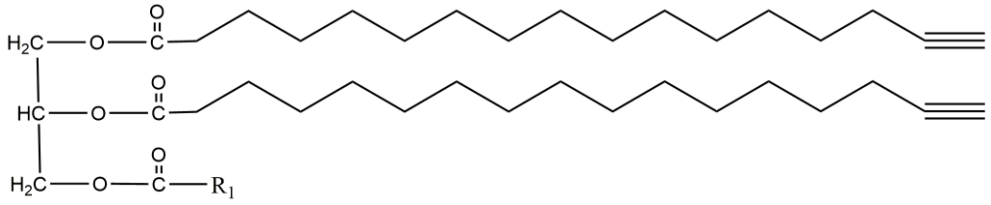

Supplementary figure 4: Structure of double alkyne-palmitate (C17:2)- labeled triacylglycerol. R_1 stands for any other fatty acid, incorporated into the molecule.

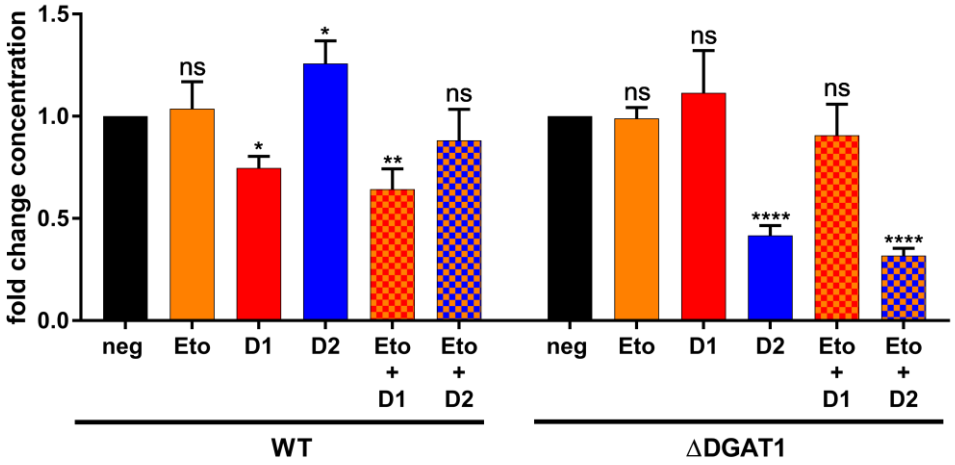

Supplementary figure 5: Fold change analysis of double alkyne-labeled TAG (dlTAG) based on relative amounts (mol per mille) from dlTAG and dlPC species from primary hepatocytes, isolated from wildtype mice (WT) or mice lacking DGAT1 (ΔDGAT1), treated with different inhibitor combinations, pulsed with alkyne-palmitate and decanoic acid. After isolation, primary mouse liver hepatocytes were plated in 24 well plates with $7.5x10^4$ cells per well. Cells were preincubated with either 50 µM Etomoxir (Eto), 3 µM DGAT1-Inhibitor (D1), 15 µM DGAT2-Inhibitor (D2) or combinations of Etomoxir with each DGAT-inhibitor (Eto+D1, Eto+D2). Cells were then co-pulsed with 50 µM alkyne palmitate (C17:2) and 50 µM decanoic acid (C10) for 1 hour. Lipids were extracted with simultaneous addition of an internal standard mix for alkyne labeled lipids and click reaction with C175-XX reagents was performed. Multiplex samples were pooled and analyzed by MS. Mass signals were identified using LipidXplorer MFQL analysis with internal standard quantification for dlTAG. Fold changes (FC) in relative concentrations (from mol per mille) of double labeled alkyne TAG for each inhibitor treatment were calculated by normalization to the negative control. The data represent mean ±SD for n=3 biological replicates. * stands for p≤0.0332, ** for p≤0.0021 and **** for p≤0.0001. ns=not significant. Isolation of hepatocytes and fatty acid pulse was done by CL, lipid extraction and MS/TLC analysis were done by KW.

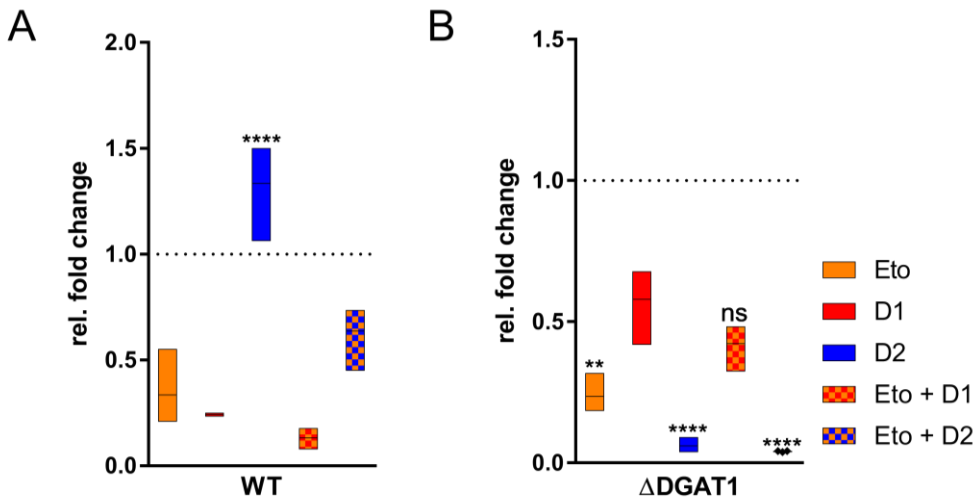

Supplementary figure 6: Detailed normalized fold change (NFC) analysis of double alkyne-labeled TAG with decanoic acid (dITAG [44:4]) from primary hepatocytes, isolated from mice lacking DGAT1, treated with inhibitor combinations and pulsed with alkyne-palmitate and decanoic acid. After isolation, primary mouse liver hepatocytes were plated in 24 well plates with $7.5x10^4$ cells per well. Cells were preincubated with either 50 µM Etomoxir (Eto), 3 µM DGAT1-Inhibitor (D1), 15 µM DGAT2-Inhibitor (D2) or combinations of Etomoxir with each DGAT-inhibitor (Eto+D1, Eto+D2). Cells were then co-pulsed with 50 µM alkyne palmitate (C17:2) and 50 µM decanoic acid (C10) for 1 hour. Lipids were extracted with simultaneous addition of an internal standard mix for alkyne labeled lipids and click reaction with C175-XX reagents was performed. Multiplex samples were pooled and analyzed by MS. Mass signals were identified using LipidXplorer MFQL analysis with internal standard quantification for dITAG. Normalized fold changes (NFC) in concentrations of each lipid species for each inhibitor treatment were calculated by normalization to the negative control and to the average class fold change. The data is represented as floating bars (min to max) with the line indicating the mean value. n=3 biological replicates. ** stands for p≤0.0021 and **** stands for p≤0.0001. ns= not significant. Isolation of hepatocytes and fatty acid pulse was done by CL, lipid extraction and MS/TLC analysis were done by KW.

In the following the results are briefly summarized. Etomoxir had no significant effect on overall dITAG levels, whereas both DGAT inhibitors did show effects like those shown with single labeled species (Supplementary figure 5, panel A). Nevertheless, effects on MCFA-aTAGs were similar both in WT and DGAT1$^{-/-}$ hepatocytes compared to the single labeled lipids. This is summarized in Supplementary figure 6, showing fold change analysis on the species dITAG [44:4], consisting of the two C17:2 and one C10-FA, representing the MCFA. Data analysis form the TLC-based experiment was only based on single labeled species. For comparability, the MS-based data presented in the results part of this thesis is only based on single-labeled species.

10.4. Internal standard validation

The validation of all measured intensities from the internal standards (IS) form the four lipid species which are presented in this work, shows the robustness of the MS system for aTAG and aDAG species. The intensities from all single measurements (n=540) were combined from all data sets presented in this thesis and a coefficient of variation was calculated.

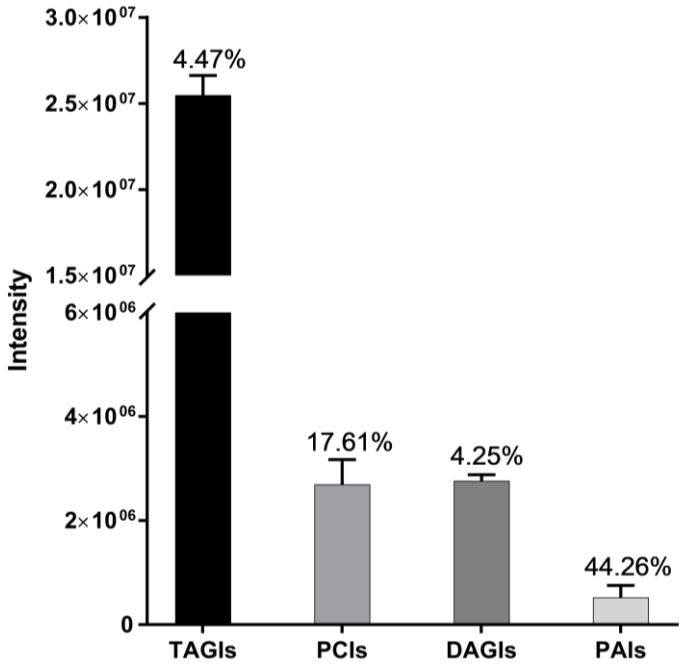

Supplementary figure 7: Intensities of the internal alkyne-labeled standards for the lipid species TAG, PC, DAG and PA with coefficient of variation (indicated percentage value). The bar graphs represent the measured intensities, combined form all experiments presented in this work. Values represent mean ±SD for n=6 experiment sets with a total sum of 540 single measured intensity values.

10.5. MFQL scripts

aCholesterol-ester-IS

```
QUERYNAME = multiCEIS;
DEFINE PR1 = 'C[53] H[89] D[4] N[4] O[2]' WITH CHG = 1;
DEFINE NL1 = 'C4 H11 N1' WITH CHG = 0;
DEFINE NL2 =  'C4 H9 D2 N1' WITH  CHG = 0;
DEFINE NL3 =  'C4 H8 D3 N1' WITH  CHG = 0;
DEFINE NL4 =  'C4 H7 D4 N1' WITH  CHG = 0;

IDENTIFY
PR1 IN MS1+
AND NL1 IN MS2+
AND NL2 IN MS2+
AND NL3 IN MS2+
AND NL4 IN MS2+

REPORT
NAME = "CE IS [%d:%d]" % ((PR1.chemsc[C] - 35), (PR1.chemsc[db] - 6.5));
MASS = PR1.mass;
chemsc = PR1.chemsc;
C = "%d" %  (PR1.chemsc[C] - 35);
db = "%d" %  (PR1.chemsc[db] - 6.5);
MASS = "%4.4f" % "(PR1.mass)";
ERROR = "%2.2f ppm" % "(PR1.errppm)";
ISpmol = 29.16;
INT73 = NL1.intensity;
INT75 = NL2.intensity;
INT76 = NL3.intensity;
INT77 = NL4.intensity; ;
```

aCholesterol-ester species

```
QUERYNAME = multiCE;
DEFINE PR1 = 'C[40..60] H[50..130] D[4] N[4] O[2]' WITH DBR = (3.5,15), CHG = 1;
DEFINE NL1 = 'C4 H11 N1' WITH CHG = 0;
DEFINE NL2 =  'C4 H9 D2 N1' WITH  CHG = 0;
DEFINE NL3 =  'C4 H8 D3 N1' WITH  CHG = 0;
DEFINE NL4 =  'C4 H7 D4 N1' WITH  CHG = 0;

IDENTIFY
PR1 IN MS1+
AND NL1 IN MS2+
AND NL2 IN MS2+
AND NL3 IN MS2+
AND NL4 IN MS2+

SUCHTHAT
isEven(PR1.chemsc[C])

REPORT
NAME = "CE [%d:%d]" % ((PR1.chemsc[C] - 35), (PR1.chemsc[db] - 6.5));
MASS = PR1.mass;
chemsc = PR1.chemsc;
C = "%d" %  (PR1.chemsc[C] - 35);
db = "%d" %  (PR1.chemsc[db] - 6.5);
MASS = "%4.4f" % "(PR1.mass)";
ERROR = "%2.2f ppm" % "(PR1.errppm)";
ISpmol = 29.16;
INT73 = NL1.intensity;
INT75 = NL2.intensity;
INT76 = NL3.intensity;
INT77 = NL4.intensity; ;
```

aCeraminde IS

```
QUERYNAME = multiCERIS;
DEFINE PR1 = 'C[44] H[80] D[4] N[5] O[3]' WITH CHG = 1;
DEFINE PR2 = 'C[44] H[80] D[4] N[5] O[3]' WITH CHG = 1;
DEFINE NL1 = 'C4 H11 N1' WITH CHG = 0;
DEFINE NL2 =  'C4 H9 D2 N1' WITH  CHG = 0;
DEFINE NL3 =  'C4 H8 D3 N1' WITH  CHG = 0;
DEFINE NL4 =  'C4 H7 D4 N1' WITH  CHG = 0;

IDENTIFY
PR1 IN MS1+
AND PR2 IN MS2+
AND NL1 IN MS2+
AND NL2 IN MS2+
AND NL3 IN MS2+
AND NL4 IN MS2+

SUCHTHAT
PR1.chemsc == PR2.chemsc

REPORT
NAME = "d18:1-Cer(%d:%d)" % ((PR1.chemsc[C] - 26),
(PR1.chemsc[db] - 3.5));
MASS = PR1.mass;
chemsc = PR1.chemsc;
C = "%d" %  (PR1.chemsc[C] - 26);
db = "%d" %  (PR1.chemsc[db] - 3.5);
MASS = "%4.4f" % "(PR1.mass)";
ERROR = "%2.2f ppm" % "(PR1.errppm)";
ISpmol = 8.43;
INT73 = NL1.intensity;
INT75 = NL2.intensity;
INT76 = NL3.intensity;
INT77 = NL4.intensity; ;
```

aCeraminde species

```
QUERYNAME =multiCER;
DEFINE PR1 ='C[39..70] H[50..130] D[4] N[5] O[3]' WITH DBR =
(4.5,10), CHG= 1;
DEFINE PR2  'C[39..70] H[50..130] D[4] N[5] O[3]' WITH DBR =
(4.5,10), CHG  1;
DEFINE NL1 = 'C4 H11 N1' WITH CHG = 0;
DEFINE NL2 =  'C4 H9 D2 N1' WITH  CHG = 0;
DEFINE NL3 =  'C4 H8 D3 N1' WITH  CHG = 0;
DEFINE NL4 =  'C4 H7 D4 N1' WITH  CHG = 0;

IDENTIFY
PR1 IN MS1
AND PR2 IN M2+
AND NL1 IN MS2+
AND NL2 IN MS2+
AND NL3 IN MS2+
AND NL4 IN MS2+

SUCHTHAT
isOdd(PR1.chemsc[C])
AND isEven(PR1.chemsc[H])
AND PR1.chemsc == PR2.chemsc

REPORT
NAME = "alkyne-d19:2-Cer(%d:%d)" % ((PR1.chemsc[C] - 27),
(PR1.chemsc[db] - 4.5));
MASS = PR1.mass;
chemsc = PR1.chemsc;
C = "%d" %  (PR1.chemsc[C] - 27);
db = "%d" %  (PR1.chemsc[db] - 4.5);
MASS = "%4.4f" % "(PR1.mass)";
ERROR = "%2.2f ppm" % "(PR1.errppm)";
ISpmol = 8.43;
INT73 = NL1.intensity;
INT75 = NL2.intensity;
INT76 = NL3.intensity;
INT77 = NL4.intensity; ;
```

aDiacylglycerol IS

```
QUERYNAME = multiDAGIS;
DEFINE PR1 = 'C[43] H[79] D[4] N[4] O[5]' WITH DBR = (3.5,15), CHG = 1;
DEFINE PR2 = 'C[43] H[79] D[4] N[4] O[5]' WITH DBR = (3.5,15), CHG = 1;
DEFINE NL1 = 'C4 H11 N1' WITH CHG = 0;
DEFINE NL2 =  'C4 H9 D2 N1' WITH  CHG = 0;
DEFINE NL3 =  'C4 H8 D3 N1' WITH  CHG = 0;
DEFINE NL4 =  'C4 H7 D4 N1' WITH  CHG = 0;

IDENTIFY
PR1 IN MS1+
AND PR2 IN MS2+
AND NL1 IN MS2+
AND NL2 IN MS2+
AND NL3 IN MS2+
AND NL4 IN MS2+

SUCHTHAT
 PR1.chemsc == PR2.chemsc

REPORT
NAME = "DAG [%d:%d]" % ((PR1.chemsc[C] - 11), (PR1.chemsc[db] - 2.5));
MASS = PR1.mass;
chemsc = PR1.chemsc;
C = "%d" %  (PR1.chemsc[C] - 11);
db = "%d" %  (PR1.chemsc[db] - 2.5);
MASS = "%4.4f" % "(PR1.mass)";
ERROR = "%2.2f ppm" % "(PR1.errppm)";
ISpmol = 16.7;
INT73 = NL1.intensity;
INT75 = NL2.intensity;
INT76 = NL3.intensity;
INT77 = NL4.intensity; ;
```

aDiacylglycerol species

```
QUERYNAME = multiDAG;
DEFINE PR1 = 'C[28..58] H[50..130] D[4] N[4] O[5]' WITH DBR = (3.5,15), CHG = 1;
DEFINE PR2 = 'C[28..58] H[50..130] D[4] N[4] O[5]' WITH DBR = (3.5,15), CHG = 1;
DEFINE NL1 = 'C4 H11 N1' WITH CHG = 0;
DEFINE NL2 =  'C4 H9 D2 N1' WITH  CHG = 0;
DEFINE NL3 =  'C4 H8 D3 N1' WITH  CHG = 0;
DEFINE NL4 =  'C4 H7 D4 N1' WITH  CHG = 0;

IDENTIFY
PR1 IN MS1+
AND PR2 IN MS2+
AND NL1 IN MS2+
AND NL2 IN MS2+
AND NL3 IN MS2+
AND NL4 IN MS2+

SUCHTHAT
isEven(PR1.chemsc[C])
AND isOdd(PR1.chemsc[H])
AND PR1.chemsc == PR2.chemsc

REPORT
NAME = "DAG [%d:%d]" % ((PR1.chemsc[C] - 11), (PR1.chemsc[db] - 2.5));
MASS = PR1.mass;
chemsc = PR1.chemsc;
C = "%d" %  (PR1.chemsc[C] - 11);
db = "%d" %  (PR1.chemsc[db] - 2.5);
MASS = "%4.4f" % "(PR1.mass)";
ERROR = "%2.2f ppm" % "(PR1.errppm)";
ISpmol = 16.7;
INT73 = NL1.intensity;
INT75 = NL2.intensity;
INT76 = NL3.intensity;
INT77 = NL4.intensity; ;
```

aPhosphatidic acid IS

```
QUERYNAME = multiPAIS;
DEFINE PR1 = 'C45 D4 H82 O8 N4 P1' WITH DBR = (2.5,15), CHG = 1;
DEFINE PR2 = 'C45 D4 H82 O8 N4 P1' WITH DBR = (2.5,15), CHG = 1;
DEFINE NL1 = 'C4 H14 P1 N1 O4' WITH CHG = 0;
DEFINE NL2 = 'C4 H12 D2 P1 N1 O4' WITH CHG = 0;
DEFINE NL3 = 'C4 H11 D3 P1 N1 O4' WITH CHG = 0;
DEFINE NL4 = 'C4 H10 D4 P1 N1 O4' WITH CHG = 0;

IDENTIFY
PR1 IN MS1+
AND PR2 IN MS2+
AND NL1 IN MS2+
AND NL2 IN MS2+
AND NL3 IN MS2+
AND NL4 IN MS2+

REPORT
NAME = "PA [%d:%d]" % ((PR1.chemsc[C] - 11), (PR1.chemsc[db] - 2.5));
MASS = PR1.mass;
chemsc = PR1.chemsc;
C = "%d" %  (PR1.chemsc[C] - 11);
db = "%d" %  (PR1.chemsc[db] - 2.5);
MASS = "%4.4f" % "(PR1.mass)";
ERROR = "%2.2f ppm" % "(PR1.errppm)";
ISpmol = 14.06;
INT73 = NL1.intensity;
INT75 = NL2.intensity;
INT76 = NL3.intensity;
INT77 = NL4.intensity; ;
```

aPhosphatidic acid species

```
QUERYNAME = multiPA;
DEFINE PR1 = 'C[36..60] H[50..130] D4 N[4] P[1] O[8]' WITH DBR = (0.5,15), CHG = 1;
DEFINE PR2 = 'C[36..60] H[50..130] D4 N[4] P[1] O[8]' WITH DBR = (0.5,15), CHG = 1;
DEFINE NL1 = 'C4 H14 P1 N1 O4' WITH CHG = 0;
DEFINE NL2 = 'C4 H12 D2 P1 N1 O4' WITH CHG = 0;
DEFINE NL3 = 'C4 H11 D3 P1 N1 O4' WITH CHG = 0;
DEFINE NL4 = 'C4 H10 D4 P1 N1 O4' WITH CHG = 0;

IDENTIFY
PR1 IN MS1+
AND PR2 IN MS2+
AND NL1 IN MS2+
AND NL2 IN MS2+
AND NL3 IN MS2+
AND NL4 IN MS2+

SUCHTHAT
isEven(PR1.chemsc[C])
AND isEven(PR1.chemsc[H])
AND PR1.chemsc == PR2.chemsc

REPORT
NAME = "PA [%d:%d]" % ((PR1.chemsc[C] - 11), (PR1.chemsc[db] - 2.5));
MASS = PR1.mass;
chemsc = PR1.chemsc;
C = "%d" %  (PR1.chemsc[C] - 11);
db = "%d" %  (PR1.chemsc[db] - 2.5);
MASS = "%4.4f" % "(PR1.mass)";
ERROR = "%2.2f ppm" % "(PR1.errppm)";
ISpmol = 14.06;
INT73 = NL1.intensity;
INT75 = NL2.intensity;
INT76 = NL3.intensity;
INT77 = NL4.intensity; ;
```

aPhosphatidylcholine IS

```
QUERYNAME = multiPCIS;
DEFINE PR1 = 'H93 D4 C50 O8 P1 N5' WITH CHG = 1;
DEFINE PR2 ='H93 D4 C50 O8 P1 N5' WITH  CHG = 1;
DEFINE NL1 = 'C9 H25 P1 N2 O4' WITH CHG = 0;
DEFINE NL2 = 'C9 H23 D2 P1 N2 O4' WITH  CHG = 0;
DEFINE NL3 =  'C9 H22 D3 P1 N2 O4' WITH  CHG = 0;
DEFINE NL4 =  'C9 H21 D4 P1 N2 O4' WITH  CHG = 0;

IDENTIFY
PR1 IN MS1+
AND PR2 IN MS2+
AND NL1 IN MS2+
AND NL2 IN MS2+
AND NL3 IN MS2+
AND NL4 IN MS2+

SUCHTHAT
PR1.chemsc == PR2.chemsc

REPORT
NAME = "PC [%d:%d]" % ((PR1.chemsc[C] - 16), (PR1.chemsc[db]
- 2.5));
MASS = PR1.mass;
chemsc = PR1.chemsc;
C = "%d" %  (PR1.chemsc[C] - 16);
db = "%d" %  (PR1.chemsc[db] - 2.5);
MASS = "%4.4f" % "(PR1.mass)";
ERROR = "%2.2f ppm" % "(PR1.errppm)";
ISpmol = 124.78;
INT73 = NL1.intensity;
INT75 = NL2.intensity;
INT76 = NL3.intensity;
INT77 = NL4.intensity; ;
```

aPhosphatidylcholine species

```
QUERYNAME = multiPC;
DEFINE  PR1  =  'C[30..60]  H[50..130]  D[4]  N[5]  P[1]  O[8]'  WITH
DBR = (4.5,15), CHG = 1;
DEFINE  PR2  =  'C[30..60]  H[50..130]  D[4]  N[5]  P[1]  O[8]'  WITH
DBR = (4.5,15), CHG = 1;
DEFINE NL1 = 'C9 H25 P1 N2 O4' WITH CHG = 0;
DEFINE NL2 = 'C9 H23 D2 P1 N2 O4' WITH  CHG = 0;
DEFINE NL3 =  'C9 H22 D3 P1 N2 O4' WITH  CHG = 0;
DEFINE NL4 =  'C9 H21 D4 P1 N2 O4' WITH  CHG = 0;

IDENTIFY
PR1 IN MS1+
AND PR2 IN MS2+
AND NL1 IN MS2+
AND NL2 IN MS2+
AND NL3 IN MS2+
AND NL4 IN MS2+

SUCHTHAT
isOdd(PR1.chemsc[C])
AND isOdd(PR1.chemsc[H])
AND PR1.chemsc == PR2.chemsc

REPORT
NAME = "PC [%d:%d]" % ((PR1.chemsc[C] - 16), (PR1.chemsc[db]
- 2.5));
MASS = PR1.mass;
chemsc = PR1.chemsc;
C = "%d" %  (PR1.chemsc[C] - 16);
db = "%d" %  (PR1.chemsc[db] - 2.5);
MASS = "%4.4f" % "(PR1.mass)";
ERROR = "%2.2f ppm" % "(PR1.errppm)";
ISpmol = 124.78;
INT73 = NL1.intensity;
INT75 = NL2.intensity;
INT76 = NL3.intensity;
INT77 = NL4.intensity; ;
```

aTriacylglycerol IS

```
QUERYNAME = multiTAGIS;
DEFINE PR1 = 'C[59] H[107] D[4] N[4] O[6]' WITH CHG = 1;
DEFINE PR2 = 'C[59] H[107] D[4] N[4] O[6]' WITH CHG = 1;
DEFINE NL1 = 'C4 H11 N1' WITH CHG = 0;
DEFINE NL2 =  'C4 H9 D2 N1' WITH  CHG = 0;
DEFINE NL3 =  'C4 H8 D3 N1' WITH  CHG = 0;
DEFINE NL4 =  'C4 H7 D4 N1' WITH  CHG = 0;

IDENTIFY
PR1 IN MS1+
AND PR2 IN MS2+
AND NL1 IN MS2+
AND NL2 IN MS2+
AND NL3 IN MS2+
AND NL4 IN MS2+

SUCHTHAT
PR1.chemsc == PR2.chemsc

REPORT
NAME = "TAG IS [%d:%d]" % ((PR1.chemsc[C] - 11),
(PR1.chemsc[db] - 3));
MASS = PR1.mass;
chemsc = PR1.chemsc;
C = "%d" %  (PR1.chemsc[C] - 11);
db = "%d" %  (PR1.chemsc[db] - 3);
MASS = "%4.4f" % "(PR1.mass)";
ERROR = "%2.2f ppm" % "(PR1.errppm)";
ISpmol = 117.74;
INT73 = NL1.intensity;
INT75 = NL2.intensity;
INT76 = NL3.intensity;
INT77 = NL4.intensity; ;
```

aTriacylglycerol speices

```
QUERYNAME = multiTAG;
DEFINE PR1 = 'C[40..80] H[50..130] D[4] N[4] O[6]' WITH DBR =
(3.5,18), CHG = 1;
DEFINE PR2 = 'C[40..80] H[50..130] D[4] N[4] O[6]' WITH DBR =
(3.5,18), CHG = 1;
DEFINE NL1 = 'C4 H11 N1' WITH CHG = 0;
DEFINE NL2 =  'C4 H9 D2 N1' WITH  CHG = 0;
DEFINE NL3 =  'C4 H8 D3 N1' WITH  CHG = 0;
DEFINE NL4 =  'C4 H7 D4 N1' WITH  CHG = 0;

IDENTIFY
PR1 IN MS1+
AND PR2 IN MS2+
AND NL1 IN MS2+
AND NL2 IN MS2+
AND NL3 IN MS2+
AND NL4 IN MS2+

SUCHTHAT
isEven(PR1.chemsc[C])
AND isOdd(PR1.chemsc[H])
AND PR1.chemsc == PR2.chemsc

REPORT
NAME = "TAG [%d:%d]" % ((PR1.chemsc[C] - 11),
(PR1.chemsc[db] - 3));
MASS = PR1.mass;
chemsc = PR1.chemsc;
C = "%d" %  (PR1.chemsc[C] - 11);
db = "%d" %  (PR1.chemsc[db] - 3);
MASS = "%4.4f" % "(PR1.mass)";
ERROR = "%2.2f ppm" % "(PR1.errppm)";
ISpmol = 117.74;
INT73 = NL1.intensity;
INT75 = NL2.intensity;
INT76 = NL3.intensity;
INT77 = NL4.intensity; ;
```

Double labeled aTriacylglycerol IS

```
QUERYNAME = multiTAGdlIS;
DEFINE PR1 = 'C70 H124 D8 N[8] O[6]' WITH CHG = 2;
DEFINE PR2 = 'C70 H124 D8 N[8] O[6]' WITH CHG = 2;
DEFINE NL1 = 'C62 H102 D8 N6 O6'  WITH CHG = 2;
DEFINE NL2 = 'C62 H106 D4 N6 O6'  WITH CHG = 2;
DEFINE NL3 = 'C62 H108 D2 N6 O6'  WITH CHG = 2;
DEFINE NL4 = 'C62 H110 N6 O6'  WITH CHG = 2;

IDENTIFY
PR1 IN MS1+
AND PR2 IN MS2+
AND NL1 IN MS2+
AND NL2 IN MS2+
AND NL3 IN MS2
AND NL4 IN MS2+

REPORT
NAME = "dlTAG-IS [%d:%d]" % ((PR1.chemsc[C] - 19), (PR1.chemsc[db] - 4));
MASS = PR1.mass;
chemsc = PR1.chemsc;
C = "%d" %  (PR1.chemsc[C] - 19);
db = "%d" %  (PR1.chemsc[db] - 4);
MASS = "%4.4f" % "(PR1.mass)";
ERROR = "%2.2f ppm" % "(PR1.errppm)";
ISpmol = 22.48;
INT73 = NL1.intensity;
INT75 = NL2.intensity;
INT76 = NL3.intensity;
INT77 = NL4.intensity; ;
```

10.6. Wt vs ΔDGAT1 experiments: total labeled lipids

The following figure shows the absolute amounts of all single alkyne labeled lipid species in the experiments done with the DGAT1$^{-/-}$ mice and the respective WT controls. This is done to rule out any false conclusions concerning the differences in the amount of certain lipid species in comparing these different biological systems.

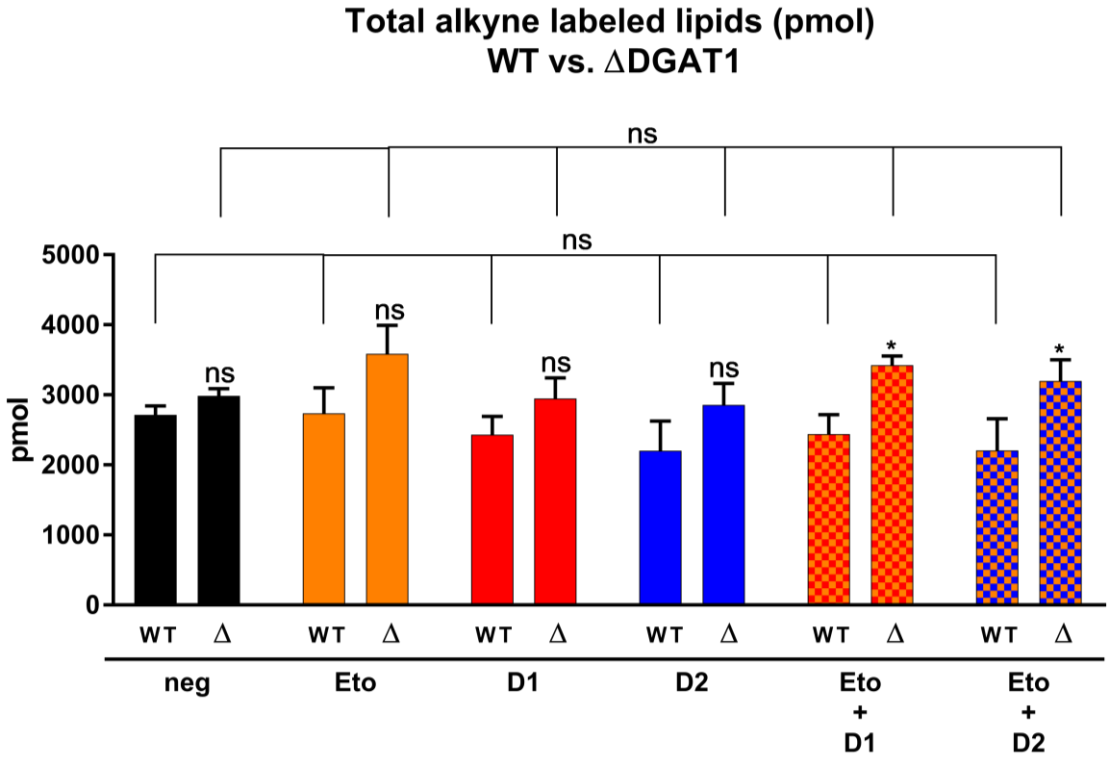

Supplementary figure 8: Absolute amount of all single alkyne-labeled lipids in pmol from primary hepatocytes, isolated from wildtype mice (WT) or mice lacking DGAT1 (ΔDGAT1), treated with different inhibitor combinations, pulsed with alkyne-palmitate and decanoic acid. After isolation, primary mouse liver hepatocytes were plated in 24 well plates with 7.5x10^4 cells per well. Cells were preincubated with either 50 µM Etomoxir (Eto), 3 µM DGAT1-Inhibitor (D1), 15 µM DGAT2-Inhibitor (D2) or combinations of Etomoxir with each DGAT-inhibitor (Eto+D1, Eto+D2). Cells were then co-pulsed with 50 µM alkyne palmitate (C17:2) and 50 µM decanoic acid (C10) for 1 hour. Lipids were extracted with simultaneous addition of an internal standard mix for alkyne labeled lipids and click reaction with C175-XX reagents was performed. Multiplex samples were pooled and analyzed by MS. Mass signals were identified using LipidXplorer MFQL analysis with internal standard quantification for aTAG, aDAG, aPC, aPA, aCE and aCer. The data represent mean ±SD for n=3 biological replicates. * stands for p≤0.0332 and ns=not significant. Isolation of hepatocytes and fatty acid pulse was done by CL, lipid extraction and MS/TLC analysis were done by KW.

There are no significant changes in the amount of labeled lipids between the treatment groups (Eto, D1, D2, Eto+D1, Eto+D2) and the respective negative control in either the WT or the DGAT1$^{-/-}$ animals, when compared internally. The amounts in each treatment group between WT and DGAT1$^{-/-}$ animals are slightly higher on the side of the DGAT1$^{-/-}$ animals, however only significantly higher in the two treatment groups where Etomoxir and either one of both DGAT inhibitors are combined. Nevertheless, in the negative controls the amounts of all labeled lipids were nearly the same, thus making the direct comparison of the two animal groups meaningful.

10.7. Supplementary data for chapters 5.3.2 and 5.5

Supplementary figures 9 and 10 refer to the experiments done in chapter 5.3.2.

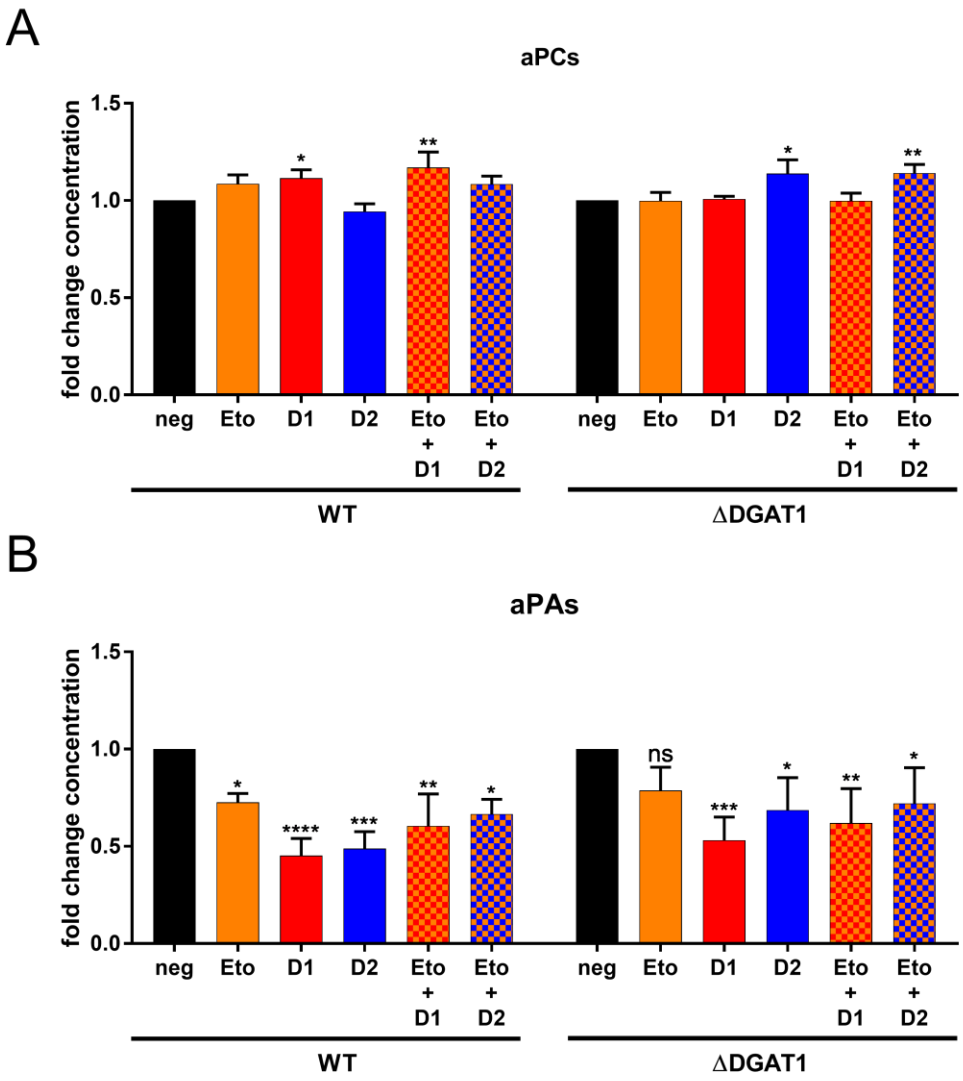

Supplementary figure 9: Fold change analysis of alkyne-labeled PC (A) and PA (B) based on relative amounts (mol per mille) from aTAG, aDAG, aPC, aPA, aCE and aCER, from primary hepatocytes, isolated from wildtype mice (WT) or mice lacking DGAT1 (ΔDGAT1), treated with different inhibitor combinations, pulsed with alkyne-palmitate and decanoic acid. After isolation, primary mouse liver hepatocytes were plated in 24 well plates with $7.5x10^4$ cells per well. Cells were preincubated with either 50 µM Etomoxir (Eto), 3 µM DGAT1-Inhibitor (D1), 15 µM DGAT2-Inhibitor (D2) or combinations of Etomoxir with each DGAT-inhibitor (Eto+D1, Eto+D2). Cells were then co-pulsed with 50 µM alkyne palmitate (C17:2) and 50 µM decanoic acid (C10) for 1 hour. Lipids were extracted with simultaneous addition of an internal standard mix for alkyne labeled lipids and click reaction with C175-XX reagents was performed. Multiplex samples were pooled and analyzed by MS. Mass signals were identified using LipidXplorer MFQL analysis with internal standard quantification for aTAG, aDAG, aPC, aPA, aCE and aCER. Normalized fold changes (NFC) in relative concentrations of alkyne PCs and PAs for each inhibitor treatment were calculated by normalization to the negative control. The data represent mean ±SD for n=3 biological replicates. * stands for p≤0.0332, ** for p≤0.0021, *** for p≤0.0002 and **** for p≤0.0001. ns=not significant. Isolation of hepatocytes and fatty acid pulse was done by CL, lipid extraction and MS/TLC analysis were done by KW.

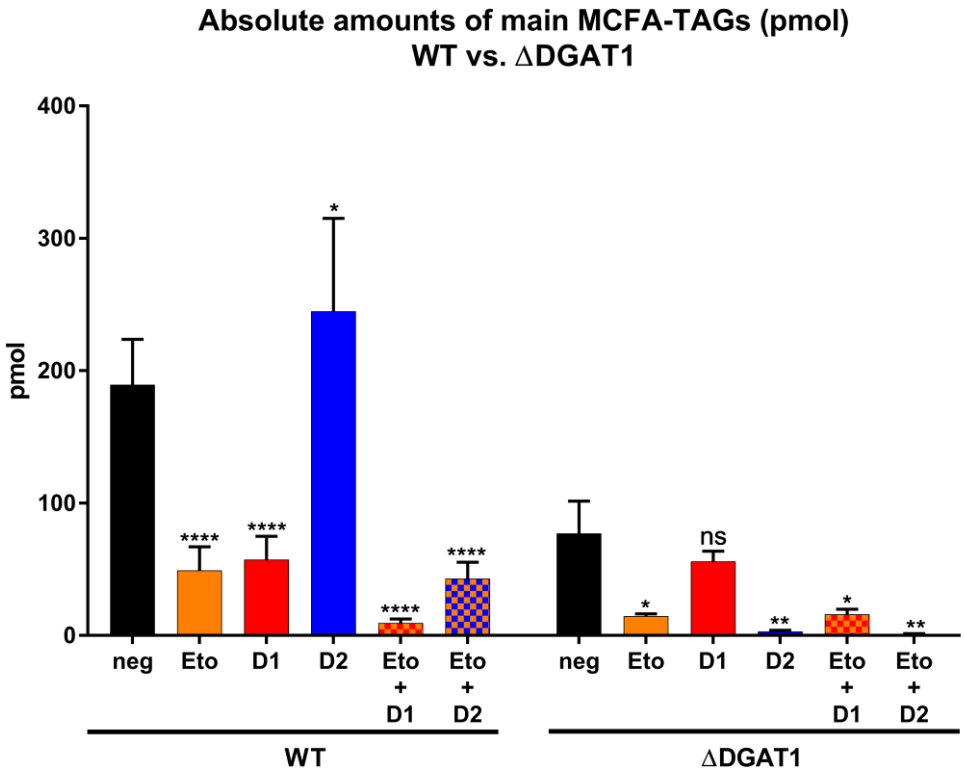

Supplementary figure 10: Absolute amounts (pmol) of the four main MCTs from primary hepatocytes, isolated from wildtype mice (WT) or mice lacking DGAT1 (ΔDGAT1), treated with different inhibitor combinations, pulsed with alkyne-palmitate and decanoic acid. After isolation, primary mouse liver hepatocytes were plated in 24 well plates with $7.5x10^4$ cells per well. Cells were preincubated with either 50 µM Etomoxir (Eto), 3 µM DGAT1-Inhibitor (D1), 15 µM DGAT2-Inhibitor (D2) or combinations of Etomoxir with each DGAT-inhibitor (Eto+D1, Eto+D2). Cells were then co-pulsed with 50 µM alkyne palmitate (C17:2) and 50 µM decanoic acid (C10) for 1 hour. Lipids were extracted with simultaneous addition of an internal standard mix for alkyne labeled lipids and click reaction with C175-XX reagents was performed. Multiplex samples were pooled and analyzed by MS. Mass signals were identified using LipidXplorer MFQL analysis with internal standard quantification for aTAG, aDAG, aPC, aPA, aCE and aCER. Absolute amounts from MCTs (Σ of [43:3], [43:2], [45:4], [45:3]) are presented in pmol. The data represent mean ±SD for n=3 biological replicates. * stands for p≤0.0332, ** for p≤0.0021 and **** for p≤0.0001. ns=not significant. Isolation of hepatocytes and fatty acid pulse was done by CL, lipid extraction and MS/TLC analysis were done by KW.

Supplementary figures 11 and 12 refer to experiments done described in chapter 5.5.

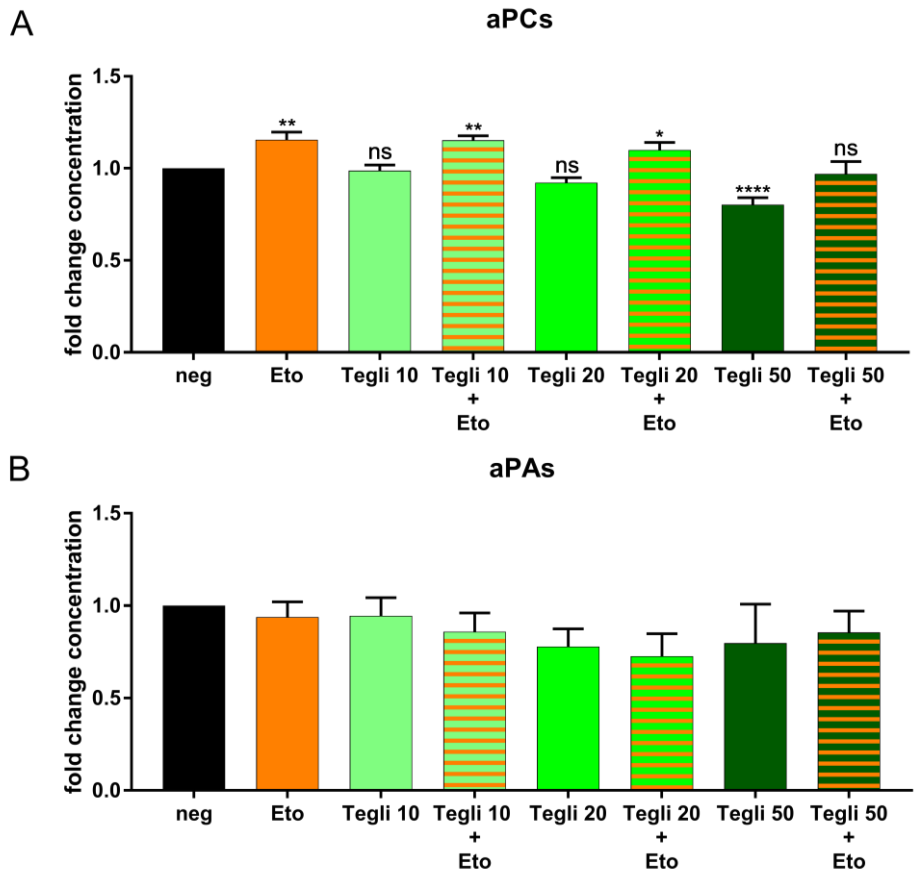

Supplementary figure 11: Fold change analysis of alkyne-labeled PC (A) and PA (B) based on relative amounts (mol per mille) from aTAG, aDAG, aPC, aPA, aCE and aCER, from primary hepatocytes, isolated from WT mice treated with different combinations of Etomoxir and Teglicar and pulsed with alkyne-palmitate and decanoic acid. After isolation, primary mouse liver hepatocytes were plated in 24 well plates with $7.5x10^4$ cells per well. Cells were preincubated with either 50 µM Etomoxir (Eto), 10 µM Teglicar (Tegli 10), 20 µM Teglicar (Tegli 20), 50 µM Teglicar (Tegli 50) or combinations of Etomoxir with each Teglicar concentration (Tegli XX + Eto). Cells were then co-pulsed with 50 µM alkyne palmitate (C17:2) and 50 µM decanoic acid (C10) for 1 hour. Lipids were extracted with simultaneous addition of an internal standard mix for alkyne labeled lipids and click reaction with C175-XX reagents was performed. Multiplex samples were pooled and analyzed by MS. Mass signals were identified using LipidXplorer MFQL analysis with internal standard quantification for aTAG, aDAG, aPC, aPA, aCE and aCER. Normalized fold changes (NFC) in relative concentrations of alkyne lipids for each inhibitor treatment were calculated by normalization to the negative control. The data represent mean ±SD for n=3 biological replicates. * stands for p≤0.032, ** stands for p≤0.0021 and **** for p≤0.0001. ns=not significant.

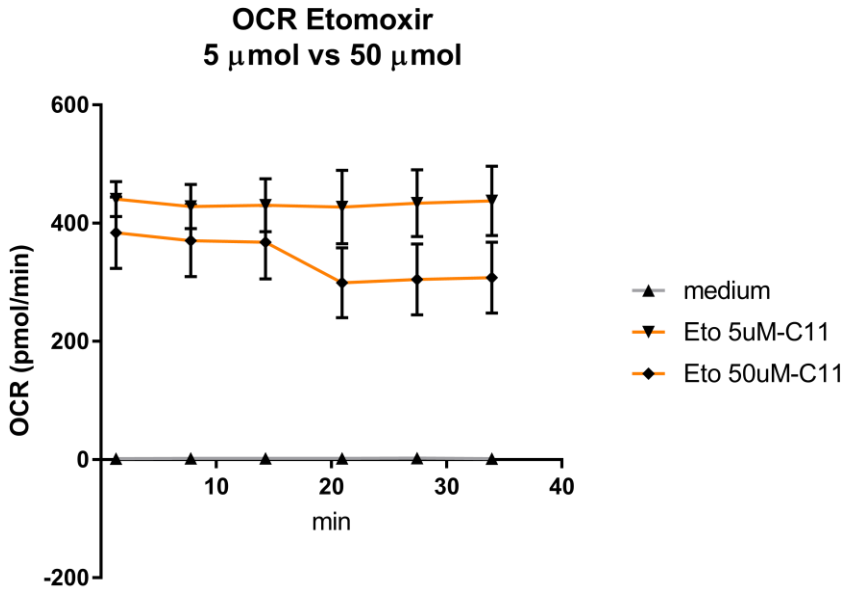

Supplementary figure 12: Live cell OCR measurement (pmol/min) in C11-FA fed hepatocytes isolated from WT mice treated with either 5 or 50 µM Etomoxir. After isolation, primary mouse liver hepatocytes were plated in a Seahorse XF Analyzer 96 well plate with 1000 cells per well. Cells were allowed to adhere for two hours before the assay procedure was started (see: Chapter 3.6.). After 3 measuring cycles of baseline OCR measurement Etomoxir was injected, and the measurement was resumed for 3 more cycles. A drop in OCR was only visible with treatment of 50 µM Etomoxir and not with 5 µM.

Acknowledgements

Although my name stands alone beneath the title of this thesis, it could not have been completed without the support and encouragement from all the people who helped me throughout the years of my PhD. With these lines I would like to express my deepest gratitude to all of you.

First and foremost, I would like to thank my doctoral supervisor Prof. Dr. Christoph Thiele for giving me the great opportunity to work in his group and offering me this interesting topic. I would like to thank him for always giving insightful advice and reliable help, when needed. I am very grateful for his good support throughout the whole period of my PhD and I am looking forward continuing my work in his group.

Likewise, I want to thank all the members of my thesis committee. I am very grateful to PD Dr. Heike Weighardt for reviewing my thesis as a second supervisor. My sincere thanks go as well to PD Dr. Reinhard Bauer and Prof. Dr. Michael Gütschow for completing my thesis committee.

I would especially like to thank Prof. Dr. Dagmar Kratky and her colleague Dr. Christina Leopold at the Medical University of Graz in Austria, for enabling the collaborative work with the DGAT1$^{-/-}$ animals, which resulted in the exciting data which greatly complements this thesis. My deepest gratitude and thanks to Dr. Christina Leopold for her excellent work in isolating and pulsing the hepatocytes. I would also like to thank Mohamed Yaghmour for helping me with the lipid extraction and the MS analysis of the samples from Austria. My earnest thanks go to Dr. Fabian Gondorf and Mario Lauterbach for great help in establishing the Seahorse analysis and helpful counsel on various occasions.

At this point I would like to thank the Deutsche Forschungsgemeinschaft (DFG) for partially funding my PhD project through various SFB initiatives.

My sincere thanks and appreciation to Dr. Jeffrey Hannam and especially PD Dr. Lars Kürschner for proofreading my thesis. My most truthful thanks go to all the present and former members of the Thiele lab, who were always open for questions and discussions, were always eager to offer help and created a genuinely nice and collegial atmosphere in the lab: present: PD Dr. Lars Kürschner, Dr. Anne Gaebler, Mohamed Yaghmour, Fabian Zink, Konstantin Beckschäfer, Heike Sievert and former: Dr. Anke Penno, Dr. Mario Schoene, Dr. Johanna Spandl, Dr. Daniel Lohmann, Dr. Ana Stevanovic, Dr. Kira Piotrowitz, Dr. Kristina Hoffmann, Dr. Kristina Klizaite, Dr. Elvira Weber, Philipp Leyendecker and Alexander Buck-Häger. Furthermore, I want to thank all the Master- Bachelor- and Lab rotation students which I supervised during the time of my PhD. I enjoyed supervising you all! I especially want to thank the students Konstantin Beckschäfer, Maria Fiedler and Jennifer Saam for sharing

so many nice moments in the lab and during various coffee breaks. I also want to express my gratitude and thanks to the whole community from the LIMES Institute. I really appreciate the very communicative environment in the institute where you can always get into contact with colleagues form different research fields, creating a great opportunity for interdisciplinary research, but also adding a nice social atmosphere through various events like the party on Carnival or on Christmas. Thank you all!

Furthermore, I want to thank all my close ones, family and friends, for sharing all the nice moments and genuine distractions from everyday life at the lab bench. I would like to thank my closest friends from the GGG for all the good times on various camping-, BBQ-, Oberkassel-campfire-and-so-on-events: Alex (Heavy), Anne, Chris, Daria, Elise, Felix, Inouk, James, Malte, Micha, Milan, Sonja and Tanja. Likewise, I want to thank all my climbing partners for all the good times at the sandstone boulders of Fontainebleau, the basalt pillars in the Eifel or the plastic rocks inside a gym: Alex (Heavy), Alex, Inouk, Phillip, Malte, Kristina, and Niko. Special thanks also to Felix, Mario and Alex for the occasional (and far too less) musical input throughout my PhD.

My warmest thanks go to my parents for always supporting me throughout every step in my life. And finally, I want to thank my most loved ones: my wife Jana and my daughter Lena. I am glad to have you both by my side and I enjoy every single moment spending with you both. You are the most important people in my life. Thank you!

“Alte Wunder, künftge Zeiten
Seltsamkeiten,
Weichet nie aus meinem Herzen”
-Novalis-